UNIVERSIDAD AUTÓNOMA DE MADRID

FACULTAD DE CIENCIAS

Departamento de Biología Molecular

NEW NON-VIRAL VECTORS FOR siRNA DELIVERY TO INHIBIT HIV REPLICATION

DOCTORAL THESIS

Nick Weber

Madrid, 2009

Doctoral Thesis:

NEW NON-VIRAL VECTORS FOR siRNA DELIVERY TO INHIBIT HIV REPLICATION

This work has been carried out to fulfill the prerequisites necessary to be awarded a Doctorate in Molecular Biology to:

Nick Weber

Project Adviser:

Dr. Mª.Ángeles Muñoz-Fernández.

PhD in Biological Sciences.

PhD in Medicine and Surgery.

Head of the Laboratorio de Inmunobiología Molecular.

Hospital General Universitario "Gregorio Marañón" (Madrid).

Signature of Approval of the Adviser.

This work has been carried out in the Laboratorio de Inmuno-Biología Molecular of the Hospital General Universitario ""Gregorio Marañón", under the guidance of Dr. María Ángeles Muñoz-Fernández. The completion of this work is due to the funding provided by Fondos de Investigación Sanitaria (Ministerio de Ciencia e Innovacíon), the Fundación para la Investigación y Prevención del Sida en España (FIPSE), and Caja Navarra.

To Mom and Dad,

and to María

ACKNOWLEDGEMENTS

In order to be able to carry out such a large project as completing a doctoral thesis, the help, collaboration, and support form many people are a huge necessity. I have been fortunate enough to benefit from the help from a tremendously knowledgeable, active and supportive group of people that is also surprisingly plentiful. Above all, I wish to thank the person who made this all possible in the first place by offering a position in her lab to a stranger from such a strange far-away place as Montana and by continually doing anything and everything necessary for this research to be carried out successfully, María Ángeles.

Next, to all the people in the lab (either those that share a lab with me or those in the many labs with which we are affiliated) who are indeed "collaborators" in the truest sense of the word and who deserve just as much as I do to have their names under the title of this work, I want to express my thanks to the following people:

To our collaborators at the Universidad de Alcalá, the crazy dendrimer creators, Rafa, Javi and especially Paula, you deserve much credit for designing, synthesizing and providing us with the main ingredients that we needed so that we wouldn't just being playing around with cells and viruses. Thank you Paula for explaining so much to me no matter how many times I asked the same questions;

To Rafa for controlling the most complicated device that I got to play around with, the confocal microscope, and for helping me capture the best images and the videos that by some strange occurrence got my mug on the national news. You deserve at least half of the spotlight for that one;

Our collaborators working in Poland, Ela, Dima and Maria, deserve credit for carrying out the structural and characteristic studies on dendrimers that were fundamental to completing this work;

To the Germans, Olivia for her hard work with the polymers, and Dr. Kissel for showing interest in me and my idea enough to send me the structures that carried with them all of his genius and expertise in polymer synthesis;

To all the chicas del labo who have all made me feel more than welcome since the very beginning, Laura, Almu, Bea, Teresa, Marjorie, Veronica, Raquel, Carmen, Nati, Lola, Pepa, and Chusa, also for their unending assistance in the lab (especially Chusa) and Susana for her help in the lab and for never refusing to patiently listen and respond to any and all of my questions no matter how asinine, thank you to all of you for all your help and especially your *ánimos* everyday. To my partners in the "best

corner of the resident's office", Claudia and Alicia, thank you for your wonderful attitudes and especially for your friendship to me, and Alicia, thank you, especially, for all your help in getting all this work down on paper in somewhat understandable English and for so much more. To Alberto, both Rafas, "*Grande*" and "*Pequeño*", Javi, Santi, Luis and Jose Luis for your positive outlooks and (sometimes) funny jokes, and to Miguel for keeping me motivated this last year especially with ideas of just how exciting research can be. To the ones who were the first to help me out at the beginning and also for answering many of my questions, Gerónimo, Jesús, and Salva. And to my "brothers in arms" (or perhaps better referred to as "brothers in dendros"), the ones with whom I've shared this treacherous course of making sense out of those darn things, Maribel and Louis, I couldn't have done this with out you. I only hope that I might have been a fraction of the amount of help to you guys in your quests as you have been to me. Keep at it, for your turns are rapidly approaching. Thank you to everyone in the lab for being a great group of people and creating a wonderful environment for someone from across the world to come and carry out his work enjoyably.

Finally, I wish to thank my family (both American and Spanish) for being the greatest family a kid could ever hope to have, for endless love and support, and in particular, Mom and Dad for always believing in me and supporting me in whatever endeavor I have chosen, whether it be science, math, sports, music, leaving to play rugby across the ocean, or carrying out biomedical research in some strange concept that has something (but we're not sure what, exactly) to do with HIV.

And to María, thank you for being you. You are my main motivation and inspiration. And so much more.

A todos:

Muchísimas Gracias!!!

TABLE OF CONTENTS

LIST OF ABBREVIATIONS

2G-NN16	2G-CBS-$(OCH_2CH_2N^+Me_2CH_2CH_2N^+Me_3I^-)_8$
2G-NN8	2G-CBS-$(OCH_2H_2NMe\ CH_2CH_2N^+Me_3{}^+I^-)_8$
A	adenine
Ag	antigen
$AgNO_3$	silver nitrate
AIDS	acquired immune deficiency syndrome
APS	ammonium persulphate
ATCC	American Type Culture Collection
AZT	azidothymidine
BBB	blood-brain barrier
bMVEC-B	bovine brain microvascular endothelial cells
BrdU	bromodeoxyuridine
C	cytosine
CA	capsid
CBS	carbosilane dendrimer
cDNA	complementary DNA
CNS	central nervous system
CO_2	carbon dioxide
Cy3	cyanine 3
Da	dalton
DAPI	4'-6-Diamidino-2-phenylindole
DEPC	diethylpyrocarbonate
DLS	dynamic light scattering
DMEM	Dulbelco's Modified Eagle Medium
DMSO	dimethyl sulfoxide
DNA	deoxyribonucleic acid
dsRNA	double-stranded RNA
dT	deoxyribose thymine
EDTA	ethylenediaminetetraacetic acid
FBS	fetal bovine serum
FITC	fluorescein isothiocyanate
G	guanine
GAPDH	glyceraldehyde 3-phosphate dehydrogenase
GE	gel electrophoresis
GT	gene therapy
h	hour

HAART	highly active antiretroviral therapy
HAD	HIV associated dementia
HBS	HEPES-buffered saline
HEC-1A	human endometrial carcinoma cells
Hep	heparin
HEPES	4-(2-hydroxyethyl)-1-piperazineethanesulfonic acid
HIV	human immunodeficiency virus
IL-2	interleukin-2
IN	integrase
IU	international unit
kDa	kilodalton
LDH	lactate dehydrogenase
LTR	long terminal repeat
M	molar (mol/l)
mA	milliamperes
MA	matrix
min	minute
miRNA	micro RNA
MOI	multiplicity of infection
mPa	millipascal
mRNA	messenger RNA
MTT	(3-(4,5-dimethylthiazol-2-yl)-2,5-diphenyl-tetrazolium-bromide)
mW	milliwatt
MW	molecular weight
NaCl	sodium chloride
N/P	amine to phosphate ratio
NC	nucleocapsid
NHA	normal human astrocytes
NIAID	National Institute of Allergy and Infectious Diseases
NIH	National Institute of Health
NMR	Nuclear Magnetic Resonance
PAGE	polyacrylamide gel electrophoresis
PALS	phase analysis light scattering
PBMC	peripheral blood mononuclear cells
PBS	phosphate buffered saline
PCR	polymer chain reaction

PEG	polyethylene glycol
PEI	polyethyleneimine
PHA	phytohemagglutinin
PIC	preintegration complex
ppm	parts per million
PR	protease
qPCR	quantitative polymer chain reaction
RISC	RNA inducing silencing complex
RNA	ribonucleic acid
RNAi	RNA interference
rpm	revolutions per minute
RPMI	Royal Park Memorial Institute
RT	reverse-transcriptase
s	second
SD	standard deviation
SEM	standard error of the mean
shRNA	small hairpin RNA
siRNA	small interfering RNA
T	thymine
TAR	*trans*-activation response RNA element
TBE	Tris/Borate/EDTA
TEER	transepithelial electric resistance
TEMED	tetramethylethylenediamine
U	uracil
V	volts
VL	viral load

SUMMARY

One of the primary limitations of RNA interference as a technique for gene regulation is effective delivery and transfection of siRNA into the target cells. Dendrimers and polyethyleneimine (PEI) polymers are nanoparticles being developed as non-viral vectors for oligonucleotide and drug delivery. Through two separate collaborations with other research groups, we have gained access to novel carbosilane dendrimers (CBS) and polyethylene glycol (PEG)-engrafted PEI copolymers in order to research the potential these vectors have at inhibiting HIV replication by siRNA delivery. Initially, stability and structural dynamics studies were carried out to examine the characteristics these structures possess when complexed with siRNA. These experiments showed that CBS protected siRNA from RNase degradation and that its structural design resulted in a gradual liberation of the siRNA cargo. Cytotoxicity assays of dendriplexes with a variety of cell types revealed a maximum safe dendrimer concentration for *in vitro* assays. Similar experiments performed with polyplexes highlighted the improvement in biocompatibility achieved by PEG engraftment. PEI-PEG polymers had minimal effects on cell viability. Next, through the use of flow cytometry and confocal and immunofluorescence microscopy, lymphocytes and astrocytes were seen to be successfully transfected with fluoro-chrome-labeled siRNA either alone or complexed to the delivery vectors. Further-more, transfection efficiency assays helped to decide the best ratios of vector amine to nucleotide phosphate for cell transfection and to determine the size and number of PEG-engraftments to achieve maximum uptake by the cells. Barriers made of cell monolayers were utilized to test the potential of dendriplexes to cross biological barriers with the objective of using this delivery method to reach cells of the central nervous system (CNS). The final set of experiments dealt with gene silencing by siRNAdelivered by these vectors. The GAPDH gene was silenced by dendriplexes nearly 50% after a short incubation, and polyplexes were seen to silence it by an average of 80% over the course of three weeks. The primary goal of the project was achieved when siRNA delivered by a PEI-PEG polymer resulted in the stable inhibition of HIV replication for 15 days to levels comparable to AZT, a top antiretroviral drug. Taken all together, these results point to the possibility of utilizing these non-viral vectors to deliver and transfect siRNA into lymphocytes or possibly cross the blood brain barrier and reach cells of the CNS, which would thus, in turn, improve the possibility of RNA interference as a potential alternative therapy for HIV infection.

Una de las primeras limitaciones del ARN pequeño de interferencia (siRNA) como técnica para la regulación de genes es su efectiva transfección y liberación del siRNA en el interior de las células diana. Los dendrímeros y los polímeros polietilenimina (PEI) son nanopartículas que se han desarollado como vectores no virales para la liberación de oligonucleótidos y fármacos. A través de dos colaboraciones con otros grupos de investigación, hemos tenido acceso a nuevos dedrímeros carbosilano (CBS) y copolímeros PEI unidos a una o más moléculas de polietilenglicol (PEG) con el fin de investigar el potencial que estos vectores tienen en la inhibición de la replicación del VIH mediante la liberación de siRNA. Inicialmente, se han llevado a cabo estudios de estabilidad y dinámica estructural para examinar las características que estas estructuras poseen cuando se acomplejan con siRNA. Los experimentos han mostrado que los CBS protegen a los siRNA de la degradación por RNasas y que la liberación del siRNA es gradual. Ensayos de citotoxicidad de dendriplexes en una selección de tipos celulares han mostrado una concentración máxima de dendrímero segura para ensayos *in vitro*. Se han llevado a cabo experimentos similares con polyplexes destacando la mejora en la biocompatibilidad lograda tras la unión de los polímeros con PEG. Los polímeros PEI-PEG apenas han tenido efecto en la viabilidad celular. A continuación, mediante el uso de citometría de flujo y de microscopía confocal o de inmunofluorescencia, se ha observado que tanto linfocitos como astrocitos se transfectan con siRNA marcado con un fluorocromo tanto solo como unido a vectores de liberación. Además, ensayos de eficiencia de transfección han ayudado a determinar los mejores ratios de carga y el tamaño y número óptimos de moléculas PEG para conseguir una máxima internalización por las células. Con el fin de usar estos métodos de liberación para alcanzar las células del sistema nervioso central (SNC), se han utilizado dos modelos distintos de barreras biológicas para testar el potencial de los dendriplexes en cruzarlas. El ultimo grupo de experimentos ha consistido en el silenciamiento de genes mediante la liberación de siRNA por estos vectores. Se ha conseguido silenciar el gen GAPDH en casi un 50% tras un corto periodo de incubación con dendriplexes y en un 80% tras tres semanas de tratamiento con poliplexes. El objetivo principal de este proyecto se ha alcanzado cuando la liberación de siRNA por un polímero PEI-PEG ha resultado en una inhibición estable de la replicación del VIH durante quince días a niveles comparables a los del fármaco antirretroviral AZT. En conjunto, nuestros resultados apuntan a la posibilidad de utilizar estos vectores no virales para transfectar y liberar siRNA en linfocitos o atravesar la barrera hemato-encefálica y alcanzar las células del SNC, lo cual mejoraría el uso potencial del ARN de interferencia como terapia alternativa en la infección por el VIH.

1. INTRODUCTION

1.1 The Human Immunodeficiency Virus (HIV)

The global HIV/AIDS pandemic is the largest threat to worldwide health, safety and economy that will likely be faced in our generation. Since the first cases of AIDS were recognized in 1981 [1], more than 25 million people have succumbed to the disease. Another 33 million individuals are currently infected with HIV, according to 2008 estimates by the World Health Organization [2]. These numbers qualify HIV/AIDS as a pandemic [3]. The geographical area most affected by HIV/AIDS lies in Sub-Saharan Africa where 33 (67%) of the 49 least developed countries[1] in the world [4] and two thirds of all HIV positive cases in the world are located. In this region, the adult prevalence[2] of HIV infection has reached 5% [2], and the pandemic has had enormous effects on public health, life expectancy, population dynamics, numbers of orphaned children and local economy because of the loss in human capital. **Figure 1** shows an example of the effect that AIDS has had on the average life expectancy in several of the worst affected countries. Sub-Saharan Africa is indeed the region that is worst affected by HIV/AIDS. However, the myriad of dangers and problems caused by this infectious disease pandemic affects the entire world. Therefore, there is a great deal of need for research into preventive strategies, developing new therapies, improving current treatment, and searching for an effective vaccine. The effect this pandemic has on social, cultural and economic issues is greatly increasing every year. And yet, there still is no vaccine or cure for the disease and treatment consists of a rigorous life-long regimen of high-cost antiretroviral medications.

[1] The UN classifies countries as "least developed" based on three criteria: (1) annual gross domestic product (GDP) below $900 per capita; (2) quality of life, based on life expectancy at birth, per capita calorie intake, primary and secondary school enrollment rates, and adult literacy; and (3) economic vulnerability, based on instability of agricultural productions and exports, inadequate diversification, and economic smallness. Half or more of the population in the 49 least developed countries are estimated to live at or below the absolute poverty line of U.S. $1 per day.

[2] Proportion of adults aged 15-49 who are living with HIV/AIDS

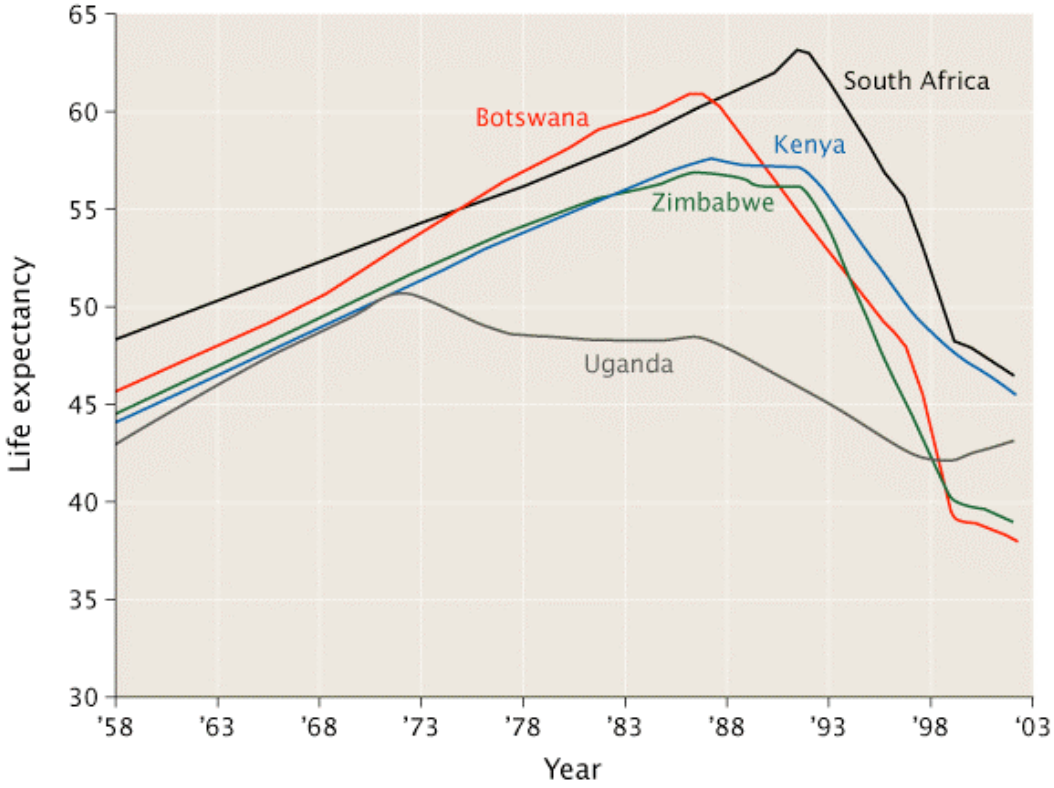

Figure 1. Life expectancy in five Sub-Saharan African countries (Botswana, Kenya, South Africa, Uganda, and Zimbabwe) from 1958 to 2003. *(Source: World Bank, World Development Indicators, 2004)*

The causative agent of AIDS is HIV, a lentivirus and member of the retrovirus family. Transmission of HIV between individuals can occur via unprotected sexual contact, through the exchange of blood or blood products such as through blood transfusions or by sharing needles for intravenous drug use, or from mother to child either during gestation, at birth or during breast-feeding. HIV primarily infects the human immune system cells CD4+ helper T lymphocytes, macrophages and dendritic cells. During the course of HIV infection, persistent viral replication, aberrant and persistent immune activation and, eventually, immunological deterioration are known to occur [5]. HIV infection consists of four stages referred to as incubation, acute infection, latency, and AIDS. Acute HIV infection involves high HIV viremia and a sudden drop in CD4+ T cells due to a very high viral replication rate and a dissemination of infected CD4+ T cells by activated CD8+ T cells. This stage persists an average of two weeks during which time the individual may exhibit flu-like symptoms [5, 6]. Afterwards, the infection enters a stage of clinical latency lasting an

average of 10 years for untreated patients, when the plasma viral load (VL) drops and CD4+ T cell counts rebound before gradually falling to levels where proper immune system function cannot be maintained. At this point, the patient is susceptible to a myriad of opportunistic infections, the contraction of which indicates a progression to AIDS, the final stage of HIV infection (Figure 2). The course of the disease progression can be accurately monitored by measuring VL and CD4+ T cell counts [7, 8]. In untreated patients, HIV infection followed by the development of AIDS is invariably fatal.

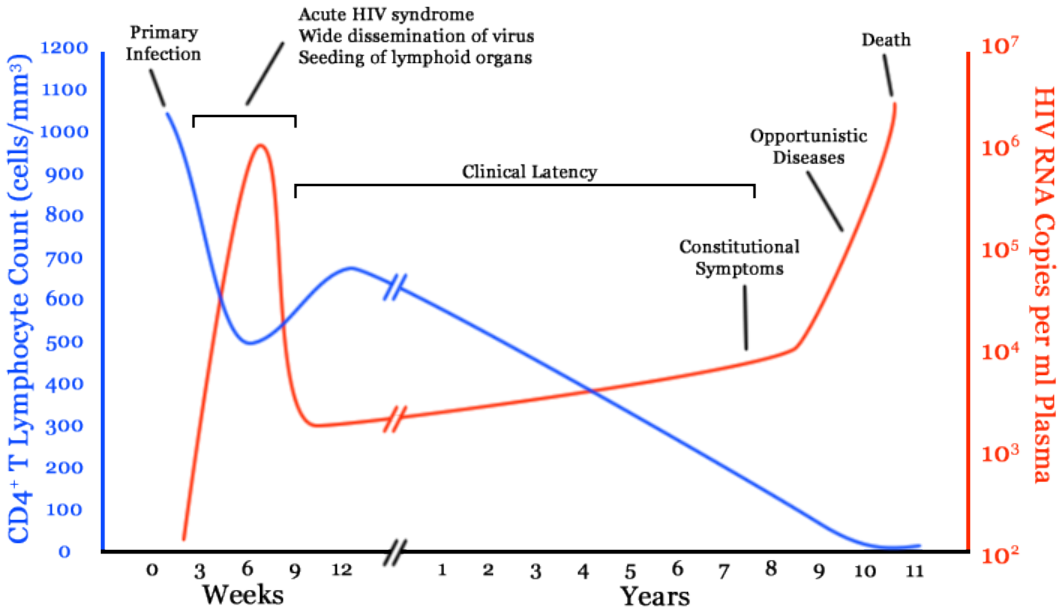

Figure 2. Generalized graph showing HIV RNA copies (viral load) and CD4+ T cell counts over the average course of untreated human HIV infection. *(Modified from Fauci et al. (1996))*

1.1.1 HIV genome

Virions of the HIV virus, like all retroviruses, consist of an envelope structure composed of viral **envelope glycoproteins** (Env) and a **lipid bilayer** that encloses viral **structural proteins** (Gag), **enzymatic proteins** (Pol) and two copies of an **RNA** genome (see Figure 4). The genome consists of nine genes that encode 15 principal proteins (**Figure 3**).

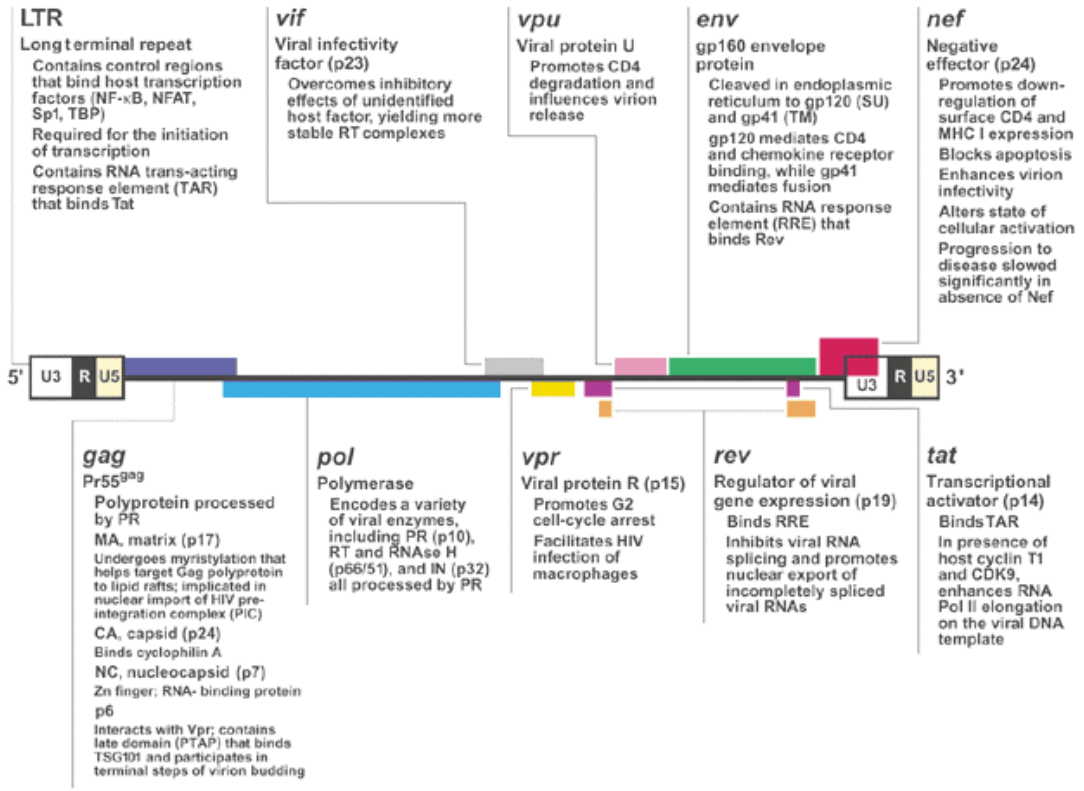

Figure 3. The HIV genome consists of 9 genes that encode 15 proteins. *(Source: Greene, et al. (2002))*

- **LTR** – The genome is flanked on both ends by a non-coding repeated sequence termed the **long terminal repeat** (LTR), which is necessary for the viral genome to be inserted into a host cell's DNA, and also functions as a transcriptional promoter.
- **Gag –** The gene *gag* encodes for the three structural proteins matrix (MA), capsid (CA), and nucleocapsid (NC), which are formed from the cleavage of the Gag polyprotein by the HIV protease.
- **Pol –** The *pol* gene encodes for a polyprotein containing all three enzymatic proteins. The transcript from this gene is produced when a frame shift occurs when the *gag* gene is being transcribed so that the *gag* stop codon is missed and the *pol* gene is transcribed as an appendage to the *gag* mRNA. This error in transcription occurs about 5% of the time [9]. The resulting polycistronic mRNA is translated into the polyprotein Gag-Pol. This polyprotein is likewise processed by protease to generate the Gag and Pol polyproteins and, subsequently, the three structural proteins

(from Gag) and the three enzymes protease (PR), reverse-transcriptase (RT), and integrase (IN). Each of these enzymes possesses a unique role in the propagation of the virus as is described below in more detail.

- **Env –** The *env* gene encodes the gp160 envelope polyprotein. This gene product is translated in the endoplasmic reticulum and transferred to the plasma membrane by way of the Golgi apparatus where it is cleaved by cellular proteases and glycosylated to form the membrane bound gp41 glycoprotein and the gp120 glycoprotein located in the Golgi lumen. The two Env glycoproteins are non-covalently bound to each other and, once they arrive at the plasma membrane, are incorporated into budding virions where they become responsible for receptor binding and fusion of the nascent virions during infection of new cells.
- **Accessory genes –** The accessory genes *vif*, *vpr*, *tat*, *rev*, *vpu*, and *nef* are six additional genes contained in HIV that distinguish it (and other primate lentiviruses) from more basic retroviruses which only possess the essential *gag*, *pol*, and *env* genes [9]. They encode proteins that play a secondary role in HIV replication. These are the products of either singly spliced or multiply spliced viral mRNA. The Env proteins come from singly spliced transcripts, while unspliced whole transcripts are the precursors for the Gag and Gag-Pol polyproteins. Tat and Rev are essential for HIV replication, whereas the remaining accessory proteins are not required for viral replication *in vitro* [10], but serve additional purposes in the viral replication cycle.

1.1.2 HIV structure

HIV virions are very efficient in their structure, possessing only the necessary components for the first phase of the viral life cycle, from cell infection to integration into the host DNA. The genome is optimized to contain the necessary genes in the smallest amount of RNA possible. It takes advantage of multiple splicing sites, all three reading frames, and extensive overlapping to accomplish this [9]. An individual virion has a diameter of 100 to 150 nm [11]. The structural organization of the virus must be extremely efficient in order to contain two copies of an RNA genome as well

as all the proteins needed to enable infection and maintain stability in an environment as hostile as the extracellular matrix (**Figure 4**).

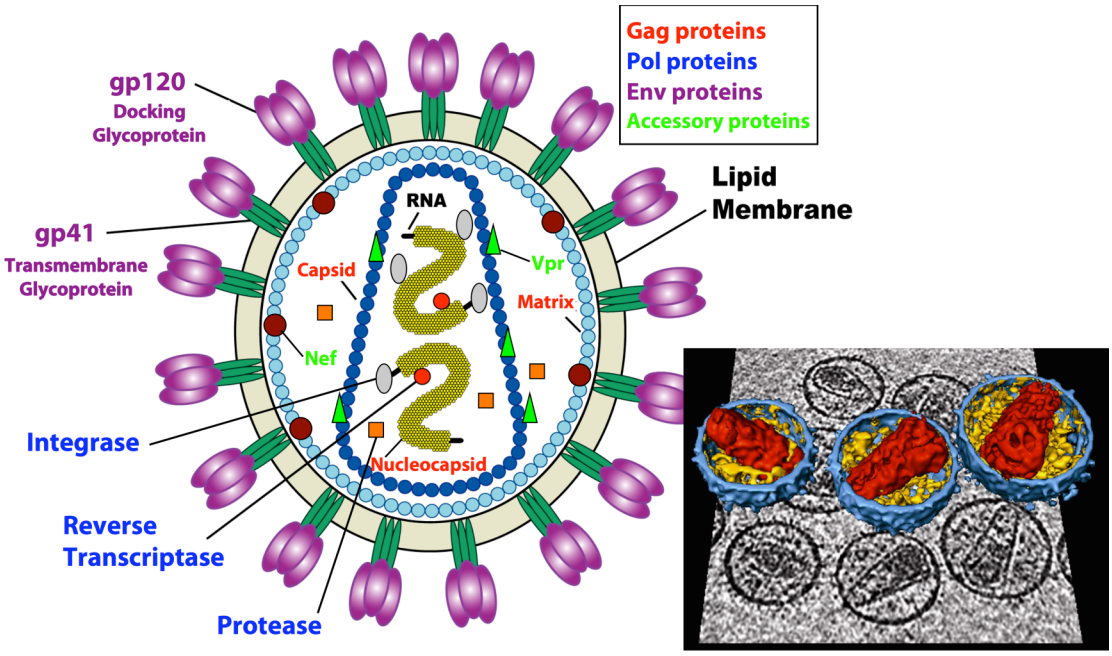

Figure 4. A model for the structure of a mature HIV virion. *(Adapted from NIAID image.)* **Inset: 3D reconstruction of authentic HIV virions from cryo-electron tomography.** *(Source: Briggs, et al. (2006))*

1.1.3 HIV replicative cycle

HIV follows a thorough step-by-step procedure consisting of two phases in order to reproduce. Every step and all of the components involved, either viral or from the host cell, are important (and in most cases essential) for HIV to maintain productive replication. A likely mode for HIV infection begins with the virus being presented to CD4+ T cells by macrophages or dendritic cells. The precise methods of cellular transmission *in vivo* have not been entirely determined, and likely depend on the route of transmission between individuals. What is more fully understood is what happens when the virion comes into contact with a susceptible CD4+ T cell. Cell entry can be achieved either by fusion or endocytosis, but fusion is required for productive infection to occur [12]. What follows is an explanation of each of the steps necessary for HIV to succeed at infecting a cell in order to replicate, and **Figure 5** illustrates HIV's replicative cycle.

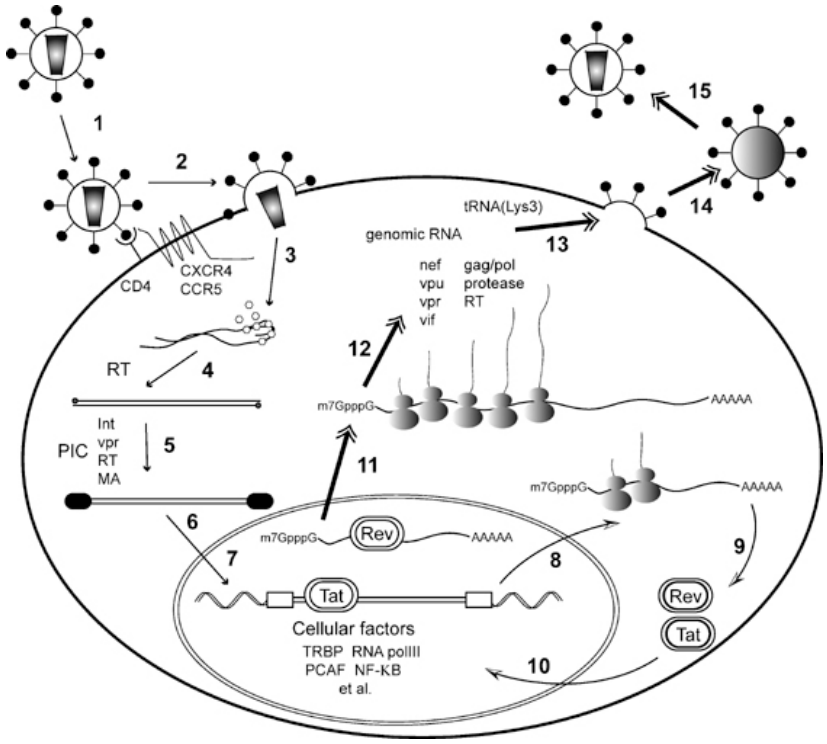

Figure 5. The replication cycle of HIV. Small arrowheads show fusion to integration. Curved arrows show early transcription of Tat and Rev. Double-headed arrows show late transcription to viral budding. *(Source: Scherer, et al. (2007))*

- **Fusion –** HIV fuses with the cell membrane upon association of the viral gp120 Env glycoprotein with the CD4 receptor and another chemokine coreceptor, primarily CCR5 for macrophage-tropic HIV strains (R5 viruses) or CXCR4 for T cell-tropic strains (X4 viruses) (**Figure 5, point 1**). Interaction of the gp120 with the target cell membrane receptor causes a conformational change in the viral protein exposing another viral glycoprotein, gp41, which brings the virus membrane close enough to the cell membrane for fusion to occur and the virus contents to enter the cell (**Figure 5, point 2**).
- **Retrotranscription –** After fusion and access to the interior of the cell is achieved, the virus undergoes uncoating of the particle's structural components (**Figure 5, point 3**), thus allowing retrotranscription of the viral RNA genome to take place. Retrotranscription is the process in which the single stranded RNA viral genetic material is retrotranscribed by the viral enzyme RT into double stranded DNA (**Figure 5, point 4**). Retrotranscriptase also contains an RNase H activity, which degrades the RNA template after the DNA strand has been synthesized.

- **Preintegration complex and nuclear import –** The viral DNA and several viral enzymes and structural and accessory proteins are packaged into a tight unit called the preintegration complex (PIC) (**Figure 5, point 5**). Formation of the PIC requires a great deal of compaction of the viral DNA [13]. The PIC travels along microtubules to reach the cell nucleus where it passes through a nuclear pore (**Figure 5, point 6**). The ability to gain access to the inside of the nucleus allows HIV to infect non-dividing cells such as resting T cells and terminally differentiated macrophages including microglia, in the brain. This is quite a feat considering nuclear pores are roughly half the diameter of the PIC. The mechanism for nuclear import is not entirely understood.
- **Integration –** Facilitated by the viral enzyme, IN, the virus genome undergoes genetic recombination with the cellular DNA and is inserted into a host chromosome (**Figure 5, point 7**). The end result of recombination determines the efficacy with which the virus replicates. Integration into a transcriptionally active region of the host DNA results in active viral replication, while it is likely that integration into heterochromatin where transcription is repressed results in latently infected cells. These latently infected cells contribute to the latent stage of HIV infection and the inability to completely eliminate the virus from the host even when the plasma VL remains at undetectable levels.
- **Transcription –** In transcriptionally active regions where HIV DNA has integrated, the HIV provirus is transcribed by the cell's transcription machinery to produce the RNA transcripts necessary for viral replication. Transcriptional efficiency depends highly on the viral proteins Tat and Rev. Tat is known to bind with elements of the cellular transcription machinery and enhance transcription of full length HIV transcripts. It does this by binding to the *trans*-activation response (TAR) RNA element, a sequence that forms the 5´- end of all HIV transcripts. Without Tat, only short incomplete transcripts are produced efficiently. Early on in the replicative cycle, short multiply spliced transcripts are produced and result in the expression of the viral proteins Tat, Rev and Nef (**Figure 5, points 8,9**). With the accumulation of Tat, partially spliced and full-length HIV transcripts can be transcribed more efficiently to produce the remaining viral proteins, including structural, enzymatic and the other accessory proteins (**Figure 5, point 10**). Rev is

essential for full-length transcripts to exit the nucleus (**Figure 5, point 11**) [14]. Insufficient levels of Tat and Rev may also contribute to viral latency, as new infectious virions are not produced in high numbers without the presence of these two proteins. When the threshold concentration of Tat and Rev is achieved, the second phase of viral replication, also called "late transcription", is initiated when the cell begins to manufacture new virions at a high level.

- **Assembly and Release –** With the transcription and translation of full-length viral transcripts into the Gag and Gag-Pol polyproteins accomplished (**Figure 5, point 12**), all the viral elements and two copies of the RNA genome assemble, under the direction of Gag, at the plasma membrane (**Figure 5, point 13**). Meanwhile, Env is translated from singly spliced transcripts in the ER and transferred via the cellular vesicular pathway to the plasma membrane. Via lateral movement, the Env glycoproteins migrate to the site of budding where all the elements to be incorporated into the nascent virion are assembled, and a new virion buds off from the cell surface (**Figure 5, point 14**).
- **Virion maturation –** The newly synthesized virion is still in an immature form, and the Gag and Gag-Pol polyproteins must be processed by protease for a mature viral particle to form (**Figure 5, point 15**). The cleavage of Gag into MA, CA, and NC initiates the formation of the conical shaped viral core around the RNA genome (see **Figure 4**) [11]. Protease also cleaves Pol into RT, IN, and PR. The resulting mature virion is now ready to infect a new CD4 expressing cell.

1.1.4 Cellular targets for HIV infection

As has already been mentioned, the primary target and breeding ground for HIV are CD4+ helper T lymphocytes and the lymphoid tissues where these cells are most concentrated, such as the thymus, lymph nodes, spleen, and other lymphoid organs [15]. Circulating T cells, dendritic cells, and macrophages are also infected by HIV. In addition to infection of cells by free HIV virions, another (and possibly more prominent) method of viral dissemination is via cell-to-cell interactions [16, 17]. This method is possibly involved in one of the proposed mechanisms by which HIV invades the central nervous system. Referred to as the "Trojan horse" hypothesis, HIV

infected monocytes enter the brain and infect astrocytes and other nervous system cells either through cell-to-cell contact or via the release of infectious virus after migrating from the blood stream across the blood-brain barrier (BBB). The other possible methods are (1) the crossing of the BBB by free virions either by migration between or via transcytosis through the endothelial cells of the barrier and (2) the release of HIV into the brain from infected BBB endothelial cells [18]. Many pathological manifestations arise, in part, because of the infection of nervous system cells including HIV-related encephalopathy and AIDS dementia complex [19, 20]. The ability of HIV to infect multiple cell types contributes to viral latency and the enormous difficulties of eradication. HIV infection of cells such as monocytes and dendritic cells cause less cytotoxicity in these cells than with helper T cells [21], resulting in a longer period for productive viral replication and a higher possibility of the virus at establishing latency. The cells that harbor integrated virus without undergoing apoptosis or being eliminated by the immune system offer a principle reason why cell transfection must be achieved for any potential therapy to be successful. Moreover, the identification and targeting of latently infected cells with novel therapeutics could potentially improve current therapy. Likewise, cell-to-cell transmission of HIV highlights the fact that reducing the viral load in circulation to below detectable levels is not sufficient to enact a cure, and that more specific antiretroviral activity at the cellular level is a necessity to address HIV infection.

1.1.5 HIV infection and the central nervous system (CNS)

HIV infection is often accompanied by neurological disorders and neuropathological abnormalities. It has been estimated that 20–30% of HIV-infected individuals eventually develop HIV associated dementia (HAD), and although the introduction of highly active antiretroviral therapy (HAART) has reduced its incidence, mild forms still persist [22]. In fact, in the HAART era, infected patients are living longer and the prevalence of HIV-associated neurological disturbances is actually rising [22-24]. In addition, HAD represents the leading cause of dementia in people under the age of 60. At present, an effective pharmacotherapy for HAD is not available. Previous approaches to cope with HAD reflect the challenging complexity inherent in the treatment of AIDS patients [25, 26]. Complicating the issue, the BBB separates the blood from the cerebral parenchyma and prevents the penetration of

drugs into the CNS. This physical barrier is characterized by tight intracellular junctions and the absence of fenestrations limiting permeability for therapeutic molecules such us the majority of the antiretrovirals. Therefore, in addition to antiretroviral treatments an additional option for therapy needs to be developed.

1.1.6 Solutions for HIV infection

Current treatment for HIV infection involves the use of multiple therapies in order to control the replication of the virus. The development of HAART has allowed HIV positive patients to survive much longer and live healthier, happier lives by means of diminishing VL and allowing the recovery of the immune system [27]. However, the complexity of this treatment causes many problems with administering it effectively. Most notably, its high cost and the need for the treatment to be thoroughly monitored by a health professional make its availability in underdeveloped countries very limited, precisely where the pandemic is most serious and treatment is most needed [2].

Despite significant advances in HIV infection treatment options, the virus still is a difficult target to contend with. At the molecular level, the low fidelity with which the virus replicates its genome, based on the retrotranscriptase's lack of proofreading, along with a high replication rate, cause a very high rate of mutation [28]. The net result, in addition to the existence of a wide spectrum of viral isolates, is that the virus can very easily generate resistances to drugs or escape mutants when a drug regimen is improperly interrupted [29]. This causes the need for changes or increases in the drug regimen resulting in higher secondary effects, another main concern with current HIV treatment [2]. HAART, or treatment consisting of a combination of several classes of antiretroviral drugs, is generally administered to try and prevent the emergence of drug resistant viral strains. However, in low- and middle-income countries, where not all antiretroviral drugs are available, the options for drug combinations are limited.

One of the main reasons that there is no cure for HIV infection despite over twenty-five years of research is the inability to address viral latency in HIV infection. HIV does not simply infect immune system cells, use the cell machinery for its own replication, and then kill the cell. It is also capable of infecting certain cells and remaining inactive inside them for large periods of time before resurfacing later to

cause as much damage to the immune system as the initial infection [12, 30]. Viral latency prevents the complete eradication of the virus, because despite the efficacy of therapy at reducing HIV replication and achieving an undetectable plasma viral load, there appears to remain pools of latently infected cells, which reinitiate viral production when activated. Therefore, treatment can never be entirely discontinued.

In the absence of a cure or vaccine for HIV infection, antiretroviral drugs have become the best method of addressing the HIV/AIDS epidemic. The first antiretroviral drugs were approved for use in the mid 1990s. HIV antiretrovirals fall into five categories: nucleoside or nucleotide reverse transcriptase inhibitors, non-nucleoside reverse transcriptase inhibitors, protease inhibitors, integrase inhibitors, and entry inhibitors [31]. These drugs manage to reduce viral replication by inhibiting the viral processes necessary for replication through the use of molecules that function by binding the viral or host proteins involved and inactivating them or by mimicking the substrate of the enzymatic reactions. In just over ten years since the use of these drugs was initiated, antiretroviral therapy has had an immense impact on the outlook of this disease. **Figure 6** shows how the estimated number of deaths globally has been affected in part by increased access to antiretroviral medication in developing countries [2].

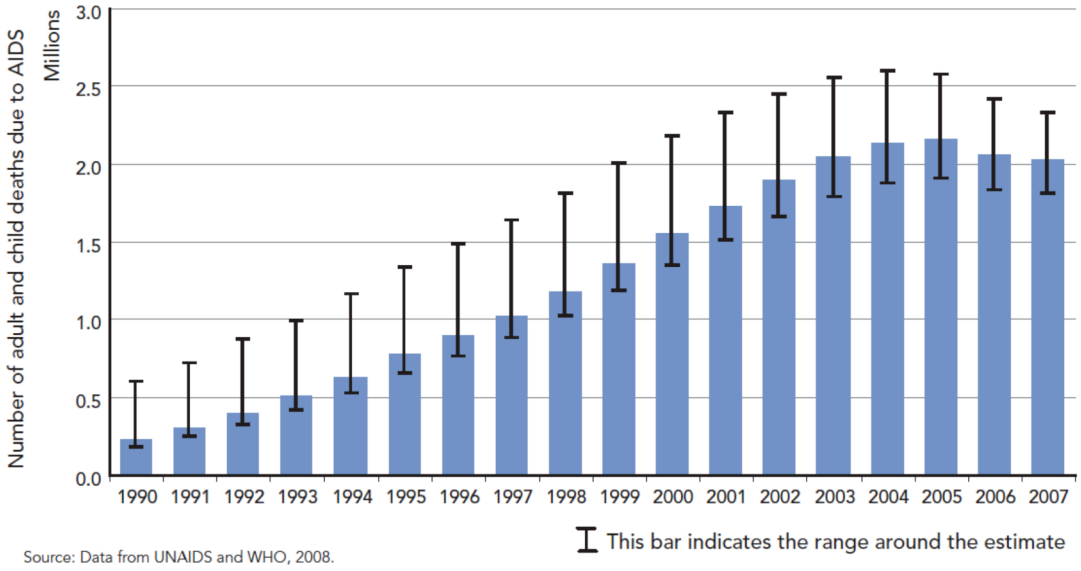

Figure 6. Estimated number of adult and child deaths due to AIDS globally, 1990-2007.

Despite these advances, the HIV/AIDS pandemic will not be eradicated without substantial new developments and innovation. HAART treatment has made an immense impact on fighting the disease, but it still possesses major drawbacks such as the necessity of maintaining greater than 95% adherence for it to be effective and the fact that it is a life-long therapy. Additional problems with drug cost and availability, treatment side effects, the emergence of drug resistance, the wide array of viral isolates, high mutability of the virus, and coinfections with other diseases such as tuberculosis or hepatitis, among many other issues, demand that research into addressing HIV infection be continued and further expanded with the objective of making new discoveries and improving current therapies.

1.2 Gene Therapy and RNA interference

The concept of altering the function, expression or translation of abnormal or disease causing genes has led to the development of such techniques as gene therapy and RNA interference (RNAi). Gene therapy deals with the introduction of genetic material (RNA or DNA) into target cells that encodes a protein that is missing or defective in order to achieve therapeutic objectives. Since it was first developed in the seventies, eighties and nineties, gene therapy has gone through major advances and tragic setbacks. However, possibly its most outstanding impact on biology and medicine was the introduction of the concept that disorders can be addressed by attacking them at their foundation, at the level of genes. The success of this idea has led to further developments in modifying specific gene functions through transcriptional, post-transcriptional or translational regulation such as antisense oligonucleotides, ribozymes and RNAi.

RNAi is an innate defense response to the introduction of double-stranded RNA into cells resulting in a sequence-specific downregulation of genes with the same or similar sequences to the introduced RNA. Andrew Fire, Craig Mello and colleagues first discovered RNAi in *Caenorhabditis elegans* in 1998 [32] for which the pair received the Nobel Prize in 2006. In the eleven years since that discovery, there has been a steady increase in research dedicated to RNAi and the utilization of RNAi to silence genes as can be seen in **Figure 7**. Both the total number of articles dealing with gene therapy or RNAi and the percentage of this topic dedicated to

RNAi have steadily increased. In 2008, 70% of the nearly 8000 articles on this topic indexed in Pubmed mentioned RNAi in the title or abstract.

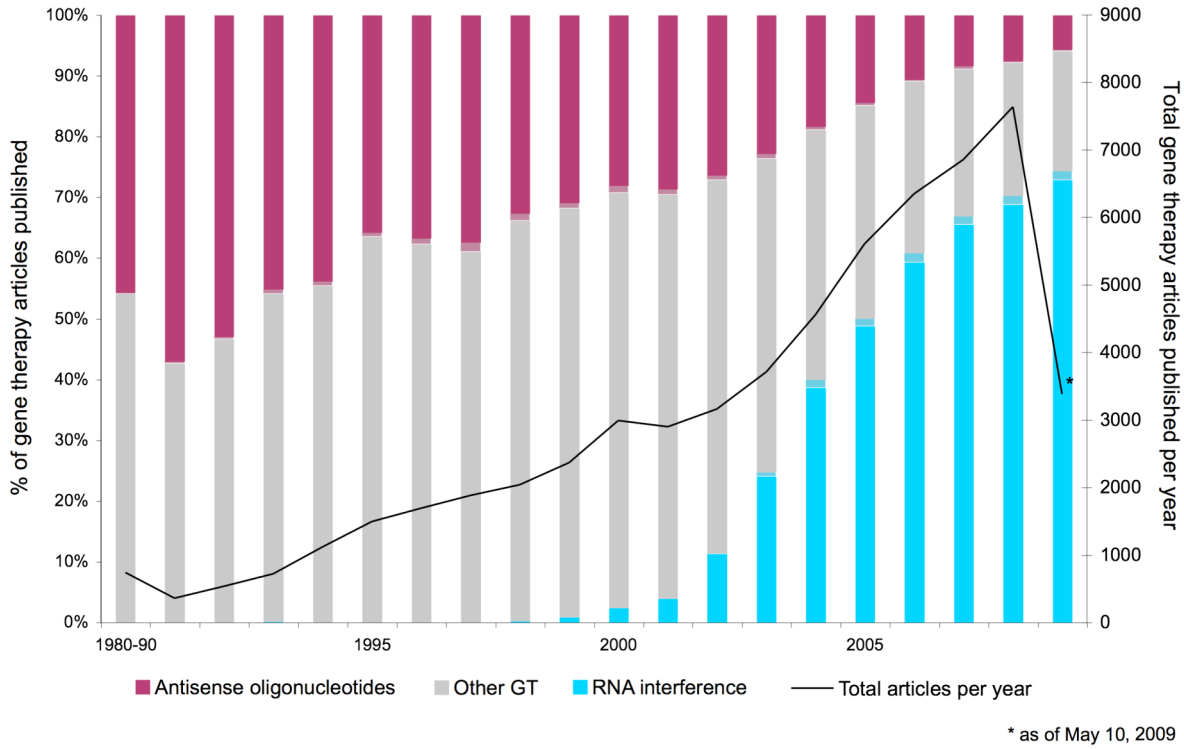

Figure 7. Gene therapy articles indexed in Pubmed. A steady increase in both total number of gene therapy (GT) articles and articles dedicated to RNAi.

1.2.1 Mechanism of RNA interference

The mechanism behind RNAi consists of several parts. First, upon the introduction of a double-stranded RNA (dsRNA) into the cell, a cellular protein termed Dicer recognizes the foreign element and cleaves it into short double-stranded RNA segments of between nineteen and twenty-three base pairs. These short segments have been termed small interfering RNA (siRNA). Second, the siRNA are incorporated into a large protein complex called the RNA inducing silencing complex, or RISC, which separates the strands and uses the antisense strand as a template to recognize complementary mRNA via Watson-Crick base pairing and degrade them. Thus, gene transcripts are downregulated post-transcriptionally but prior to translation. In this way, the RNAi mechanism effectively silences the

production of genes from exogenous RNA invaders in a sequence-specific manner (**Figure 8**) [33].

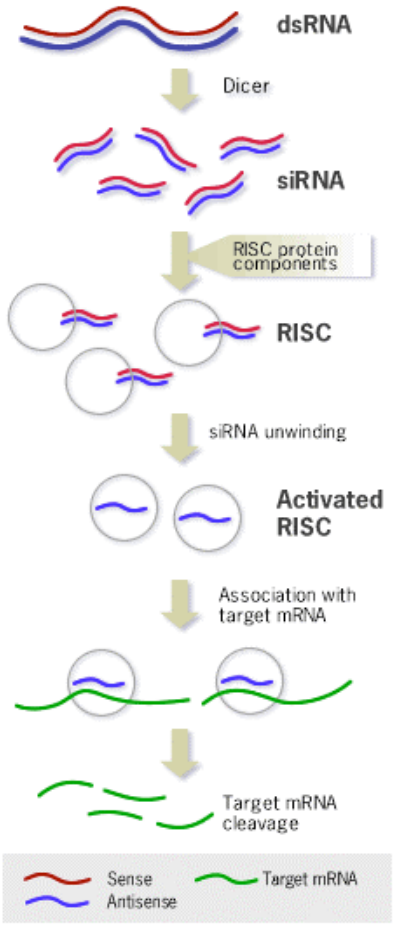

Figure 8. Mechanism for gene silencing by RNAi. *(Source: www.5ibio.com/html/RNA/RNAi/20061111/1427.html)*

The RNAi mechanism pathway can be initiated with either long double-stranded RNA or by skipping the cleaving step performed by Dicer and directly introducing siRNA into the cell cytoplasm. In this way, the RNAi mechanism can be hijacked, and a gene can be targeted for downregulation by designing and transfecting the cell with siRNA possessing a complementary sequence to the target mRNA. One of the benefits of skipping the step involving Dicer is that the introduction of large dsRNA induces an innate immune interferon response in mammals which is avoided with treatments of the smaller siRNA [34]. In-depth studies have determined the size and structure of the siRNA products of Dicer digestion in great detail, and their design

and synthesis have been optimized in order to achieve the highest efficiency in gene silencing. The general structure of siRNA consists of two complementary RNA strands 21 nucleotides long. The two RNA strands form complementary base-pair interactions in such a way that on each strand only the first 19 nucleotides (from 5′ to 3′) bind with the first 19 nucleotides of the other strand leaving an overhang of two nucleotides on each 3′ end (**Figure 9**). The two nucleotide overhangs on each end come about as a result of the way Dicer cleaves the longer dsRNA, and they function to identify the siRNA for incorporation into the RISC complex to act as the template for target mRNA recognition [35].

Figure 9. In this example of a typical siRNA, base-pairs form between the "core" 19 nucleotides of the two strands leaving an overhang of two nucleotides on each end of the siRNA. In this case the overhangs consist of two deoxynucleotides (thymine) instead of ribonucleotides to improve stability and resistance to nucleases. *(Source: www.invitrogen.com)*

1.2.2 Other utilizations of the RNAi mechanism

Several other regulators of gene expression such as micro RNAs (miRNA) and small hairpin RNAs (shRNA) also utilize the RNAi mechanism to downregulate specific genes. It has been discovered that miRNAs are endogenous short auto-complementary RNA strands that buckle in on themselves to form stem-loop structures, are processed by Dicer in the same way as dsRNA, and function as naturally occurring gene regulators by targeting specific mRNA transcripts and inhibiting their translation [36]. It seems that miRNA are naturally encoded and expressed in the genome of most animals and plants, and they function as one of the many tools cells have for regulating gene expression. Similarities and differences between miRNA and siRNA are constantly being found leading to a further understanding of the RNAi mechanism and ways to take advantage of it for therapeutic objectives. shRNA is a powerful laboratory tool to specifically target genes for downregulation that differs from siRNA in that instead of transfecting siRNA, plasmids expressing small hairpin transcripts are transfected into the target cells [37]. The shRNA transcripts form miRNA-like stem-loop structures and are

incorporated into the RNAi pathway in the same way. Transfection of shRNA expressing plasmids results in longer-lasting gene silencing activity due to the constant recycling of active siRNA via transcription of the transfected plasmid. However, achieving transfection of the larger plasmid into the target cells is more challenging than the smaller siRNA.

1.2.3 Applications of RNA interference

In only just over a decade of research on RNAi, a great deal of achievements has already been made in this area. Thus far, the primary use of RNAi has been as a tool for the identification of genes. The sequencing of the human genome has allowed researchers to identify previously unknown genes. However, in many cases, only the gene sequence is known without any knowledge of the function of the coded protein. By very effectively targeting and silencing a gene of any sequence, RNAi is being utilized as a rapid and highly specific method for testing loss-of-function phenotypes [38, 39]. The ability to knockdown a specific gene in such a simple way is a huge advancement from previous laboratory methods of gene regulation such as other forms of gene therapy or transgenic models. Molecular biologists are beginning to utilize this technique for a myriad of other objectives. In addition to testing individual gene function, whole siRNA libraries have been developed including genome-wide screens that can test the involvement of any of the approximately twenty-one thousand human genes in everything from hereditary diseases and oncogenesis to viral infection.

However, RNAi is not only a powerful laboratory tool. Research in siRNA and shRNA as therapeutics is constantly expanding. A huge array of medical afflictions such as genetic disorders, cancers, neurodegenerative disorders, and infectious diseases such as HIV and hepatitis are being addressed by applying RNAi research to human cells *in vitro*. Considering the great achievements reached and the tremendous potential of RNAi, it is not surprising that *in vivo* studies were initiated very soon after its initial discovery. Much like the difficulties encountered in transfecting target cells with siRNA *in vitro*, systemic application of siRNA *in vivo* must overcome many hurdles before this technique can be utilized in designing new therapies. The primary obstacles for siRNA are degradation by nucleases in the blood stream and achieving localized targeting. The first *in vivo* studies with RNAi either

involved localized administration or targeting tissues in the liver or spleen where systemically administered siRNA is more readily taken up. To address stability of siRNA in the blood stream, methods for achieving cell transfection have also needed to serve double as protective agents as well as drug delivery vehicles (covered further in section **1.3 Drug Delivery**).

Gene therapy took a tremendous hit in 2003 when one of the initial clinical trials involving gene transfer resulted in leukemia in five out of twenty subjects including one death [40-42], despite successfully abating a genetic disorder called X-linked severe combined immunodeficiency. It turned out that the retroviral delivery agent that was used to achieve transfection and integration of the induced gene into the target hematopoietic stem cells caused the activation of an oncogene promoter resulting in the leukemia. Following this episode, many clinical trials with gene therapy were put on hold and a greater effort was put on optimizing the method of delivery and transfection with an emphasis on research into non-viral vectors. Despite the difficulties encountered with extending gene therapy to clinical trials, several so-far-successful clinical trials with RNAi are currently being carried out (**Table 1**).

Table 1. RNAi in clinical trials.

Company	Disease	Product	Status
Allergan	AMD	Sirna-27/AGN211745	phase II
Quark Pharma.	AMD	RTP801i-14	phase II
Opko Health	AMD	Bevasiranib	phase III
Benitec/City of Hope	HIV/AIDS	Lentivirus vector	phase I
Nucleonics Inc.	HBV	NUC B1000	phase I
Alnylam Pharma.	RSV	ALN-RSV-01	phase II
Senetek PLC	glioblastoma multiforme	ATN-RNA	phase I
Calando Pharma.	ovarian cancer	CALAA-01	phase II
Quark Pharma.	acute renal failure	AKli-5 (I5NP)	phase I/II
TransDerm Inc.	pachyonychia congenita	TD101	phase Ib
Santaris Pharma.	HCV	SPC3649	phase I

Based on Refs. [34, 43, 44]

1.2.4 Targeting HIV with RNA interference

Very early on in the development of RNAi as a gene silencing technique, studies were started with the idea of utilizing this technique to treat or prevent HIV infection. Initial experiments showed that siRNA and shRNA could successfully inhibit HIV replication *in vitro* in either cell lines or primary lymphocytes by

targeting viral RNA sequences [45-48]. **Figure 10** shows the HIV genes that have been targeted by RNAi, which have achieved varying levels of success at reducing viral replication. The fact that the HIV genome is transcribed in its entirety in order to produce the viral structural and enzymatic proteins [49] means that siRNA targeted to any region of the HIV genome will result in a downregulation of all viral products not only the gene that is specifically targeted [50]. Further studies revealed that when undergoing longer periods of treatment with siRNA or shRNA, HIV was able to mutate in order to avoid pressure from RNAi and escape treatment even when RNAi was targeted a highly conserved region of the HIV genome [45]. Even more interestingly, the virus was found to be able to mutate in a way that the secondary structure of its RNA transcripts changed so that the sequence targeted by RNAi was occluded from access by the RISC complex [51]. As had been the case with so many other anti-HIV therapies, it seemed that this new technique would not be immune to viral drug resistance. In any case, much has been achieved by attempting to utilize RNAi for the inhibition of HIV including targeting cellular factors necessary for viral replication such as CCR5 [46, 52, 53], *in vivo* studies with antibody-delivered anti-HIV siRNA to human immune system cells transplanted into immunodeficient mice [54], and several clinical trials in HIV-infected patients [43]. These accomplishments have been made despite (and by always keeping in mind) the multiple difficulties that must be solved like delivery, transfection, siRNA degradation, and viral escape.

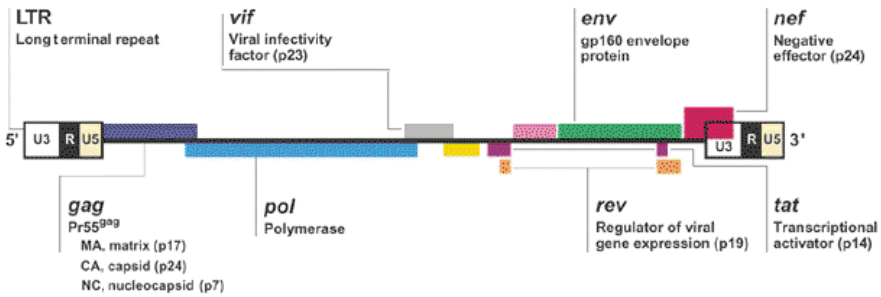

Figure 10. HIV genes successfully targeted by RNAi:
5´LTR (Refs. [45, 55, 56]); *gag* [57-59]; *pol* [58, 59]; *vif* [60-62]; *tat* [55, 61, 63, 64]; *rev* [63-65]; *env* [65, 66]; *nef* [62, 67]. *(Image from Greene, et al. (2002))*

1.2.5 Problems that face RNA interference

Despite the enormous possibilities of RNAi, there still exist many problems that need to be addressed. As previously mentioned, obstacles in delivery, target cell transfection, stability/degradation, transient activity, secondary effects, toxicity caused by delivery vector, and resistance all hinder the path of carrying out *in vivo* experiments with RNAi and further developing RNAi as a new therapy for clinical use. As will be described in the next section, a great deal of these issues can be addressed by using the correct delivery vector. Because of this, a great deal of research is being put into finding a suitable partner and chauffeur for these valuable small nucleic acid molecules. The ideal delivery agent should protect the siRNA from degradation, transport it to the target cells or tissues, facilitate its transfection into the cytoplasm of the cells and all the while remain fairly innocuous and cause little or no adverse effects.

1.3 Drug Delivery

As has already been mentioned, the main limiting problems with developing gene therapy and RNAi into pharmaceuticals are their ineffectiveness *in vivo* and the difficulties in converting them into clinical therapies. Although some success has been achieved by localized delivery to such areas as the eye, skin, or local tumors [68-72], systemic RNAi therapy still faces many issues [34]. These problems arise from the difficulty of directing the plasmids or oligonucleotides to target cells or tissues and then being able to successfully transfect them into the cell [73-75] where they can exert an effect. *In vivo*, free oligonucleotides are rapidly filtered from the blood by the kidneys or are processed by the reticulo-endothelial system and delivered to the liver and spleen [43]. This causes problems if the target cells are located in other regions of the organism. Furthermore, oligonucleotides, siRNA and plasmids are very unstable once in circulation because of the presence of nucleases and serum proteins in the bloodstream which sequester and degrade these potential therapeutic agents. The area of study dedicated to addressing these problems is termed “drug delivery”. Despite the existence of several methods that allow successful transfection of cells with oligonucleotides *in vitro*, transferring these methods to *in vivo* studies is often unfeasible.

1.3.1 Physiological obstacles to systemic RNAi therapy.

There exist numerous problems with applying systemic RNAi therapy *in vivo* (**Figure 11**). Aside from the stability, degradation and filtration issues in the bloodstream (**Figure 11a**), there are several other barriers that must be overcome if the delivery system can achieve stability in circulation. Crossing the vascular endothelial barrier presents a problem for most delivery systems (**Figure 11b**). This is especially true in the CNS where difficulties in crossing the BBB with small molecule pharmaceuticals are widely recognized. It is believed that particles with diameters greater than 5 nm do not readily cross the vascular endothelial barrier. Some organs including the liver, spleen, lungs, and kidneys can be reached with larger molecules due to accumulation in the reticulo-endothelial system, which is a method of eliminating foreign particles from circulation. Likewise, some tumors can be accessed with larger molecules because of increased vasculature permeability in tumors referred to as the enhanced permeability and retention effect [34]. However, for diseases involving leukocytes or other parts of the immune system, obtaining stable circulation in the bloodstream may be sufficient to reach all the cells affected by the disease. HIV infection and other immunological disorders fall under this category. Although, the extent to which the virus may infect other non-immune system cells such as neuronal cells [76] and establish regions of latently infected cells that do not circulate throughout the blood stream is still under investigation. Once across the endothelial barrier, the extracellular matrix poses a myriad of obstacles like polysaccharides and fibrous proteins that hinder the progression of the treatment on their path to the target cells (**Figure 11c**).

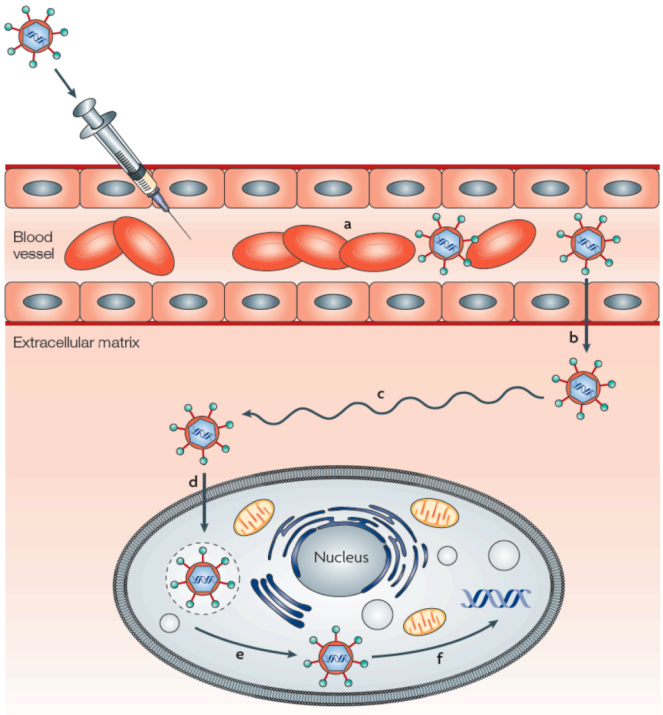

Figure 11. Physiological Barriers to the systemic delivery of siRNA vectors. A systemic delivery system confronts numerous obstacles in reaching its objective: a) filtration, degradation and phagocytosis in the blood stream; b) crossing the endothelial barrier; c) transversing the extracellular matrix to the target cell; d) cell transfection; e) endosomal escape: f) delivery of siRNA to cell cytoplasm. *(Source: Whitehead, et al. (2009))*

Whether the target cells must be reached by crossing the endothelial membrane and penetrating the thick forest of the extracellular matrix or are reached from within the blood stream, the barrier of crossing the cell membrane and gaining access to the interior of the cell is the next obstacle that must be overcome (**Figure 11d**). Indeed, cell transfection/uptake is one of the principle topics in which research in drug delivery is dedicated [77]. The methods by which particles are taken up are receptor mediated endocytosis and membrane fusion [78]. Viral vectors utilize the viruses' evolutionarily developed methods for evading obstacles and gaining entrance to the cell interior. Many of these vectors utilize cell membrane receptors to facilitate fusion with the membrane, which allows for the deposit of their genetic payload to the interior of the cell. Non-viral vectors face greater challenges in achieving entry into the cell. Non-targeted vectors are believed to interact with the cell membrane via electrostatic interactions that facilitate endocytosis. Targeted vectors utilize ligands that are recognized by cell membrane receptors and their association initiates endocytosis [79]. Endocytosis of delivery vehicles results in their localization into

endosomal vesicles from which the delivery system must achieve escape (**Figure 11e**). If all these obstacles can be overcome, the final step to be completed is the release of the intact and functional DNA or siRNA so that it can exert its effect (**Figure 11f**). In the case of plasmid DNA delivery for gene therapy, the additional problem of achieving access to the cell nucleus must be addressed.

1.3.2 Methods for transfection *in vitro*.

As mentioned in the previous sections, in order to achieve any silencing effect with RNAi, the siRNA or shRNA expressing plasmids must overcome the obstacle course of hurdles and reach the interior of the cell. It has generally been accepted that the cellular uptake of free oligonucleotides does not readily occur for most cell types *in vitro*. Our experiences have indicated otherwise for lymphocytic and astrocytic cell lines and primary lymphocytes [80]. Notwithstanding, the majority of research that utilizes RNAi depends on a delivery vector of some kind. Drug delivery vectors can be divided into two different categories. Viral vectors are chiefly used to transport and deliver genes, while non-viral vectors are the method of choice for smaller oligonucleotides such as siRNA.

1.3.3 Viral Vectors

Viruses possess a highly evolved method of hijacking cells and depositing their genetic material into the cell interior in order to utilize the cellular machinery for reproduction. This capability has been taken advantage of by scientists attempting to insert therapeutic genes in the place of the viral genetic material [81]. By removing the viral genome or removing essential viral genes from the viral particles, the altered virus loses its virulence and functions only as an innocuous transporter of the drug. In this way, researchers can achieve very specific delivery to the cells of interest with very high transfection efficiency. More highly developed retroviral vectors utilize not only the structural components of the virus but also the enzymes used by the virus to transcribe its genome from RNA into DNA, direct it into the nucleus, and insert it into the DNA of the host cell (**Figure 12**). These vectors are highly useful for integrating genes into cells so that they are repeatedly transcribed and thus can achieve an intransient effect. Despite the advances in molecular biology that allow the creation of these theoretically innocuous vectors, there still are many problems surrounding their

use in patients. Many viral vectors are immunogenic and have issues with stability. Many can only infect dividing cells. Causing even more worry, retroviral vectors can insert the therapeutic genes into regions of the genome that can cause undesired gene activation. This was the case in the clinical trail that used gene therapy to treat SCID-X1 children in which five of the twenty subjects developed leukemia [40-42]. In the end, these vectors have been derived from highly virulent pathogens and they still possess many of their disease causing attributes, and there exists a great amount of public uncertainty to the use of this technology since there always exists the risk of contamination with replication competent viruses.

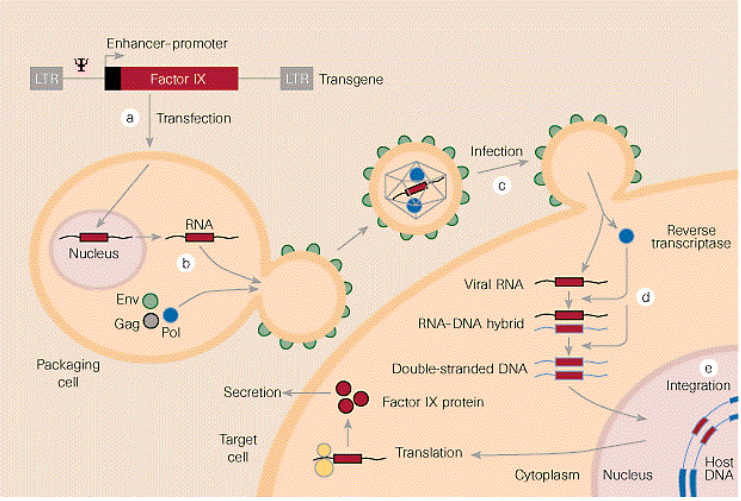

Figure 12. Retroviral vectors exploit the life cycle components of their naturally occurring counterparts to introduce a transgene into target cells (in this case Factor IX). *(Source: Verma et al. (1997))*

1.3.4 Non-viral Vectors

In many cases, viral vectors are not a feasible option, and fortunately, there exist many kinds of non-viral vectors that can function just as well as viral vectors. Non-viral vectors can be based on lipids, peptides, polymers, nanoparticles or a combination of more than one of these (**Figure 13**). Lipid-based vectors are referred to as liposomes and are comprised of the same phospholipid molecules as cell membranes. They are taken up by cells via endocytosis and release their payload into the cell interior when the lipoplex phospholipids are rearranged from interactions with the phospholipids of the cell membrane in the endosomes [82]. The disadvantages of this type of vector are problems with stability, particle uniformity, incapability of

targeted delivery, and rapid clearance from circulation due to uptake. Peptide-based vectors link small peptides with oligonucleotides either via covalent bonds or electrostatic interactions between basic amino acid residues and the negatively charged oligonucleotide backbone. The peptides can be designed to specifically target certain cell types or to facilitate cell uptake. Cell-penetrating peptides are one example of this type of delivery vehicle. They are able to translocate the cell membrane and escort their cargo into the cell [83]. Translocation of the cell occurs by direct membrane penetration, endocytosis, or via the formation of a transitory structure.

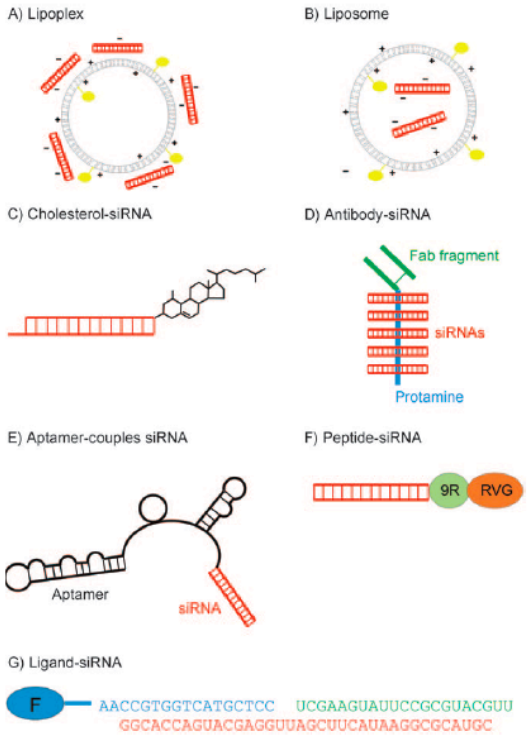

Figure 13. Examples of non-viral delivery vectors for siRNA. *(Source: Kurreck (2009))*

Polymer-based delivery systems utilize cationic polymers to bind DNA or other oligonucleotides. In addition to forming complexes with the DNA, many polymers are capable of condensing it down to a size that makes cell transfection possible (~100 nm) [84] (**Figure 14**). The DNA is condensed in a method similar to the way that histones and other nuclear proteins cause DNA to form supercoiled chromatin [85] (at a compaction ratio of as much as 1000-fold in interphase). The benefits of using polymers are a great deal of flexibility in structural design, the possibility of attaching functional groups to the polymers, DNA condensing

capability, and the relative ease of polymer synthesis and handling compared to viral vectors which require the use of recombinant technology and involve the dangers inherent with working with attenuated viruses. Polymers also generally do not produce the same immune response as viral vectors, so they are better adapted for *in vivo* experiments.

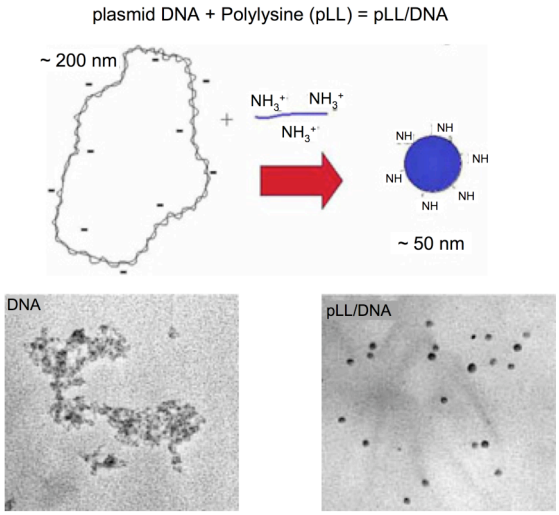

Figure 14. The polycation polylysine is capable of condensing DNA to a size that is more suitable for cellular uptake. *(Source: Gene Delivery Group, University of Oxford Dept. of Clin. Pharmacology)*

The possibility of utilizing functional groups attached to the polymers can accomplish many different objectives. For example, targeting moieties or targeting peptides can function to direct the polymer vector to very specific cell receptors and therefore specific cells or tissues. As was commented before, receptor-mediated endocytosis results in the compartmentalization of the polyplexes into endosomes and eventually lysosomes where degradation of the polyplex will occur. Therefore, endosomal escape is a necessity for the DNA or siRNA to reach the cytoplasm. This can be accomplished via the use of endosomalytic features such as the attachment of fusogenic peptides. Some polycations such as polyethyleneimine (PEI) possess tertiary and secondary amine nitrogens that allow the polymer to become further protonated when in a lower pH environment such as that which exists inside endosomes. This additional protonation of the polycations, a characteristic that has been designated the "proton sponge" effect, is thought to cause swelling and eventual rupture of the endosomal membrane [86]. Nuclear localization signal peptides can potentially give the polymers access to the nucleus so that their cargo plasmid DNA

can be expressed by the cellular transcription machinery [87]. Also, hydrophilic shielding moieties such as poly(ethylene glycol) (PEG) can be attached to polymers to increase the time in circulation by increasing their biocompatibility and resistance to uptake by the reticulo-endothelial system and clearance from the blood stream [88]. These shielding attachments can also protect DNA or siRNA from degradation by serum nucleases as they reduce the interactions of the polyplex with blood components. Shielding moieties are grafted to polymers in several different ways, and research into the effect that number, size and length of PEG shielding moieties have on the overall biocompatibility of the polymers has revealed much about these groups [89]. This work will expand on that research as results with polymers possessing PEG moieties of different sizes and numbers will be reported here.

1.3.5 Nanoparticles

The constantly evolving field of research referred to as nanotechnology offers other methods for drug delivery. Nanoparticles (referring to particles with a diameter from 1 to 100 nm [90]) are being developed to function as drug delivery vehicles including transporters of DNA and oligonucleotides. Nanoparticles used for drug delivery share many of the same characteristics as polymers, but have a more highly specialized design and synthesis. Dendrimers, for example, are nanoparticles derived from polymer synthesis technology, but possess specific attributes such as monodispersity and symmetry (**Figure 15**). Like polymers, most nanoparticles used in drug delivery contain cationic groups that can bind oligonucleotides via electrostatic interactions. Due to their small size, nanoparticles can facilitate the uptake of DNA or oligonucleotides by cells by 1) condensing the nucleic acids considerably in size, and 2) possessing the size necessary to be taken up by endocytosis. Some nanoparticles such as gold- or silica-based nanoparticles have obtained results in DNA transfection, but their entry depends on the use of other cell transfection methods like polymer or liposomal transfectants or through the use of a particle accelerator gun. Carbon nanotubes have shown positive results in delivering DNA to cell lines *in vitro* [91, 92] and siRNA into myeloid, dendritic and cancer cells *in vivo* [93, 94]. However, the most highly utilized type of nanoparticle for gene therapy applications is dendrimers.

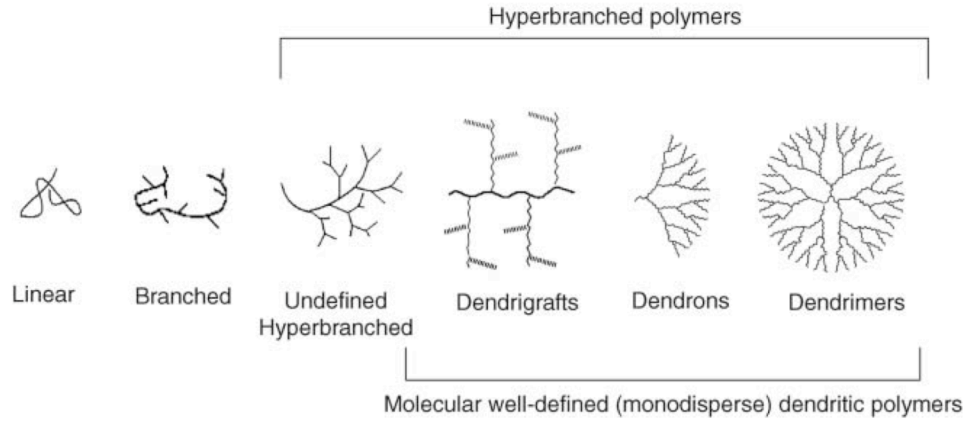

Polymers to dendritic structures.

Figure 15. Polymers to dendritic structures. Molecular synthesis technology can be applied to polymer science to improve structure and function of different drug delivery vehicles. *(Source: Boas, et al. (2006))*

1.3.6 Dendrimers

Dendrimers are defined as nanoscopic, monodisperse, polybranched, synthetic polymers [95]. The term "dendrimer" comes from the Greek "*dendros*" for tree because of the tree-like or branching nature of the dendrimer structure. Due to a diameter size of from 1.5 to 15 nm [96], dendrimers are considered to be nanoscopic. Dendrimers are synthesized under highly controlled conditions so that the product is as close to completely monodisperse as possible. This characteristic comes from a system of synthesis in which many steps are followed to gradually create a uniform structure and all of the dendrimer molecules have the exact same structure. The reason for creating nanoparticles with such a specific structure is for the functionality that arises because of that structure. As in the case with proteins, the macromolecules that dendrimers were largely designed to imitate, structure determines function. The highly systematic synthesis allows for a great deal of control in size, shape and terminal group functionality [97, 98]. Dendrimers are synthesized by two different methods [99]. One method of synthesis called "divergent synthesis" generates the molecule from the core outwards, while the other, "convergent synthesis", initially starts with the external functional groups and generates the dendrimer by joining the external branches together and working from the outside in.

The dendrimer structure can be divided into three different parts:

1. a central core from which the arms extend outward that contains a microenvironment protected by the external structural components,

2. multiple branching arms that radiate out from the central core whose structure, length and number can all be altered depending on the desired size and functionality, and
3. external functional groups located at the periphery of the branches and, therefore, on the molecular surface. These groups generally provide the primary functionality of the dendrimer.

Similarly, the dendrimer structure can be viewed as having layers, or "generations". The number of generations that a particular dendrimer has depends on the number of branching or focal points that exist in the branching arms as they extend outward from the core **(**Figure 16**)** [100]. Since at each focal point, the number of arms extending outwards increases by at least a multiple of two, the higher the generation, the greater the number of functional groups at the extremities. For a typical dendrimer that doubles the number of exterior branches at each focal point, a fourth generation dendrimer would possess thirty-two functional groups at the periphery.

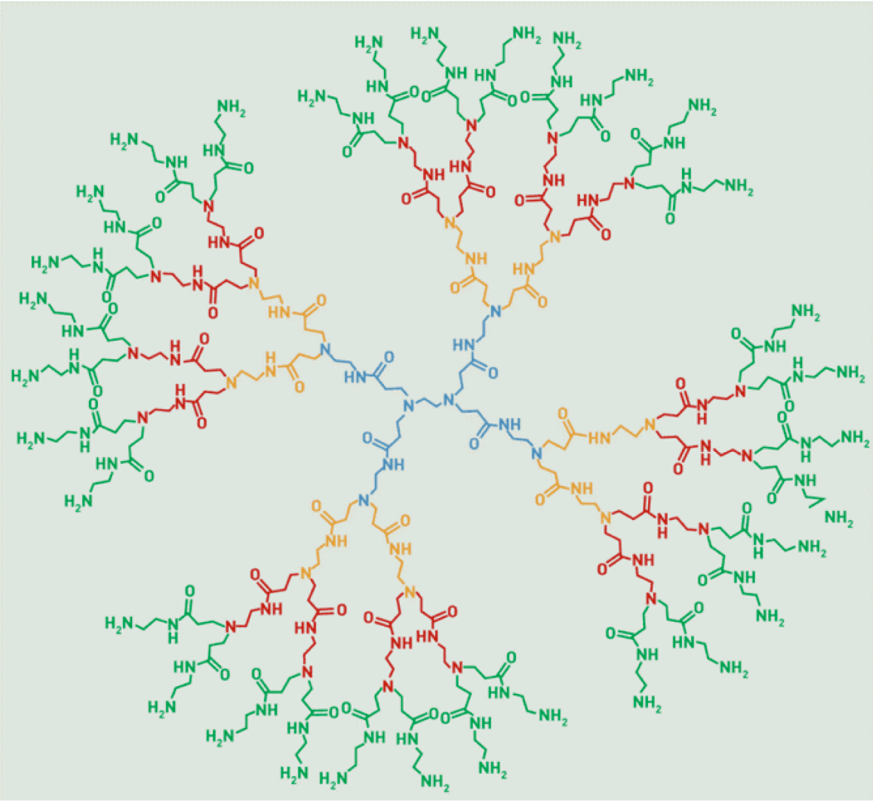

Figure 16. In this fourth generation polyamidoamine (PAMAM) dendrimer, the core and first generation are shown in blue, and each successive generation is shown in a different color. *(Source: Castriciano, et al. (2008))*

Monodispersity refers to the homogeneity in which the dendrimers are synthesized (i.e., all dendrimer molecules are made with the same structure, generation, and amount of branching). The branching structure of dendrimers allows them to possess multiple functional groups on the branch extremities all radiating out from a central core [101]. A primary advantage of dendrimers is the flexibility in which they can be generated. This allows for a wide variety of functional groups to be located along the branches as well as at the far extremities. The structure of the molecule depends entirely on the function it is designed to carry out. Internal pockets near the core of the dendrimer can provide microenvironments to contain and protect small molecules [99]. In other cases, external charged groups function to tightly bind oppositely charged molecules such as DNA or oligonucleotides via electrostatic interactions. The amine-terminated carbosilane dendrimers used in this study possess external amines, which have been quaternized to attach an additional methyl group to each amine nitrogen. This alkyl substituent occupies the nitrogen's lone electron pair in a covalent bond resulting in a positive charge for the amine. This net positive charge located at the periphery of the dendrimer allows it to bind the negatively charged phosphate groups of the DNA or RNA backbone.

The size of dendrimers depends on the structure and, in particular, the number of generations that the dendrimers possess. Dendrimers range in size from around 1.5 nm to 15 nm in diameter. This size range categorizes dendrimers as nanoparticles and allows them to imitate proteins in terms of their interactions with small molecules or other macromolecules [102]. **Figure 17** shows how dendrimers can approximate protein structures and other bioassemblies in size. This characteristic is essential for these synthetic molecules to achieve functions based on biological interactions. Such functions include imaging probes, vaccine adjuvants, and the encapsulation, delivery and/or controlled release of pharmaceuticals [103-105].

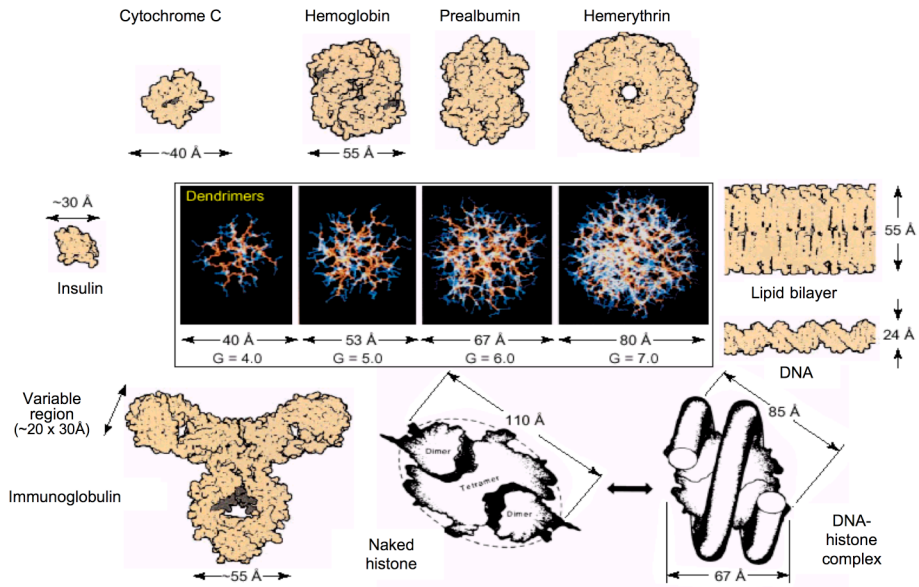

Figure 17. Dimensionally scaled comparison of PAMAM dendrimers of several different generations with proteins and other bioassemblies. *(Source: Esfand, et al. (2001))*

In addition to their size, dendrimers benefit from their unique structural characteristics in order to function as biologically useful molecules. As with a tree, which optimizes the quantity of solar light it can harvest and the amount of moisture in the soil it can absorb through the use of dendritic architecture to spread out its branches, leaves, and roots, dendrimers make use of this structural characteristic to optimize their biological interactions at a molecular level (**Figure 18**) [106]. Furthermore, the highly branched nature of the structure results in a high density of functional groups at the molecular surface. This attribute, in addition to maximizing the efficiency of the dendrimer in forming molecular interactions, could also theoretically allow for the utilization of several different types of peripheral groups on the same molecule in order to achieve multiple functionalities. A possible example would be dendrimers with cell targeting moieties as well as cationic functional groups to bind oligonucleotides and achieve cell specific delivery.

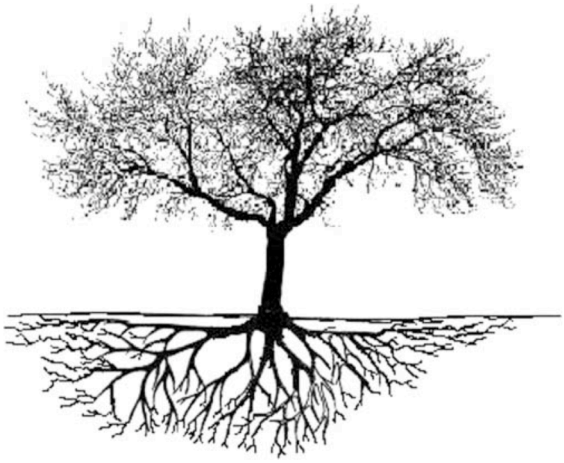

Figure 18. Dendritic architecture exists in the branches and roots of trees. *(Source: Boas, et al. (2006))*

1.4 Creation of an effective combination

Dendrimers and cationic polymers represent only some of the nanoparticles being utilized today for research in biomedical fields such as drug delivery. The aim of this study was to harness the molecular capabilities of these particles, and use them in conjunction with RNAi, a relatively new and powerful tool for the manipulation of gene expression at the cellular level. HIV infection, one of the most important and deadly infectious disease pandemics that affect the world today, was chosen as a target for this research. Specifically, complexes consisting of siRNA and dendrimers or polymers were utilized therapeutically on the hard-to-transfect CD4+ T lymphocytes that constitute the primary cell population susceptible to infection with HIV. Additionally, astrocytes were tested as a secondary cell model for HIV infection. The results should lead to further understanding in the dynamics of nanoparticle and siRNA complexation, the biocompatibility of such complexes, and their capabilities at achieving cell transfection and successful gene downregulation.

2. OBJECTIVES

The toll taken by the HIV pandemic on the global human population has been immense. The importance in developing therapeutic strategies against this disease has allowed for a huge amount of research into the molecular biology of the virus and the human immunological characteristics of infection. A large amount of the current scientific knowledge of cell biology has arisen as a result of this research.

RNAi has emerged as a powerful molecular biology tool for the specific downregulation of genes, which is being expanded to clinical applications, as well. Meanwhile, nanoscopic synthetic polymer structures are increasingly being applied to the field of biomedicine. Drug delivery applications by nanoparticles have the potential of creating effective pharmaceuticals. By combining RNAi with nanotechnology in the form of siRNA-delivering polymers and dendrimers, a whole realm of therapeutic applications arise.

Specifically, the difficulty in transfecting HIV-susceptible lymphocytes and reaching the CNS with pharmaceuticals offers the opportunity of applying this novel drug delivery system to the challenge of inhibiting HIV replication.

With this in mind, the specific objectives of this work were:

1. To determine the feasibility of second-generation amine-terminated carbo-silane dendrimers and polyethyleneimine-*graft*-poly(ethylene glycol) block copolymers as suitable drug delivery vectors for siRNA in terms of the structural characteristics and dynamics of the complexes they form.

2. To assay the biocompatibility and cytotoxicity of the dendrimers and polymers when used to deliver siRNA to various cell lines and primary cells *in vitro*.

3. To detect and analyze the cell transfection efficiency, uptake dynamics, and capabilities at crossing biological barriers for the dendriplexes and polyplexes.

4. To measure the biological activity of siRNA delivered to the target cells by the dendrimers and polymers at silencing targeted genes and, especially, reducing the replication of HIV.

3. MATERIALS AND METHODS

3.1 Reagents

3.1.1 Dendrimers

Carbosilane dendrimers (CBS) were all synthesized by the group "Química de Metalodendrímeros" of the Inorganic Chemistry Department of the Universidad de Alcalá de Henares as has been previously reported [107]. The method of preparation of the dendrimers follows a divergent procedure (synthesis from the core outwards). This method allows for more flexibility in deciding the final product. As the dendrimer is synthesized from the core outward, each successive generation results in a fork at the exterior point of all the branches and results in a doubling of the total number of exterior branches. The number of exterior branches can be described by the equation:

$$R = 2^{n+1},$$

where R is the total number of exterior branches and n is the dendrimer generation. By controlling the generation of the dendrimer, the length and number of branches as well as the size and density of the molecule can be controlled. This method of synthesis also allows many options for the functional groups at the extremities [108].

The dendrimers in this work possess two specific characteristics that make them suitable for our application. First, they have a silicon-oxygen bond in each of the branches. This allows for a time-controlled degradation. Second, the dendrimers possess external amine groups that can be quaternized to provide positively charged functional groups at the extremities [107, 109]. The resulting positive charge of the external amine groups is utilized for the formation of electrostatic interactions with the negatively charged backbone of oligonucleotides.

The degradation of the dendrimer structure occurs via the gradual hydrolysis of the Si–O bonds when the dendrimers are exposed to water. For this reason, all procedures during synthesis was carried out under the protective conditions of an argon atmosphere using standard Schlenk techniques or an argon-filled glove box, and all reactants and products were carefully protected from exposure to the environment right up until the initiation of the experiments. Once the dendrimers are dissolved in an aqueous solution, the slow hydrolysis of the Si–O bond gradually releases the external end of each branch from the dendrimer core thus resulting in the liberation of the cargo that is bound to the functional groups at the far extremities of the dendrimer.

In this work, two distinct dendrimers were used. They are 2G-CBS-(OCH_2-H_2NMe $CH_2CH_2N^+Me_3{}^+I^-)_8$ and 2G-CBS-($OCH_2CH_2N^+Me_2CH_2CH_2N^+Me_3I^-)_8$**,** and will be referred to as 2G-NN8 and 2G-NN16, respectively, based on the number of positive charges each one possesses (**Figure 19**). The difference between the two dendrimers is the degree of quaternization of the exterior amine groups on each branch. At pH 7.4 (physiological pH), the two dendrimer variants possess 8 and 16 positive charges as has been shown by ^1H nuclear magnetic resonance (NMR) and ^{13}C NMR spectroscopy measurements [107].

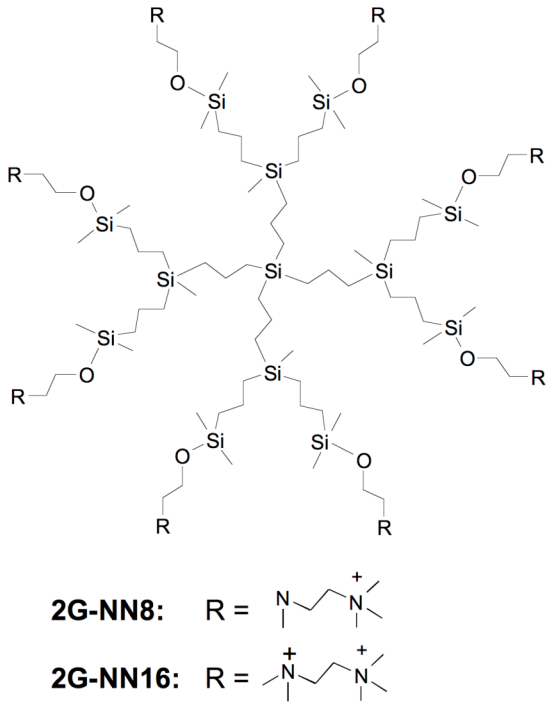

Figure 19. Structure of generation two amine-terminated carbosilane dendrimers, 2G-NN8 and 2G-NN16.

3.1.2 Polyethyleneimine-*graft*-poly(ethylene glycol) Block Copolymers

Block copolymers were prepared by grafting linear PEG onto branched PEI. In addition to four copolymers, the core PEI polymer (molecular weight (MW): 25 kDa) with no attached PEG moiety was also tested. The four copolymers used consisted of the 25 kDa PEI core grafted with a varying number of PEG chains of different molecular weights so that the PEI/PEG ratio was as close to 1 as possible. The nomenclature used for naming the polymers designates the MW of the polymer in parentheses and uses a subscript to refer to the number of PEG chains and the degree

of grafting so that the copolymer termed PEI(25k)-PEG(2k)$_{10}$ possesses ten PEG moieties of 2 kDa each, and the copolymer termed PEI(25k)-PEG(20k)$_1$ possesses one PEG moiety of 20 kDa. The four copolymers were analyzed by NMR to determine PEI content, which is shown in (Table 2). To couple the PEG moieties to the PEI polymers, a two-step reaction was performed with hexamethylene diisocyanate consisting of activation of the monomethyl-PEGs and coupling of the PEGs with PEI. This resulted in a water-soluble copolymer containing hydrolytically stable urethane and urea bonds. Spectroscopic testing (NMR and FTIR) was used to verify the molecular structure of the copolymer products [110].

Table 2. Formulas, PEI and PEG content, and structure of copolymers utilized in this study.
(Derived from figures provided by Merkel O and Kissel T in collaboration with this work)

	PEI(25k)	PEI(25k)-g-PEG(20k)$_1$	PEI(25k)-g-PEG(5k)$_4$	PEI(25k)-g-PEG(2k)$_{10}$	PEI(25k)-g-PEG(550)$_{30}$
PEI content	100 %	53 %	55 %	55 %	57 %
PEI MW	25 kDa	25 kDa	25 kDa	25 kDa	25 kDa
PEG MW		20 kDa	5 kDa	2 kDa	550 Da

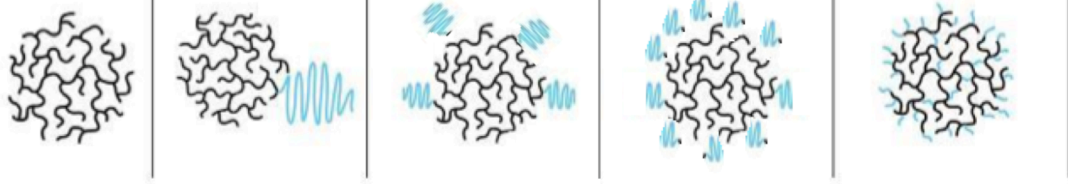

3.1.3 siRNA

All anti-HIV siRNA sequences were chosen from previously published results [53] [57] and [67] and had inhibited HIV replication in experiments using transiently transfected cells. All siRNA were purchased from Dharmacon, Inc. (Lafayette, CO). The sequences of the various siRNA were *siP24*, sense: GAU UGU ACU GAG AGA CAG GCU, antisense: CCU GUC UCU CAG UAC AAU CUU; *siGAG1*, sense: GAG AAC CAA GGG GAA GUG ACA dTdT, antisense: UGU CAC UUC CCC UUG GUU CUC dTdT; *siNEF*, sense: GUG CCU GGC UAG AAG CAC AdTdT, antisense: UGU GCU UCU AGC CAG GCA CdTdT; *siGL3*, sense: CUU ACG CUG AGU ACU UCG AdTdT, antisense: UCG AAG UAC UCA GCG UAA GdTdT. The siRNA *siP24* labeled with the fluorochrome cyanine 3 (Cy3) or fluorescein

isothiocyanate (FITC) on the 5' end of the sense strand was utilized to detect the entrance of siRNA into cells. A positive control siRNA designed to silence the expression of the housekeeping gene glyceraldehyde 3-phosphate dehydrogenase (GAPDH) (*siGAPDH*) was used to indicate successful transfection and biological activity of siRNA. In siRNA functionality experiments a siRNA of random sequence was used as a negative control to test for sequence-specific effects (*siRandom*). This siRNA was siCONTROL Non-Targeting siRNA #2 designed and screened by Dharmacon to have no silencing effect on any human, mouse or rat genes. The sequences and molecular weights for the siRNA are contained in **Table 3**.

Table 3. Sequences and molecular weights of siRNA utilized in this work.

Name	base-pairs	Sense Sequence	Mol. wt (g/mol)
siP24	21	GAU UGU ACU GAG AGA CAG GCU	13307
siGAG1	23	GAG AAC CAA GGG GAA GUG ACA dTdT	14601
siNEF	21	GUG CCU GGC UAG AAG CAC AdTdT	13330
siGL3	21	CUU ACG CUG AGU ACU UCG AdTdT	13167
siP24-Cy3*	21	Cy3-GAU UGU ACU GAG AGA CAG GCU	13815
siP24-Fl	21	FITC-GAU UGU ACU GAG AGA CAG GCU	13844
siGAPDH	21	†	13263
siRandom	21	UAA GGC UAU GAA GAG AUA CUU	13278

*in later experiments using p24-Cy3, the Cy3 fluorochrome was substituted by DY547 with similar excitation and emission characteristics (siRNA MW 13799.6 g/mol)

†proprietary information of Dharmacon, Inc. Achieves a "high efficiency of silencing glyceraldehyde-3-phosphate dehydrogenase," accession number NM_002046. (http://www.dharmacon.com)

3.2 Cells

3.2.1 Cell Lines

3.2.1.1 SupT1 cells

The established cell line SupT1 (human leukemia T-lymphocytes), obtained from American Type Culture Collection (ATCC) (Manassas, VA) (cat. CRL-1942) was maintained in complete RPMI 1640 growth medium (Biochrom AG) supplemented with 10% heat-inactivated fetal bovine serum (FBS), 2mM L-glutamine, 1% ampicillin, 1% cloxacillin, 0.32% gentamicin, 10mM 4-(2-hydroxyethyl)-1-piperazineethanesulfonic acid (HEPES), 1mM sodium pyruvate and 4.5 g/L glucose at 37°C in a 5% CO_2 atmosphere.

3.2.1.2 U87MG cells

The human glioblastoma-astrocytoma epithelial-like cell line U87MG (ATCC HTB-14) was routinely grown in Dulbleco's Modified Eagle Medium (DMEM) (Gibco) containing 10% FBS, 1% penicillin/streptomycin, and 2 mM L-glutamine at 37°C in a humidified atmosphere of 5% CO_2.

3.2.1.3 L929 mouse fibroblasts

The murine fibroblast cell line L929 (ATCC CCL-1) was routinely grown in DMEM (Gibco) containing 10% FBS, 1% penicillin/streptomycin, and 2 mM L-glutamine at 37°C in a humidified atmosphere of 5% CO_2.

3.2.1.4 Human Endometrial Carcinoma cells (HEC-1A)

These human endometrial cells (ATCC HTB-112) were derived from a human endometrial adenocarcinoma. HEC-1A were grown in RPMI medium (Gibco) supplemented with 10% FBS, 2mM L-glutamine, 1% cloxacillin, 1% ampicillin and 0.32% gentamicin in 12 well polycarbonate transwell permeable supports containing 0.4 μm pores (Costar, Cambridge, MA) at 37°C in a humidified atmosphere of 5% CO_2.

3.2.1.5 Bovine Brain Microvascular Endothelial cells (bMVEC-B)

bMVEC-B cells (Lonza, Walkersville, MD, USA) were grown in EBM-2 Basal medium supplemented with platelet-poor horse serum, ascorbic acid, β-ECGF, heparin and penicillin /streptomycin/fungizone on the same type of 0.4 μm pore poly-carbonate transwell permeable support coated with rat tail collagen type I (10 $\mu g/cm^2$) (Sigma, Missouri, USA) and coated over with fibronectin (5 $\mu g/cm^2$) (Sigma, Missouri, USA). Complete EBM-2 medium was changed 48–72 hours after seeding and every other day thereafter during 11 days to obtain a confluent barrier.

3.2.2 Primary Cell Cultures

3.2.2.1 Peripheral Blood Mononuclear Cells (PBMC)

PBMC were obtained from healthy HIV-negative blood donors by standard Ficoll-Hypaque density centrifugation, activated with the mitogen

phytohemagglutinin (PHA) (2 µg/ml), and maintained in RPMI 1640 complete growth medium supplemented with 10% FBS, L-glutamine and antibiotics along with interleukin-2 (IL-2) (20 U/ml).

3.2.2.2 Normal human astrocytes (NHA)

NHA that were isolated from the cerebrum of 5-month-old human fetuses were purchased from Cambrex (CC-2565, Walkersville, MD, USA). NHA cells were cultured by plating the cells at a density of 15×10^3 cells/cm^2 in expansion media (AGM Bullet Kit media, Cambrex) according to the manufacturer's protocol. The cells were incubated at 37 °C with 5% humidified CO_2 and allowed to reach about 95% confluence. After this, they were harvested using 0.25% trypsin and 1 mm Ethylenediaminetetraacetic Acid (EDTA) for 5 min at 37 °C.

3.2.2.3 Erythrocytes

Erythrocytes were obtained from donor blood that had been centrifuged in Ficoll-Hypaque gradient to separate them from PBMCs. The cells were diluted in 500 µl phosphate buffered saline (PBS) and seeded in 24 well plates (3×10^5 cells/well) and were immediately treated according to the experimental protocol.

3.3 Virus stocks

3.3.1 HIV-1 NL4-3

The X4-HIV virus strain NL4-3 was obtained through the AIDS Research and Reference Reagent Program, Division of AIDS, NIAID, NIH: pNL4-3 from Dr. Malcolm Martin [111]. NL4-3 was successfully grown by infecting $1 – 2 \times10^6$ MT-2 T cells at 1 multiplicity of infection (MOI) in 2 ml medium for 2 hours with regular mixing. These cells were then brought up to 6 ml and stored in an upright 25 ml flask until 80 – 90% of the cells had formed syncitia at which point the cells were added to 15×10^6 more cells in a total volume of 15 ml. At 80 – 90% syncitia, the cells were collected and spun and the supernatant was stored at -80°C.

Cell supernatant was titrated for HIV by adding serial dilutions (50 µl) to $2 – 3 \times10^4$ MT-2 cells/150µl in 96 well plates and detecting syncitia formation up until seven days. The virus concentration was calculated according to the equation:

$$\log DI_{50} = n - 0.5 + \sum R_i/n_i$$

with DI_{50} being the viral content in 50 µl; n = the greatest serial dilution with syncitia detection in all wells; R_i/n_i = the number of syncitia positive wells divided by the total number of wells for all further dilutions.

3.3.2 HIV-1 Ba-L

This R5-HIV virus strain Ba-L was obtained through the AIDS Research and Reference Reagent Program, Division of AIDS, NIAID, NIH: HIV-1 Ba-L from Dr. Suzanne Gartner, Dr. Mikulas Popovic and Dr. Robert Gallo [112]. The R5-tropic HIV strain was grown in normal PBMCs.

3.4 Dendriplexes

3.4.1 Dendriplex formation

Dendriplexes were formed by mixing equal volumes of dendrimer and siRNA dissolved in OPTIMEM® I free of serum or antibiotics at concentrations depending on the +/- charge ratio and molar concentration desired according to the formula,

$$D_{NN16} = \frac{P^-}{N^+} \cdot M_{siRNA} \cdot r_{+/-}$$

where D_{NN16} is the molar quantity of dendrimer, P^- is the number of nucleotides in the siRNA duplex, N^+ is the number of quaternized amines in the dendrimer (which also represents the molar charge of the dendrimer), M_{siRNA} is the molar quantity of siRNA, and $r_{+/-}$ is the +/- charge ratio (dendrimer to siRNA). As with polyplex formation, the molar siRNA quantity and +/- charge ratio were based on the experiment to be carried out. In the majority of the experiments, 2G-NN16 was used, which offers 16 quaternized amines (N^+ = 16), and the siRNA possessed 42 negatively charged phosphates (P^- = 42). Substituting these values into the equation above leaves,

$$D_{NN16} = 2.625 \cdot M_{siRNA} \cdot r_{+/-}$$

This implies that for every mole of siRNA, 2.625 times the +/- ratio number of moles of dendrimer was needed to form the dendriplex. The dendriplex mixture was left to incubate 15 to 20 min prior to proceeding with experimentation with the dendriplex.

3.4.2 Gel Electrophoresis (GE)

In order to visualize complexation, dendriplexes were run on 3% agarose gels containing 0.017% ethidium bromide at 90V for 30min. The gels were photographed using a Molecular Imager Gel Doc and Chemi Doc System (BioRad) and the siRNA bands that had migrated in the gel were quantified using Quantity One 1D Analysis Software. For experiments on the gradual liberation of siRNA from dendriplexes, at each time point the total quantity of siRNA that had been initially complexed with the dendrimer was compared to the siRNA that had been liberated. This was accomplished by splitting the dendriplex samples evenly into two aliquots. One aliquot was treated with heparin (2 U/μg siRNA) to free any remaining siRNA from complexation with the dendrimer. The difference in intensities of the bands from the two aliquots indicated the amount of siRNA retained in the dendriplex.

3.4.3 Strength of Union

Heparin exclusion experiments were utilized to test the strength of the union between dendrimer and siRNA. These were carried out by mixing dendriplexes (+/- ratio 4) of 2G-NN8 or 2G-NN16 with varying concentrations of Heparin (0.1, 0.15, 0.2, 0.3, and 0.6 IU/μg siRNA). The mixture was run on a 20% polyacrylamide gel for 2 h at 15 mA that was then immersed in a 0.0017% ethidium bromide solution for 5 min followed by a 5 min wash in water. The gels were photographed and the bands were quantified using the program ImageJ (1.38x, NIH, USA).

3.4.4 Size and zeta potential

Size and zeta potential measurements on dendrimers were carried out by Dzmitry Shcharbin, Elżbieta Pędziwiatr, and Maria Bryszewska from the Department of General Biophysics, University of Lodz, Poland. All dendriplex samples intended for dynamic light scattering analyses were prepared at 25°C using 0.15 mol/l HEPES buffer (containing 6 mmol/l HEPES and 144 mmol/l NaCl), pH 7.4, which was filtered with a 0.22-mm filter to remove any trace particulates. Complexes of 2G-NN16 and siGAG1 were prepared at a 500 nM siRNA concentration and at +/- charge ratios between 0 and 16. Particle size of complexes was measured by dynamic light scattering (DLS) using a Malvern Zeta-Sizer Nano S90 (Malvern, UK). The light scattered at 90° from the incident light was fit to an autocorrelation function using the

method of cumulants. The particle size of a sample was determined from the average of 12 cycles in a Malvern disposable plastic cuvette at 25^{o}C.

Zeta potential experiments were carried out by phase analysis light scattering (PALS) using a Malvern Instruments Zetasizer 2000 (Malvern, UK) at 25^{o}C. The electrophoretic mobility of the scattering (DLS) samples was determined from the average of 6 cycles of an applied electric field in a standard rectangular quartz cell. The zeta potential of complexes was determined from the electrophoretic mobility by means of the Smoluchowski approximation. All data are expressed as a mean value ± SEM of 4 independent experiments. Statistical significance was assessed using Student-Fisher test.

3.4.5 Nuclear magnetic resonance (NMR)

^{1}H-NMR spectra were recorded with Varian Unity VXR-300 and Varian 500 Plus Instruments. Chemical shifts (δ, ppm) were measured relative to residual ^{1}H resonances for chloroform-d1 and dimethyl sulfoxide-d6, which were used as solvents. NMR spectra experiments were carried out by Paula Ortega and the Inorganic Chemistry Department at the Universidad de Alcalá, Spain. Spectra were taken at various time points after CBS dendrimers similar to 2G-NN8 and 2G-NN16 were dissolved in deuterated water. These other dendrimers, which possess only a single amine group on each branch outside of the Si–O bonds, were tested in order to provide an approximation of how the internal Si–O bonds behave, and because equivalent NMR results could not be obtained for 2G-NN8 or 2G-NN16, as the additional functional groups of the extra ethylamines located further outside of the branch peripheries contribute additional resonance peaks making interpretation of the NMR chemical shift graph much more complicated. The results highlighted the gradual hydrolysis over time of the Si–O bond of the branches of the dendrimers, which can be assumed to be the case for 2G-NN8 and 2G-NN16 because of the structural similarities between the types of CBS dendrimers.

3.4.6 Protection from RNase digestion

For protective effect experiments, dendriplexes (+/- ratio of 2) or siRNA alone were incubated with 0.25% RNase (Promega, Madison WI, USA) at 37ºC for 30 min and were then loaded on a 3% agarose gel containing 0.017% ethidium bromide and

run at 90V for 30 min. Additional experiments to quantify the protective effect were performed in which dendriplex (+/- ratio 4) or siRNA alone were treated with RNase as before, incubated at 70ºC for 30 min to inactivate the RNase, and treated with heparin (2 IU/µg siRNA) to liberate the siRNA from the dendrimer in order to quantify it after being run on a 3% agarose gel.

3.5 Polyplexes

3.5.1 Polyplex formation

Complexes of siRNA and polymers were formed by mixing equal volumes of siRNA and polymer. The necessary quantity of siRNA was diluted with OPTIMEM® I medium free of serum or antibiotics at concentrations depending on the molar concentration desired. The according amount of polymer was added to the siRNA solution depending on the N/P ratio, or the number of polymer nitrogen atoms per nucleotide phosphate, according to the equation,

$$n_{polymer} = \frac{43.1 \frac{g}{mol \bullet charge}}{\%PEI\ content / 100\%} \cdot P^{-} \cdot M_{siRNA} \cdot r_{N/P}$$

where $n_{polymer}$ is the mass of the polymer in grams, *%PEI content* is the percentage content of PEI in the polymer, P^{-} is the number of nucleotides in the siRNA duplex, M_{siRNA} is the molar quantity of siRNA, and $r_{N/P}$ is the ratio of polymer amines to siRNA phosphates (referred to as the N/P ratio). The N/P ratio is similar to the +/- ratio for dendriplexes since a large percentage of polymer amines are positively charged and bind the negatively charged phosphate-sugar backbone of the siRNA according to the ratio of amine nitrogen atoms to phosphates. This ratio along with the molar siRNA quantity was assigned values depending on each experiment. A higher N/P ratio would be used in order to ensure total complexation with the siRNA and a better transfection efficiency, while the N/P ratio would be decreased in order to improve biocompatibility by minimizing the quantity of polymer necessary to transfect the desired amount of siRNA.

After mixing siRNA and polymer together, polyplexes were incubated for 20 min. The optimal incubation time was determined by dynamic light scattering. Complex formation attributes such as complexation and condensation of siRNA was investigated by gel retardation assays.

3.5.2 Gel Electrophoresis

For gel retardation assays, non-denaturing 20 % polyacrylamide gels (PAGE) were composed of 15 ml Rotiphorese Gel 40 solution, (Carl Roth GmbH, Karlsruhe, Germany), 3 ml 10× TBE buffer, 12 ml double-distilled, DEPC-treated water, 150 µl 10 % APS (Carl Roth GmbH, Karlsruhe, Germany), and 30 µl TEMED (Carl Roth GmbH, Karlsruhe, Germany). Gels were used freshly after polymerization to avoid RNase contamination and loaded with free siRNA as control (C) and complexed siRNA with increasing N/P ratio in a total volume of 10 µl per slot. Gels were run in 1 x TBE buffer for 1 h at a maximum of 100 V and 15 mA per gel followed by bathing in a 0.0017 % ethidium bromide solution in 1× TBE buffer.

3.5.3 Size and zeta potential

All size and zeta potential measurements of polymers were carried out by Olivia Merkel and the Department of Pharmaceutics and Biopharmacy, Philipps Universität Marburg, Germany lead by Dr. Thomas Kissel. For dynamic light scattering, 50 pmol siRNA per measurement were mixed with the according amount of polymer for an N/P ratio of 10 in a total volume of 50 µl. Following the 20 min incubation, the polyplex was diluted in 5% glucose at pH 7.4 to give a total volume of 500 µl. Measurements were performed using a Zetasizer Nano ZS from Malvern Instruments (Herrenberg, Germany) equipped with a 10 mW HeNe laser at a wavelength of 633 nm at 25°C and analyzed in CONTIN mode. The instrument was checked periodically with Nanosphere Size Standards (polymer microspheres in water, 199 nm ± 6nm) from Duke Scientific (Palo Alto, CA). For data analysis, the viscosity and refractive index of water at 25°C (0.89 mPa·s and 1.333, respectively) were used. The measurements were performed in triplicate. Neither the position nor attenuator were fixed but were optimized by the device. For the optimization experiments, long-term measurement of sizes was recorded over roughly one hour. The zeta potentials (surface charge) of freshly prepared polyplexes were determined using the standard capillary electrophoresis cell of Zetasizer Nano ZS from Malvern Instrument at 25°C. Average values were calculated with the data of 10 runs with standard deviation.

3.6 Cytotoxicity

3.6.1 Lactase dehydrogenase (LDH) assay

3.6.1.1 Lymphocytes

To test cytotoxicity, cells were submitted to treatment of dendrimers, dendriplexes, polymers or polyplexes and toxic effects were assessed by measuring cell membrane rupture and release of LDH into the supernatant via the CytoTox96® Non-Radioactive Cytotoxicity Assay kit (Promega). In all experiments, the transfection medium, whether it is dendrimer, dendriplex, polymer, polyplex or Lipofectin®, was never removed prior to the end of the experiment. SupT1 cells were seeded 24 h prior to treatment in 96 well plates in complete medium (1.5×10^5 cells in 190 µl/well) and were submitted to treatment (10 µl) of 2G-NN16 alone or complexed with siRNA at varying +/- charge ratios. Three to 24 h later, 100 µl of the cells were extracted, spun at 1500 rpm for 5 min, the supernatant was separated and the cells were put aside to be run through the flow cytometer. The supernatant was analyzed for LDH according to kit protocol. Measurements were reported in relation to a positive control for cell death (TritonX-100 (0.1% w/v)) after subtracting the background as determined by untreated control cells. The values were calculated according to the following formula:

$$\text{Cytotoxicity}(\%) = \frac{\text{X - C}}{\text{Tr - C}} \times 100$$

where X represents the color intensity of each sample, C is the background (untreated cells), and Tr is the positive control (TritonX-100). All points were performed in triplicate. A toxicity limit was set at 10% LDH release [113]. Experiments with polymers and polyplexes at varying N/P ratios were also carried out utilizing the same protocol except only measuring results at 3 h.

3.6.1.2 Astrocytes

U87MG astrocytes were seeded the day prior to treatment in 96 well plates in complete medium (5×10^4 cells in 200 µl/well). After allowing the cells to attach to the well bottoms, treatments of varying concentrations of dendrimer were added to the wells. Supernatant samples were taken at 3, 5 and 24 h and measured for the presence of LDH indicating membrane rupture as before.

3.6.2 3-(4,5-dimethylthiazol-2-yl)-2,5-diphenyl-tetrazolium-bromide (MTT) Assay

3.6.2.1 Lymphocytes

SupT1 or PBMC were seeded in 96 well plates in OPTIMEM® I medium containing 10% FBS (1.5×10^5 cells in 190 µl/well) and submitted to 10 µl treatment of siRNA alone or complexed with 2G-NN16 at varying +/- charge ratios. Twenty h later, 20 µl of MTT substrate solution (5 mg/ml) was added to the cells to measure mitochondrial activity. After 4 h, the supernatant was removed and the formed crystals were dissolved in 200 µl DMSO and absorbance was measured in a plate reader (Biowhittaker microplate reader 2001, Innogenetics) at 550 nm with a reference of 690 nm. All points were performed in triplicate.

3.6.2.2 Astrocytes

U87MG or NHA were seeded the day prior to treatment in 96 well plates in complete medium (5×10^4 cells in 200 µl/well). After allowing the cells to attach to the well bottoms, treatments of varying concentrations of dendrimer were added to the wells. After 3, 5, 24 or 72 h, the medium was removed and replaced with 200µl OPTIMEM® I medium containing MTT substrate solution (0.5 mg/ml) and mitochondrial activity was measured as before.

3.6.2.3 L929 fibroblasts

Cytotoxicity of PEI-PEG copolymers was tested on L929 cells via MTT assays by Olivia Merkel and the Department of Pharmaceutics and Biopharmacy, Philipps Universität Marburg lead by Dr. Thomas Kissel. Briefly, L929 cells were seeded in 96 well plates (8×10^3 cells in 200 µl/well) 24 h prior to the experiment. Polymer solutions were prepared in serum-free DMEM medium. In each well, 100µl of polymer solution was mixed with 100 µl of full serum containing medium. Cells were incubated with polymer treatments for 24 h, and then, the medium was replaced with 200 µl DMEM containing MTT substrate solution (0.5 mg/ml) and mitochondrial activity was measured as before.

3.6.3 Cell Proliferation

SupT1 were seeded in 96 well plates 24 h prior in complete medium containing 2% FBS (1×10^5 cells in 100 µl/well). The following day, the serum was brought up to 10% and the cells were submitted to treatment with siRNA alone or dendriplex. After 20 h and 48 h, cell proliferation was measured by detecting the incorporation of bromodeoxyuridine (BrdU) in newly synthesized DNA according to kit protocol (Chemicon International, Temecula, CA, USA). Experiments following the same protocol were also carried out with U87MG cells.

3.6.4 Absolute Cell Numbers

SupT1 cells were seeded and submitted to treatment the same as for LDH experiments with mock treatment and TritonX-100 used as controls. The commercial cationic lipid reagent Lipofectin® (Invitrogen, Calsbad, CA, USA) was used as a comparative control according to kit transfection protocol for cells in suspension. Seventy-two h later, healthy and viable cells were counted from 10 µl samples from each well using a Neubauer slide under a light microscope.

3.6.5 Hemolytic Activity and Erythrocyte Aggregation

The hemolytic activity and erythrocyte aggregation caused by treatment of dendrimers, dendriplexes or polymers on human erythrocytes was investigated to measure the cytotoxic effects of these macromolecules on red blood cells, the most numerous type of blood cell [114, 115]. For experiments with dendrimers or dendriplexes, erythrocytes were diluted in 500 µl PBS and seeded in 24 well plates (3×10^5 cells/well) [116]. As a positive control, cells were treated with Triton X-100 at 0.2%, and PBS was used as a negative control. Erythrocytes were then treated with different concentrations of dendrimer and dendriplex. After 1 hour of incubation, 100 µl of supernatant was obtained for evaluation of the hemoglutination, cell number and hemoglobin release levels by the plate reader spectrophotometer at a wavelength of 550 nm using 690 nm as a reference.

For experiments with polyplexes, the red blood cells were washed in HEPES-buffered saline (HBS) until the supernatant was clear and colorless and were then diluted with HBS to 5×10^8 cells/ml. Polyplexes were prepared at an N/P ratio of 10 in a total volume of 125 µl (7.5 µM siRNA). One percent Triton X-100 in HBS (100%

lysis) and pure HBS (0% lysis) were used as controls. Forty microliter aliquots of polyplex solutions were mixed with 40 µl erythrocyte suspensions. Samples were incubated for 30 min at 37 °C under constant shaking. After centrifugation at 850×g, supernatant was analyzed for hemoglobin release at 541 nm (Ultrospec 3000, GE Healthcare, Munich, Germany). The pellet was resuspended with 50 µl HBS and used for monitoring of erythrocyte aggregation. For quantification of hemoglobin released by cells treated with polyplexes, a UV spectrum of a 1:1 dilution of Triton X-100 lysed erythrocytes revealed maxima at 541 nm and 576 nm. All samples were measured in triplicate.

3.6.6 Microarrays

Astrocytoma cells were spread in a P6-culture plate at a density of 8×10^5 cells/well and cultured overnight. Then cells were incubated with 2G-NN16 (24 µg/ml) for 3 or 5 h. Finally, U87MG were detached mechanically, rinsed in PBS, and centrifuged. RNA was extracted using RiboPure-Kit (Ambion) following the kit protocol. RNA was measured in a Nanodrop® ND-1000-UV/Vis Spectrophotometer and RNA integrity was verified using a 2100 Bioanalyzer (Agilent). For each 1 µg sample of total RNA was amplified and labeled using Low RNA Amplification plus Kit One Color (Agilent) following the manufacturer's instructions. Briefly, RNA was denatured and reverse transcribed to cDNA. This cDNA was then transcribed *in vitro* to RNA using T7 RNA polymerase. Amplified RNA was cleaned up using RNeasy MiniKit (Quiagen). Antisense RNA quantification was performed with the Nanodrop® Spectrophotometer and verification of the antisense RNA integrity in the Agilent Bioanalyzer. Hybridization and scanning of microarrays were performed as specified in "One-color microarray-based gene expression analysis" v5.0.1 using all reagents recommended by Agilent and 4×44K whole genome human microarrays (Agilent Technologies). These microarrays contained more than 40,000 oligonucleotides representing human transcripts and more than 3,000 control spots. Slides were scanned using a G2565BA Agilent-scanner and data was obtained by FeatureExtraction v9.1. The open software Bioconductor was used for normalization and statistical analysis.

3.7 Transfection efficiency

3.7.1 Flow Cytometry

At different time points following treatment with dendriplexes, polyplexes, dendrimers, or siRNA alone (at varying concentrations, N/P ratios or +/- charge ratios), cells were analyzed by flow cytometry to determine two attributes, 1) the percentage of the cell population that could be deemed viable, and 2) the percentage of the viable cell population that exhibited fluorescence representing successful uptake of the Cy3-labeled siRNA (siRNA, dendriplex, and polyplex treated cells only). Cells were washed with either trypsin or glycinic acid to remove any siRNA from the membrane exterior. When cells washed with acid produced identical results as non-washed cells, this step was occasionally omitted in order to maintain high cell retention.

Following treatment with siRNA alone or dendriplexes, U87MG cells were likewise analyzed by flow cytometry to determine the transfection efficiency of Cy3-labeled siRNA in the viable cell population. We also studied the transfection intensity at 3 hours, by x-mean values. Cells were washed with glycinic acid to remove any siRNA on the membrane exterior.

3.7.2 Confocal Microscopy

SupT1 cells that had been treated with Cy3-labeled siRNA alone, in dendriplex or with a mock treatment were collected after 20 h incubation spun and resuspended in OPTIMEM® I medium. Cell membranes were labeled by incubating the cells with a 1:20 dilution of anti-CD45-FITC antibody (Beckman Coulter, Fullerton, CA, USA). Without being fixed, the "*in vivo*" cells were attached to a slide with poly-L-lysine then viewed and photographed with a Leica TCS SP2® confocal microscope using different excitation wavelengths (488 and 543 nm). Un-labeled photographs were analyzed by three independent viewers to determine percentage of cells positive for uptake of siRNA. Videos were made of the live cells by capturing still images every 30 s during a 5 min span.

Polyplex-treated cells were prepared the same as dendriplex-treated cells except that they were collected 24 h after treatment and were also labeled with 4'-6-Diamidino-2-phenylindole (DAPI) (Calbiochem, San Diego, CA) (5 µg/ml) in order to detect cell nuclei. The confocal microscope also utilized an excitation wavelength

of 405 to view the DAPI-stained nuclei. Unlabeled photographs were analyzed by three independent viewers to determine cell viability as well as uptake.

3.7.3 Immunofluorescence Microscopy

U87MG cells were seeded on coverslips in 24 well plates 24 h prior to being treated with siRNA alone or dendriplexes at +/- ratios of 4 or 8. Twenty-four h later, the coverslips were collected, rinsed with PBS, and stained with DAPI (5 μg/ml). The coverslips were mounted on microscope slides with DakoCytomation-Fluorescent-Mounting-Medium (Denmark), and photographed with a Nikon Eclipse E800 immunofluorescence microscope using filters of 400-420 nm (DAPI) and 575-590 nm (Cy3).

3.8 Capability of dendriplexes to pass through biological membranes

3.8.1 Polarized epithelial cells (HEC-1A)

To obtain a tight monolayer, HEC-1A were grown in RPMI-1640 medium with 10% FCS on a 0.4 μm pore polycarbonate permeable support (Costar, Cambridge, MA). Briefly, 2×10^5 cells were seeded per filter insert and were grown for 7 days as described elsewhere [117]. In the basolateral zone of the chamber PBMCs that had been activated with PHA (2 μg/ml) and IL-2 (60 IU/ml) were cultured in RPMI-1640 medium with 10% FCS. Prior to initiating the experiment, the transepithelial electric resistance (TEER) of the monolayer was measured with an Epithelial Voltohmmeter (World Precision Instruments), and only when a measurement of > 300 Ωcm^2 was obtained would the barrier be considered fully formed [118]. HEC-1A that were being grown concurrently on coverslips were monitored with a light microscope to estimate the growth progress and confluency of the cells. Magnified images were taken of naked cells using a Nomarski prism and cells dyed with silver nitrate ($AgNO_3$) to label the tight cell junctions. When the monolayer was deemed to be 100% confluent, siP24-Fl alone or siP24-Fl/2G-NN16 dendriplexes were added to the apical zone. Five or 72 h following treatment, the PBMCs were collected and analyzed by flow cytometry to determine the percentage of viable cell population that exhibited fluorescence representing successful transcytosis and subsequent transfection of the fluorochrome-labeled siRNA [119]. The HEC-1A that were concurrently grown on coverslips were also submitted to the

treatments and monitored by a microscope to detect any cell death or cell detachment from the barrier. No negative effects from the treatments that caused the barrier to be broken were observed.

3.8.2 Bovine brain microvascular endothelial cells (bMVEC-B)

5×10^5 cells/cm^2 of bMVEC-B were seeded in complete EBM-2 basal medium on a 0.4 μm pore polycarbonate permeable support coated with rat tail collagen type I (10μg/cm2) (Sigma, Missouri, USA) and coated over with fibronectin (5μg/cm2) (Sigma, Missouri, USA). Complete EBM-2 medium was changed 48-72 hours after seeding and every other day thereafter during 11 days to obtain a confluent barrier. Barrier formation was analyzed by measuring the TEER as described above. In the basolateral zone of the chamber, activated PBMCs or U87MG cells were cultured in the corresponding medium. When the monolayer was formed, siP24-Fl alone or in dendriplex was added to the apical zone. Five or 72 h later, the PBMCs or U87MG cells were collected and analyzed by flow cytometry as mentioned above.

3.9 Transfection via electroporation

3.9.1 GAPDH silencing via electroporation of siRNA

SupT1 cells were washed and resuspended in serum-free OPTIMEM® I medium. Either 4×10^6 or 8×10^6 cells/point were mixed with siRNA varying in concentration from 10 nM to 0.5 μM in OPTIMEM® I at a cell concentration of 10×10^6 cells/ml in a cuvette and incubated on ice for 15 min prior to subjecting the cuvette to an electropulse (250V, 1050F) (EasyjecT Plus® Multipurpose Electroporation System). The cells were left to recover at room temperature for 15 min before being added dropwise to 2 to 4 ml warm complete medium. Cells were harvested from 2 to 6 days after electroporation and the RNA was extracted according to the SV Total RNA Isolation System kit protocol (Promega). Total RNA quantities were normalized between points by measuring RNA concentrations with a Nanodrop® ND-1000-UV/Vis Spectrophotometer. Reverse transcription polymerase chain reactions (PCR) were performed as before [120] using the ImProm-II™ Reverse Transcription System (Promega) and real-time PCR using Brilliant® SYBR® Green QPCR Master Mix (Stratagene, Cedar Creek, TX, USA) were performed to quantify

GAPDH gene expression at the mRNA level using the housekeeping gene β-actin to normalize mRNA quantities. The primers used to amplify the GAPDH gene were TGG-GGA-AGG-TGA-AGG-TCG-G (forward) and GGG-ATC-TCG-CTC-CTG-GAA-G (reverse) (Eurogentec S.A., Belgium) and the primers for β-actin amplification were GGC-TTC-CCC-AGT-GTG-ACA-T (forward) and GGG-GTG-TTG-AAG-GTC-TCA-AA (reverse) and an annealing temperature of 58C was used in real-time PCR.

3.9.2 HIV inhibition via electroporation with siRNA

PBMC that had been stimulated for 2 days with PHA were infected with HIV NL4-3 at 0.5 MOI in a total volume of 1 ml during two hours with frequent mixing. Three days later, the infected cells were collected and spun (1200 rpm, 10 min) and washed once with cell culture medium at room temperature. One million cells/point were resuspended in 500 µl OPTIMEM® I (room temperature), mixed with the corresponding siRNA treatment, transferred to a cuvette, subjected to an electropulse (250V, 1050F), and immediately transferred to 15 ml of warm culture medium. Samples of cells and supernatant were collected every 24 h starting 24 h post-treatment and tested for transfection of siRNA and HIV viral concentration, respectively. Transfection of siRNA was detected via flow cytometry, and HIV replication was measured by assaying the HIV antigen (Ag) p24 with ELISA kit (INNOTEST® HIV Antigen mAb, Innogenetics, N.V., Belgium) according to the kit protocol.

3.10 Treatment with dendriplex

3.10.1 GAPDH silencing

3.10.1.1 SupT1

SupT1 cells were seeded in 24 well plates in complete medium (1×10^6 cells in 900 µl/well) and were submitted to 100 µl treatment of siGAPDH (500 nM) either alone, complexed with 2G-NN16 at a +/- ratio of 2, or with Lipofectin® according to manufacturer protocol. Cells were harvested 48 h later and RNA was extracted and GAPDH mRNA was quantified by qPCR as mentioned above.

3.10.1.2 U87MG

U87MG cells were seeded in 6 well plates (3×10^5 cells/well) 24 h prior to being treated with siRNA alone, dendriplexes (250 nM siRNA, +/- ratio of 8), or dendrimer alone (24 μg/ml). Forty-eight h later, the cells were trypsinized (0.25%) and collected, RNA was extracted, and GAPDH mRNA was quantified by qPCR as mentioned above.

3.10.2 HIV inhibition

3.10.2.1 PBMC and SupT1

PBMC that had been previously stimulated with PHA for up to 3 days or SupT1 cells were infected with HIV NL4-3 at 0.05 or 0.01 MOI, respectively. The cells were washed twice with warm medium before being plated and treated with siRNA or dendriplexes at varying concentrations and +/- ratios. The dendriplex treatment was added to the infected cells within an hour of the end of the incubation with HIV. The dendriplex was formed in serum- and antibiotic-free OPTIMEM® I and incubated 15 min, room temp for the complex to form prior to adding it to the plated cells. Samples were collected every 24 h starting 24 h after treatment, spun, and the supernatant was collected and assayed for viral concentration using the HIV protein *p24* ELISA kit according to kit protocol. The dilution factors depended on the MOI and the time point in which the sample was collected but ranged from 10^{-1} to 10^{-4}.

3.10.2.2 U87MG

Astrocytoma cells were seeded in 6 well plates in complete medium and infected with either the X4-tropic HIV-1 NL4-3 or the R5-tropic HIV-$1_{Ba\text{-}L}$ at 1 MOI. The cells were washed twice with warm medium and treated with siRNA, dendrimers, or dendriplexes at varying concentrations and +/- ratios. Supernatants were collected 3 days after the initiation of treatment and saved in a -20ºC freezer. Amplicor HIV-1 Monitor Test was used to determinate HIV-1 RNA in supernatant samples. The test was performed according to the manufacturer's instructions and indicates the quantity of genomic viral RNA in the collected supernatants by quantitative polymer chain reaction (qPCR).

3.11 Treatment with polyplex

3.11.1 GAPDH silencing

SupT1 cells were seeded in 24 well plates in complete medium (1×10^6 cells in 900 µl/well) and were submitted to 100 µl treatment of siGAPDH (500 nM) either alone or complexed with polymers at an N/P ratio of 10 for all polymers possessing PEG chains and 5 for PEI(25k). Cells were harvested 48 or 72 h later and RNA was extracted and GAPDH mRNA was quantified by qPCR as mentioned above.

For repetitive treatment experiments, SupT1 cells were seeded in 24 well plates in complete medium (1×10^6 cells in 900 µl/well) and maintained in passage for 22 days. This was accomplished by collecting samples of 400-500 µl containing cells every 2 or 3 days starting 3 days after the initial treatment and replacing the lost volume with 400 µl fresh medium and 100 µl of new treatment. Only PEI(25k)-$PEG(2k)_{10}$ and PEI(25k)-$PEG(20k)_1$ were tested. The same siRNA concentration and N/P ratios were used as before. The samples were centrifuged, and RNA was extracted from the cells and tested for GAPDH expression by qPCR as mentioned above.

3.11.2 HIV inhibition

SupT1 cells were seeded in 24 well plates in complete medium (1×10^6 cells in 900 µl/well) and were submitted to 100 µl treatment of siNEF, siCOCKTAIL, or siRandom (500 nM) either alone or complexed with polymers at an N/P ratio of 10 for all polymers possessing PEG chains and 5 for PEI(25k) 16–20 h prior to being infected with HIV NL4-3 (100 ng/1×10^6 cells) for 2 h with mixing every 30 min. The cells were then washed two times with warm medium and counted. One hundred thousand cells in 200 µl/point were seeded in 96 well plates. Transfection was confirmed by flow cytometry. After 72 h, supernatant samples were collected and analyzed for viral *p24* protein content as described above.

Longer-term HIV inhibition experiments were carried out by treating SupT1 cells with polyplexes (50 µl treatment to 5×10^5 cells in 450 µl/point) at the same siRNA concentrations and N/P ratios as before, infecting them with HIV NL4-3 (as explained above, 24 h after treatment), and maintaining them in passage for up to 15 days (initially 5×10^5 cells seeded in 1 ml/point). Supernatant samples were taken

every 2-3 days by removing 500 µl and centrifuging at 1500 rpm for 5 min to ensure only supernatant was collected. On the same day that samples were collected, the polyplex treatments were administered again by adding 100 µl polyplex and 400 µl fresh complete medium to each point. If the total volume had fallen considerably below 1 ml/well, samples of less than 500 µl would be collected so that the total volume would return to 1 ml upon the addition of treatments. The antiretroviral nucleoside analog reverse transcriptase inhibitor azidothymidine (AZT) (0.5 µM) was used as a control for HIV inhibition.

4. RESULTS

4.1 Dendriplex formation and stability

4.1.1 siRNA/CBS dendriplex complexation

siRNA/CBS dendriplexes were formed in OPTIMEM® I and tested for stability using gel electrophoresis. Three percent agarose gels were used to detect retention of the siRNA due to its union with the dendrimer at varying +/- ratios. Full retention of the siRNA in the lane wells indicated full complexation and condensation of the siRNA by the dendrimer vehicles and the formation of a stable complex. Various trials revealed that siRNA retention is seen starting with a +/- ratio of 1 with full retention achieved with +/- ratio from 2-4 for both the CBS dendrimers 2G-NN8 and 2G-NN16. As seen in (**Figure 20**), dendriplexes formed between siP24-Cy3 and 2G-NN8 or 2G-NN16 were stable and did not migrate in the gel at +/- ratios of 2, 4, 6 or 8. The siRNA-dendrimer complex was clearly retained in the gel wells as is apparent by the fluorescence emitted by the ethidium bromide stained siRNA oligonucleotides in the wells of the gel.

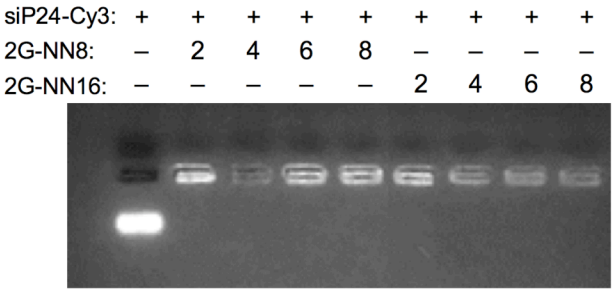

Figure 20. Retention of siP24-Cy3 by 2G-NN8 or 2G-NN16. Numbers indicate +/- charge ratios of dendriplex.

4.1.2 Strength of dendriplex union

To be effective at achieving cell delivery, dendriplexes must possess a union of sufficient strength to withstand encounters with other macromolecules during cell transfection and intracellular trafficking, but still be able to release the oligonucleotide cargo after reaching the cell cytoplasm. In order to test the relative strength of the union between siRNA and CBS dendrimer, we measured dissociation behavior of the complexes when exposed to heparin, a polyanion possessing a very high charge density, which competes with the siRNA for binding the dendrimer. PAGE was utilized to adequately visualize and quantify the siRNA released from the dendriplex

as the concentration of heparin added to the sample increased. It was found that 2G-NN8 binds siRNA more strongly, as a slight release of siRNA is not seen until heparin concentration reaches 0.2 IU Hep/µg siRNA (**Figure 21A**), while the release of siRNA from 2G-NN16 begins at 0.15 IU/µg (**Figure 21B**). Moreover, there is a substantially larger amount of siRNA released at 0.2 IU/µg with 2G-NN16 (60%) than with 2G-NN8 (8%).

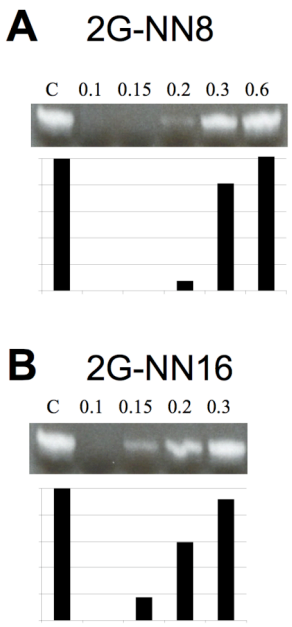

Figure 21. Strength of union assay. Competition for binding with dendrimer results in the release and migration of siRNA as heparin concentration increases. (A) 2G-NN8, (B) 2G-NN16. Relative intensities of the siRNA bands in the gel are shown by the black bars below each lane.

4.1.3 Dendriplex size and zeta potential

To measure the hydrodynamic particle diameter and zeta potential of dendriplexes, DLS was utilized. Addition of 2G-NN16 led to changes of zeta potential of siGAG1. From a +/- charge ratio of 1 up to 3, a sharp and significant increase of zeta potential from -20 to +5 was observed. When dendrimer concentration was increased from a +/- charge ratio of 4 up to 16, a continuous but more gradual increase of zeta potential was observed. Based on these data, the dendriplex composed of 2G-NN16 and siGAG1, when formed in HEPES buffer, appeared to possess a +/- charge ratio of 3 (**Figure 22A**). The particle size of the dendriplexes estimated by

intensity at different NN16/siGAG1 charge ratios is presented in **Figure 22B**. At a charge ratio of between 3 and 8 the size of dendriplexes ranged from 300 to 370 nm. Further addition of dendrimer led to an increase in dendriplex size.

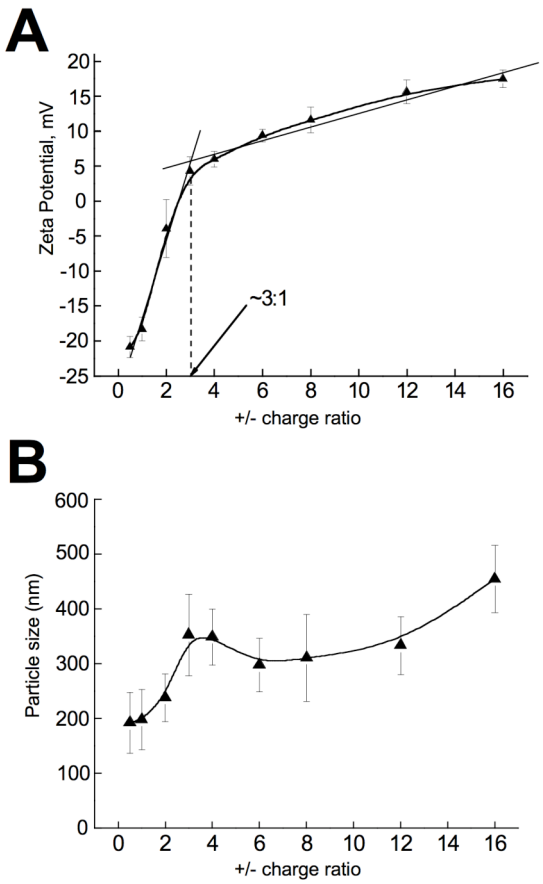

Figure 22. Zeta potential and particle size of dendriplex. (A) Zeta potential of 500 nM siGAG1 upon addition of 2G-NN16 at varying +/- charge ratios. (B) Particle size (estimated by intensity) of the same dendriplex formations. Dendriplex formed in 0.15 mM HEPES buffer, pH 7.4, 25ºC.

4.2 Polyplex formation and stability

4.2.1 PEI-PEG copolymers/siRNA polyplex complexation

PEI-PEG/siRNA polyplexes were formed using a similar protocol as dendriplexes. Initial studies on siRNA complexation and condensation characteristics at varying N/P ratios were carried out via gel electrophoresis. If the ratio of polymer to siRNA was sufficient to fully condense the siRNA, the siRNA did not migrate in the gel and appeared at or near the lane well. The existence of PEG moieties on the polymers had an effect on the polymer's ability to complex with siRNA, as did the size/number of moieties, albeit to a lesser extent. Unmodified PEI was most efficient

in complexation and condensation of siP24-Cy3, and at an N/P ratio of 3, siRNA was almost fully retained in the gel well and was condensed entirely at an N/P ratio of 5 where a strong decrease in fluorescence was observed (**Figure 23A**). The PEG modified copolymers were only slightly less efficient at complexing siRNA. For all three of the higher grafted copolymers, PEI(25k)-PEG(550)$_{30}$, PEI(25k)-PEG(2k)$_{10}$, and PEI(25k)-PEG(5k)$_4$, full complexation was achieved at N/P ratios between 6 and 8 (**Figure 23B-D**). However, a substantial amount of the siRNA was already partially retained at the N/P ratio of 5, as could be seen by the siRNA smear in this lane. PEI(25k)-PEG(20k)$_1$ revealed practically the exact same results for siRNA complexation as PEI(25k) (**Figure 23E**).

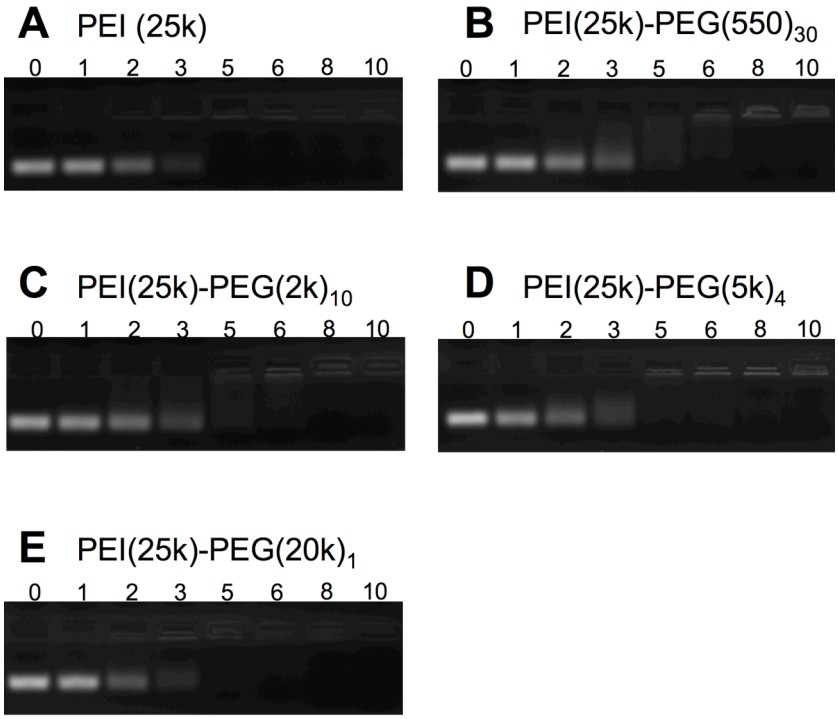

Figure 23. Complexation and condensation of siP24-CY3 by PEI (25k) (A) and its PEGylated versions (B - E). N/P ratio of polyplex samples is indicated above each lane.

4.2.2 Polyplex size and zeta potential

As had been done for dendrimers, DLS was used to analyze the particle size and zeta potential of polyplexes formed with the different polymers. **Figure 24** shows results for the five polymers bound to siGL3 at an N/P ratio of 10 [89]. This N/P ratio was used because changes in particle size for PEI(25k)-PEG(2k)$_{10}$/siGL3 were shown

to stabilize at an N/P ratio of 10 when increasing the N/P ratio from 5 up to 50 (data not shown) [89]. Particle size was directly related to the size of the PEG blocks that a polymer had as copolymers with larger PEG blocks formed smaller particles than copolymers with smaller PEG blocks. The larger particle size formed by PEI(25k)-PEG(550)$_{30}$/siGL3 (300-400 nm) was evidence of less siRNA condensation ability by this highly grafted polymer. On the other hand, polymers with less PEG grafting formed stable particles of 130-150 nm revealing the possibility that the siRNA can interact with the PEI core without interference from the PEG moieties for these copolymers, especially for PEI(25k)-PEG(20k)$_1$ which possesses only a single PEG moiety and appears to condense the siRNA the most. The copolymers were all stable and did not increase in size during an incubation of at least 20 min, while particles of siRNA with the homopolymer PEI(25k) increased in size by 35% (data not shown) [89]. This indicates that the PEG moieties prevented aggregation via a steric shielding effect for polyplexes consisting of the copolymers.

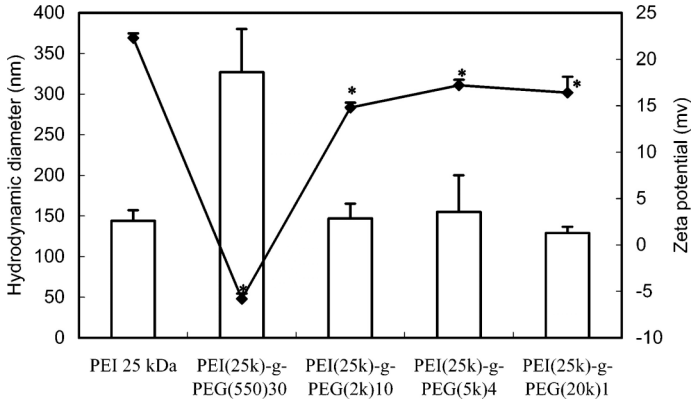

Figure 24. Particle size and zeta potential for polyplexes with siRNA in 5% glucose at N/P ratio of 10. (♦) ζ potential; (bar) particle size. *p < 0.05. *Borrowed from Mao, et al. (2006) with permission.*

The surface charge of the polyplexes is shown by the ζ-potential (**Figure 24**). Ungrafted PEI(25k) polyplexes had a high positive charge with a ζ-potential of +22.3 mV. The copolymers showed reduced ζ-potential values compared to PEI(25k). Particles containing PEI(25k)-PEG(550)$_{30}$ had a full shielding effect by the PEG. The other three copolymers exhibited higher ζ-potentials (+15 – 17 mV) with no statistical differences among them [89].

4.3 Time-controlled liberation of siRNA from dendriplex

4.3.1 Gradual hydrolysis of Si–O bonds of dendrimer branches

The carbosilane dendrimers were designed to undergo a gradual degradation via hydrolysis of its internal Si–O bonds when dissolved in an aqueous solution. This degradation of the exterior dendrimer branches would result in the liberation of any cargo that had been bound to the charged peripheral amines, as the external section of the branches would break away from the core. In the case of cargoes such as oligonucleotides, siRNA, or plasmids, functionality could only be restored to the nucleic acids once they had been released from the dendrimer escort core. Through experimentation on the union between CBS dendrimers, including 2G-NN8, and antisense oligonucleotides, this liberation of cargo was previously estimated by Bermejo, et al. to be between 6 and 24 h [107]. In addition, the structural degradation of the branches was demonstrated via NMR [109]. **Figure 25** shows proton NMR spectroscopy results highlighting the gradual hydrolysis over time of the Si–O bond of the branches of a CBS dendrimer similar to 2G-NN8 and 2G-NN16, but possessing only a single amine group outside of the Si–O bond. The results indicated that the timeframe for hydrolysis was from 1 to 12 hours with total hydrolysis not occurring until after 5 h.

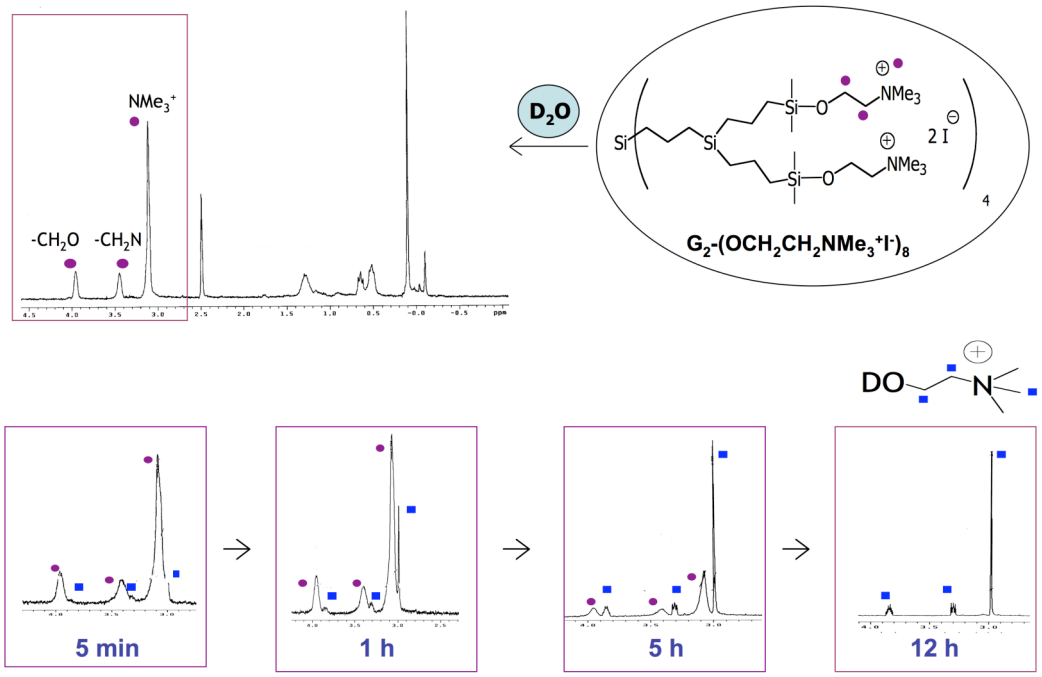

Figure 25. Proton NMR spectroscopy performed at different time points after dilution in heavy water (D_2O) shows the gradual hydrolysis of Si–O bonds of an amine-terminated carbosilane dendrimer possessing the same core as 2G-NN8 and 2G-NN16. Purple dots indicate peaks associated to functional groups of the unhydrolized exterior dendrimer branches, while blue squares show peaks for the functional groups of the hydrolysis product.

4.3.2 Gradual liberation of siRNA from dendriplex

To determine the kinetics of the interaction between 2G-NN16 CBS dendrimers and siRNA and analyze the gradual dendriplex degradation experimentally, samples of dendriplexes were visualized by gel electrophoresis at various time points after dendriplex formation. As before, siRNA migration indicated free siRNA that had been liberated by the dendrimer, while a lack of siRNA migration indicated a stable non-degraded dendriplex. Each sample was split into two fractions, and one of the fractions was treated with heparin (2 IU/µg siRNA) to force the dissociation of siRNA from the dendrimer and reveal the quantity of siRNA still complexed to the dendrimer at each time point. **Figure 26A** shows the bands of liberated siRNA free to migrate in the gel at different time points. For both +/- charge ratios of 2 and 4, but particularly at a ratio of 4 (fourth lane), retention of siRNA by 2G-NN16 can be seen up through 12 h followed by a gradual liberation. **Figure 26B**

shows the graphical analysis of the intensities of the siRNA bands. The percentage of siRNA complexed to and retained by 2G-NN16 can be determined by the differences between the intensities of the dendriplex bands and the heparin-treated dendriplex bands. This difference was a substantial value up until 24 h when it dropped to zero. These results indicate a gradual time-controlled degradation of the dendrimer and liberation of its siRNA cargo from between 12 to 24 h.

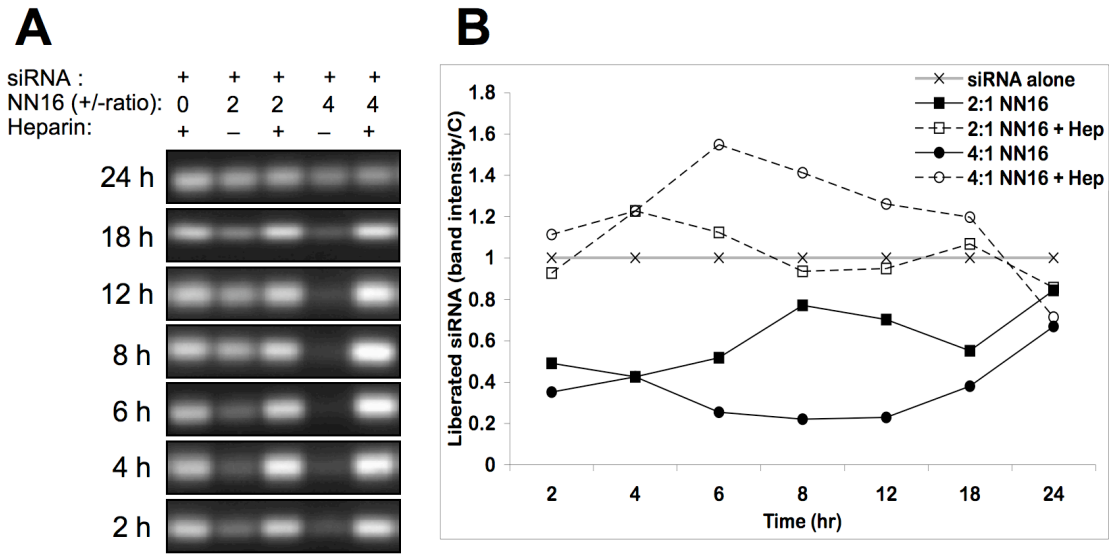

Figure 26. Hydrolysis of dendrimer Si–O bonds results in a time-dependent liberation of siRNA from complexation with 2G-NN16. (A) Images of siRNA migration in gels after various time periods of incubation with dendrimer. Lanes treated with heparin indicate total siRNA contained in dendriplex. (B) Graphical analysis of siRNA band intensities.

4.4 Protection from RNase digestion

4.4.1 siRNA/CBS dendriplex protective effect

Agarose gel electrophoresis was used to characterize a possible protective effect that CBS dendrimer has on siRNA. As shown in **Figure 27**, naked siRNA was seen to be completely degraded in the presence of RNase, while siRNA retained in the gel wells due to its union with CBS showed very little sign of RNase degradation. Furthermore, the small amount of siRNA that was not bound to the dendrimer and was free to migrate in the gel disappears when in the presences of RNase.

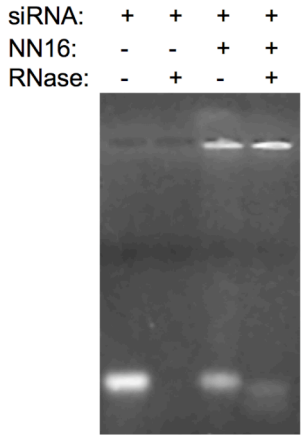

Figure 27. Protection from degradation by RNase. siRNA complexed with 2G-NN16 is not degraded by RNase.

To further corroborate these results, similar experiments were run with the additional step of using heparin to liberate the dendrimer-complexed siRNA after incubation with RNase. The resulting siRNA gel bands represent the total quantity of siRNA that was not affected by RNase digestion. **Figure 28** shows the siRNA gel bands along with a graphical representation of their relative intensities. 2G-NN16 dendrimer protected siRNA from degradation by RNase by around 40% over non-complexed siRNA.

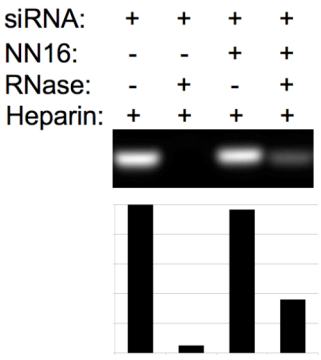

Figure 28. Quantification of protective effect 2G-NN16 dendrimer has over siRNA.

4.4.2 siRNA/PEI-PEG polyplex protective effect

The protective nature that PEI polymer and PEI-PEG copolymers have over siRNA when exposed to RNase was shown by Mao, et al. (2006) [89]. The relative extent to which the polymers exerted a protective effect depended on the size/number

of PEG moieties as copolymers containing larger/fewer moieties exerted a higher level of protection while PEI(25k) and PEI(25k)-PEG$(550)_{30}$ offered very little protection from RNase degradation (protective effect: PEI(25k)-PEG$(20k)_1$ > PEI(25k)-PEG$(5k)_4$ > PEI(25k)-PEG$(2k)_{10}$ > PEI(25k) > PEI(25k)-PEG$(550)_{30}$) (data not shown).

4.5 Cytotoxicity

4.5.1 Cytotoxicity of dendrimers

The main cellular targets for HIV infection are lymphocytes. Therefore, in-depth analysis of possible cytotoxicity on this cell type caused by treatments with siRNA and its proposed delivery vehicles were carried out. Dendrimers alone and dendriplexes were tested on lymphocytes for a toxic effect using an array of assays to measure cell viability, membrane rupture, metabolic activity, and cell proliferation. The experimental dendrimer concentrations were based on the amount necessary to form complexes with functional concentrations of siRNA. For instance, the top limit of siRNA concentration used to achieve a biological function (500 nM) requires only 12 μg/ml 2G-NN16 to obtain a +/- charge ratio of 2.

4.5.1.1 Effect on lymphocytes

4.5.1.1.1 Lactase dehydrogenase (LDH) assays

To test membrane rupture, LDH assay was utilized on the lymphocytic cell line SupT1 with 10% LDH release representing a limit above which treatments were considered toxic. At 3 h post-treatment, 2G-NN16 alone was determined to exert a toxic effect when used at concentrations above 15 μg/ml. Meanwhile, when complexed with siRNA (250 nM), a toxic effect was not reached until slightly more than 25 μg/ml 2G-NN16 (**Figure 29**) corresponding to a +/- charge ratio of 8.

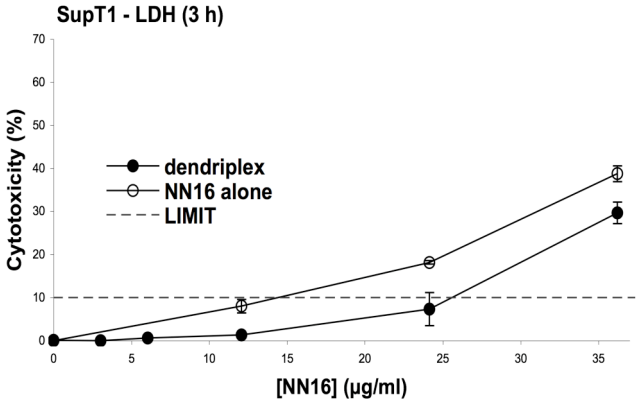

Figure 29. LDH release from SupT1 cells treated with varying concentrations of dendriplex or dendrimer alone. (Values are relative to cells treated with Triton X-100)

4.5.1.1.2 MTT assays

Mitochondrial metabolism was measured by MTT assay for both SupT1 cells and primary PBMC treated with dendriplex. In both cell types, mitochondrial activity remained higher than a viability limit of 80% when subjected to dendriplex treatments of up to 24 µg/ml (**Figure 30**).

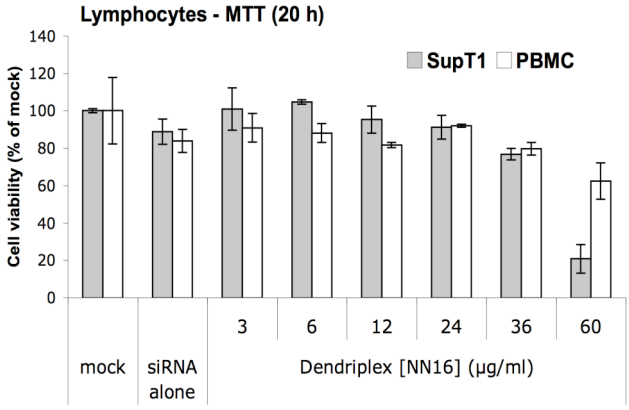

Figure 30. MTT reduction by SupT1 and PBMC treated with dendriplex at varying concentrations. (Values relative to untreated control cells)

4.5.1.1.3 Viability via flow cytometry

Cell viability was measured using flow cytometry where cells were deemed viable if they fell within the established area of healthy cells in size/complexity dot plots. The gates designating viable cells were established based on the average size and complexity of healthy control cells. **Figure 31** shows an example dot plot for

SupT1 cells treated with siP24-Cy3. The cells that were considered to be healthy all fell inside the gated region labeled "viable". In addition to determining percentage viability, transfection efficiency was determined by measuring only the "viable" cell population for fluorescence.

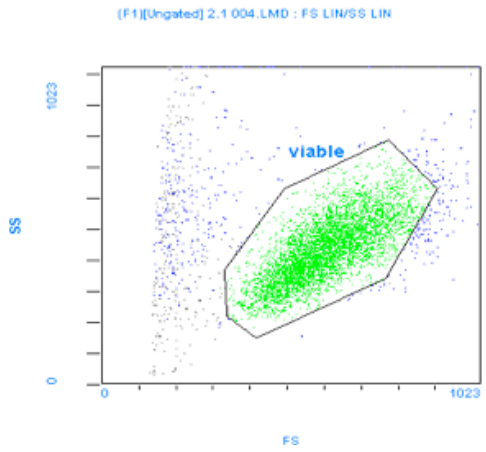

Figure 31. Example dot plot obtained from control cells indicating viable SupT1 cells.

Cells treated with varying concentrations of dendrimer or dendriplex were analyzed by flow cytometry to detect the percentage of events that fell within the healthy gates on the dot plot. Again results show that dendrimer alone is slightly more toxic than when complexed with siRNA (**Figure 32**). At higher dendrimer concentrations (above 25 µg/ml), more cell loss is detected at 24 h than at 3 h. The results mirror LDH toxicity results in that at 25 µg/ml, around 10% of the cell population cannot be deemed viable.

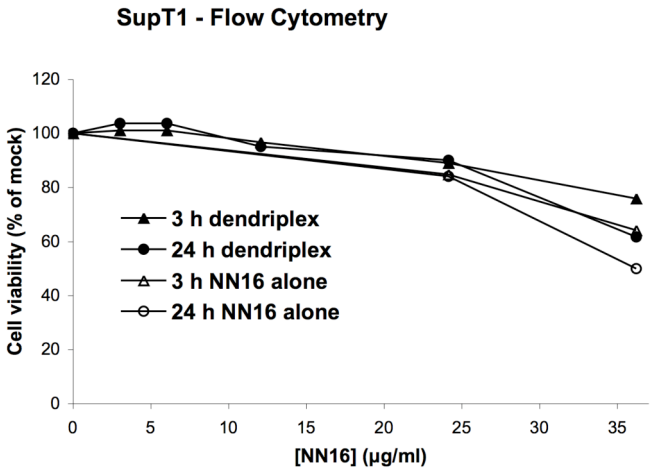

Figure 32. Percentage viable SupT1 cells after treatment with 2G-NN16 dendrimer alone or complexed with siRNA after 3 and 24 h determined from flow cytometry analysis.

4.5.1.1.4 Absolute cell counts

The results already described provided evidence that the structural integrity and metabolic function of cells were not damaged from treatment with 2G-NN16/siRNA dendriplex up to a certain concentration. However, more subtle effects on cells can be measured with simple cell counts and by measuring proliferation rates for samples undergoing treatment. Absolute cell counts were made by counting the cells contained in equal volumes of different samples through the use of a Neubauer slide and a light microscope. Results revealed that treatment with dendriplex caused a slight diminishing of total cell numbers with increasing dendrimer concentration (**Figure 33**).

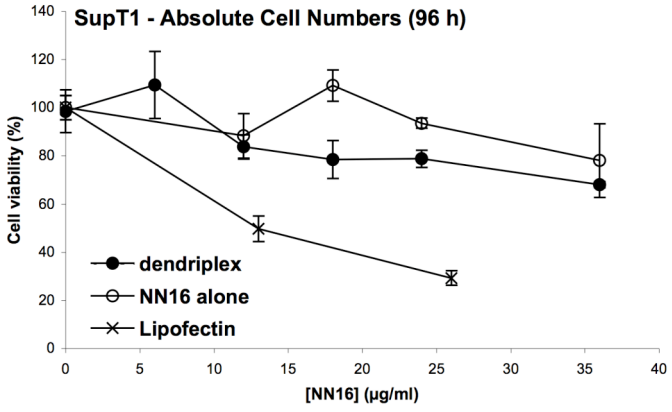

Figure 33. Cell counts 96 h after SupT1 cells were treated with dendrimer alone or complexed with siRNA. Lipofectin was utilized as a comparative control. (Results are from one experiment representative of various experimental repetitions)

4.5.1.1.5 Cell proliferation

As another method of quantifying cell numbers, a bromodeoxyuridine (BrdU) proliferation kit was utilized. This test corroborated the previous results showing that dendriplex did not induce proliferation in SupT1 cells after either 20 or 48 h (**Figure 34**).

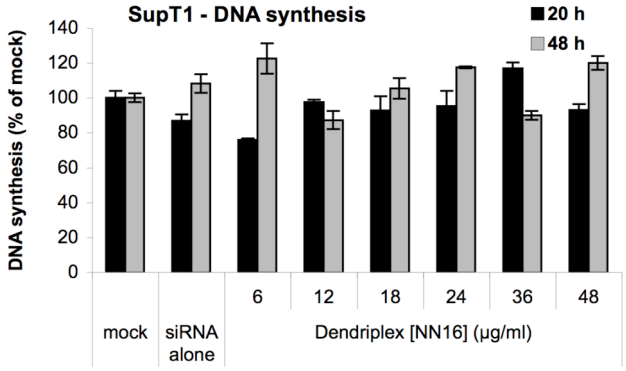

Figure 34. Proliferation in SupT1 cells treated with varying concentrations of dendriplex or siRNA alone (BrdU assay).

4.5.1.2 Effect on astrocytes

With the cytotoxicity levels of CBS dendrimers and dendriplexes on lymphocytes determined, next, the astrocytic cell line U87MG and NHA primary human astrocytes were tested. Being one of the prime cell types of the central nervous system infected by HIV, astrocytes are another candidate for antiviral siRNA therapy. If the treatment is able to cross the blood brain barrier and reach these cells, it must be able to achieve a biological effect without causing cytotoxicity. Therefore, several *in vitro* assays to determine the degree of cytotoxicity of the treatment on these cells were carried out.

4.5.1.2.1 LDH assay

LDH release was first tested with U87MG cells for 3, 5 and 24 h incubation times with varying concentrations of 2G-NN16 dendrimer alone (**Figure 35**). Despite

fluctuations for points at lower concentrations, the percentage LDH release relative to cells treated with Triton X-100 was almost always below 10% for all time points and dendrimer concentrations.

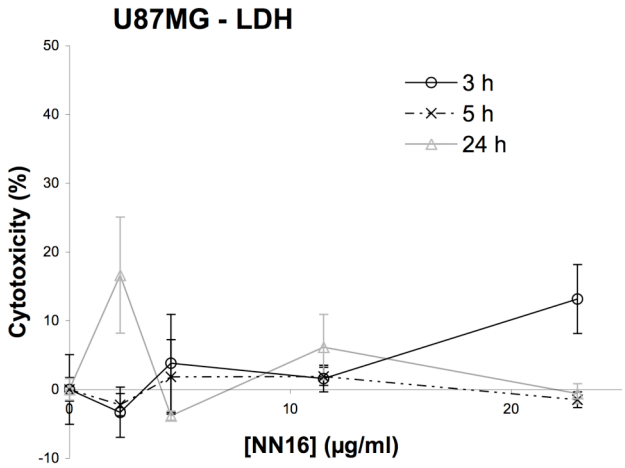

Figure 35. LDH release from U87MG cells 3, 5 and 24 h after being treated with 2G-NN16 dendrimer alone. (Values are relative to cells treated with Triton X-100)

4.5.1.2.2 MTT assays

Mitochondrial function for U87MG cells and NHA primary cells treated with CBS dendrimer was measured. Results for MTT assays with U87MG cells showed that the dendrimer did not negatively affect the metabolic function of the cells up to concentrations of nearly 25 µg/ml for incubation times of 24 or 72 h (**Figure 36**).

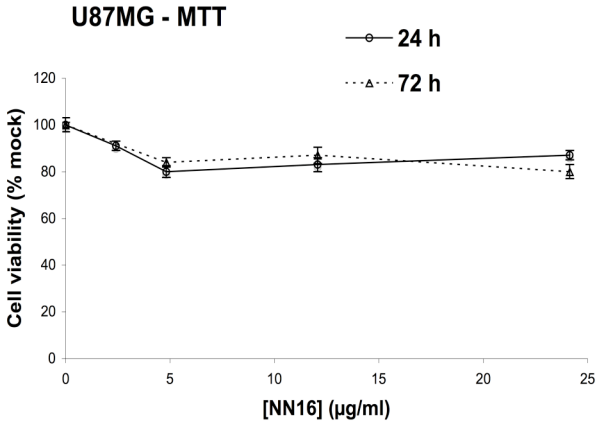

Figure 36. MTT reduction by U87MG after 24 or 72 h incubation with dendrimer alone at varying concentrations.

When these same cells were tested with four different siRNAs either alone or complexed with 2G-NN16 at a dendrimer concentration of 24 µg/ml, metabolic function remained stable up through 72 h (**Figure 37**).

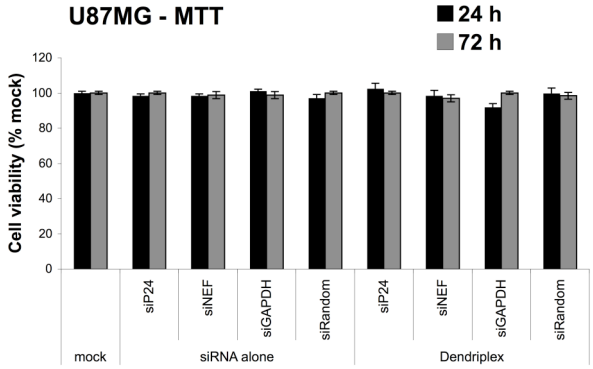

Figure 37. MTT reduction by U87MG cells treated with siRNA alone (250 nM) or complexed with dendrimer (+/- ratio, 8; [2G-NN16] = 24 µg/ml).

Similarly, primary NHA human astrocytes retained proper mitochondrial function when treated with the same dendrimer concentrations after either 24 or 72 h (**Figure 38**).

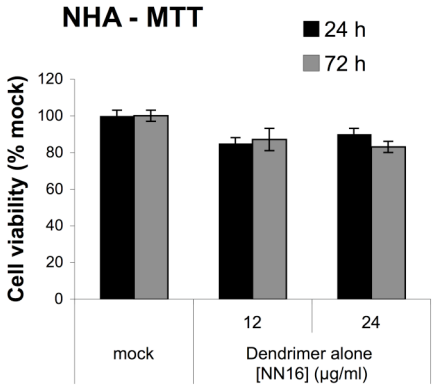

Figure 38. MTT assay shows the toxic effect of 2G-NN16 dendrimer alone on NHA cells after 24 or 72 h incubations.

4.5.1.2.3 Cell proliferation

Utilizing the same test that was used with lymphocytes, U87MG astrocytes were tested for cell proliferation by quantification of BrdU incorporation in the newly synthesized DNA of replicating cells. The measurements were assessed relative to

results for untreated cells. In spite of a slight increase in cell proliferation for dendrimer concentrations above 25 µg/ml, the results show that dendrimers at working concentrations had little effect on cell proliferation and indeed did not cause a reduction in cell replication (**Figure 39**). These data are further evidence of a lack of cytotoxicity by the CBS dendrimer 2G-NN16.

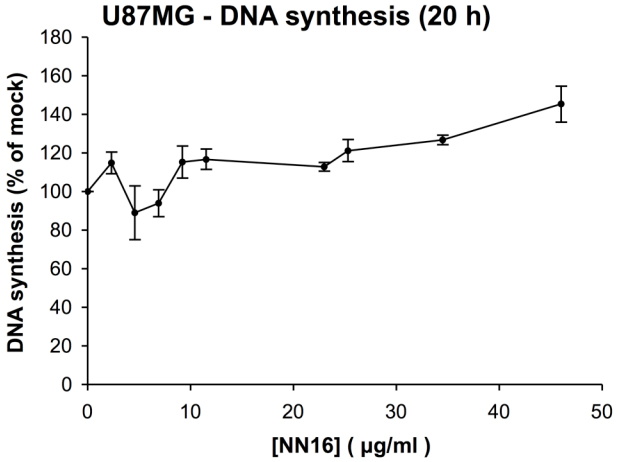

Figure 39. Proliferation in U87MG cells 20 h after treatment with varying concentrations of 2G-NN16 alone as measured by incorporation of BrdU in newly synthesized DNA (BrdU assay).

4.5.1.2.4 Microarray gene profiles for dendrimer-treated U87MG

The effect of 2G-NN16 in U87MG global gene expression profile was studied using Agilent 4x44K whole genome human microarrays. Analysis of microarrays from U87MG exposed to 23µg/ml (5µM) 2G-NN16 compared to control U87MG did not reveal any statistically significant gene expression variation, as the lowest adjusted *p*-value obtained by Limma-software was 0.66 (**Figure 40**). The lack of variation in the gene expression profile from control cells gave further evidence that 2G-NN16 did not negatively effect the astrocytic cell line in any way. Furthermore, as no gene inducing apoptosis or cell cycle arrest was seen to be over-expressed or under-expressed, the likelihood of more long-term detrimental effects from the dendrimer treatment was minimal.

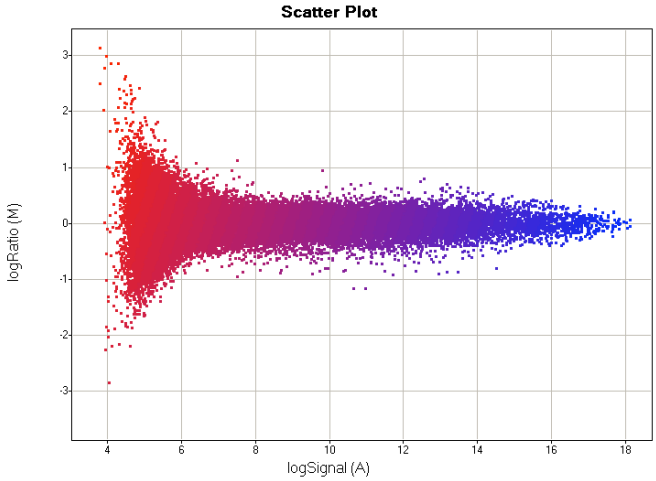

Figure 40. Microarray scatter plot shows no statistically significant gene expression variation. *(p≥0.66)*

4.5.1.3 Effect on erythrocytes

4.5.1.3.1 Hemolytic activity

The possible cytotoxic effects dendrimers could have on erythrocytes were measured by detecting erythrocyte membrane rupture and release of hemoglobin by colorimetric tests. As with other cytotoxicity tests, the release of hemoglobin was relatively low up to a dendrimer concentration well above 25 µg/ml (**Figure 41**). Also, as with other tests, siRNA/2G-NN16 dendriplexes exerted less of an effect on the cells than dendrimer alone.

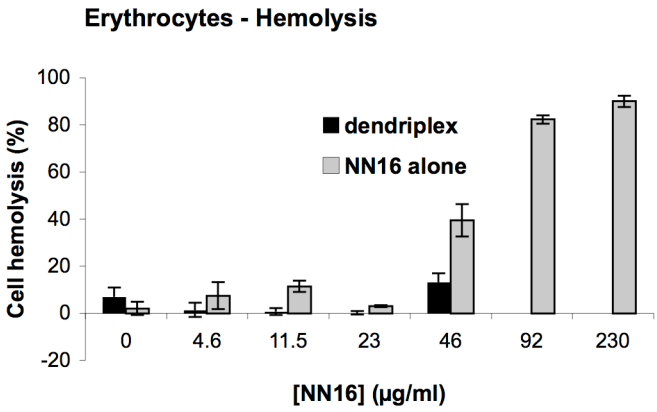

Figure 41. Graphical representation of hemoglobin released from erythrocytes 1 h after being treated with dendrimers or dendriplexes at varying concentrations. (Values are relative to cells treated with Triton X-100)

4.5.2 Cytotoxicity of polymers

Experiments on the cytotoxicity of PEI-PEG copolymers on several cell types were also carried out. In tests similar to those carried out on dendrimers, mitochondrial function, membrane rupture, cellular aggregation and cellular viability were assayed using lymphocytes, erythrocytes and murine fibroblasts.

4.5.2.1 Effect on L929 mouse fibroblasts

4.5.2.1.1 MTT assays

Following an incubation time of 24 h with varying concentrations of polymers, including PEI(25k), PEI(25k)-PEG$(550)_{30}$ and other copolymers possessing characteristics similar to the copolymers used throughout the remainder of this study, the mitochondrial activity was measured revealing an approximate toxicity limit for each polymer tested. The polymer with the greatest toxic effect on these cells was the unmodified PEI(25k) (**Figure 42**). The unshielded charged amines of the PEI likely caused more damage to the cells being tested. In contrast to PEI(25k), the copolymer with the largest PEG moiety engraftment, PEI(25k)-PEG$(30k)_1$, and the one with the largest number of PEG moieties, PEI(25k)-PEG$(550)_{30}$, were around ten fold less toxic. The copolymer with PEG moieties of 5 kDa, PEI(25k)-PEG$(5k)_2$, showed cytotoxicity at levels falling between the toxicity limits for the ungrafted and the highly grafted copolymers. This higher toxicity is likely caused by the fact that only two PEG engraftments of 5 kDa in size are not sufficient to shield all the charged amines of the PEI and protect the cells from the damage caused by interaction with the positive charges.

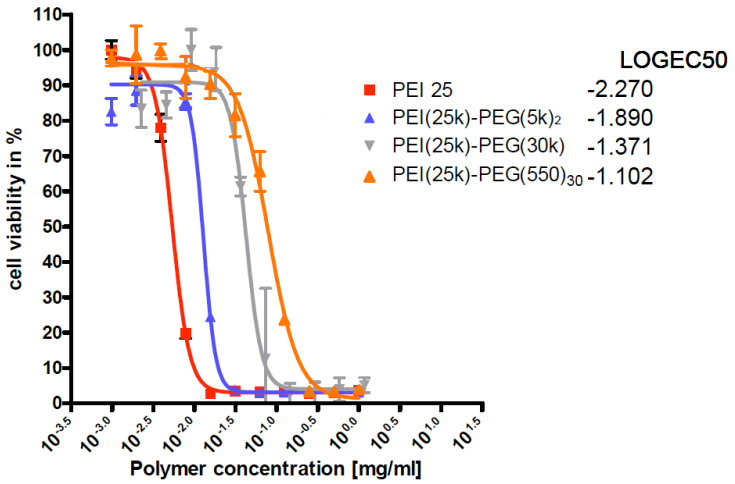

Figure 42. MTT reduction by L929 fibroblasts after treatment with polymers. The value for the median effective concentration required to produce an effect of 50% toxicity (EC50) was calculated from the regression curves applied to the toxicity results and is reported in the graph legend.

4.5.2.2 Effect on Lymphocytes

4.5.2.2.1 LDH assays

4.5.2.2.1.1 LDH release by SupT1

Next, the cytotoxicity of all the polymers was tested on lymphocytes, the main cell type susceptible to HIV infection. As these cells would be the primary target for an anti-HIV therapy involving siRNA delivered with either dendrimers or polymers, it was important to establish what the cytotoxicity limits were for each possible drug delivery candidate. It was also a way to compare different methods of improving the biocompatibility of the polymers via PEGylation. PEGylation can make up for the slightly lower efficiency at siRNA complexation it causes by reducing the overall toxic effects caused by the polymer. Therefore, higher concentrations of PEG-grafted polymers can be utilized without causing the same level of cytotoxicity. Upon comparing the cytotoxicity caused after 3 h incubation with polyplexes composed of siRNA and each of five different polymers on SupT1 cells via LDH assays, a clear trend appeared (**Figure 43**). Un-grafted PEI(25k) polymer exerted the highest toxicity, as was to be expected. But as the number of PEG moieties grafted to the polymer increased and the size of the PEG moieties decreased, the toxic effect subsided. PEI(25k)-PEG(20k)$_1$ was only slightly less toxic than similar concentrations of un-grafted PEI(25k). However, PEI(25k)-PEG(5k)$_4$, PEI(25k)-PEG(2k)$_{10}$, and PEI(25k)-PEG(550)$_{30}$ caused gradually decreasing cytotoxicity when polyplexes containing these polymers were incubated with the SupT1 cells.

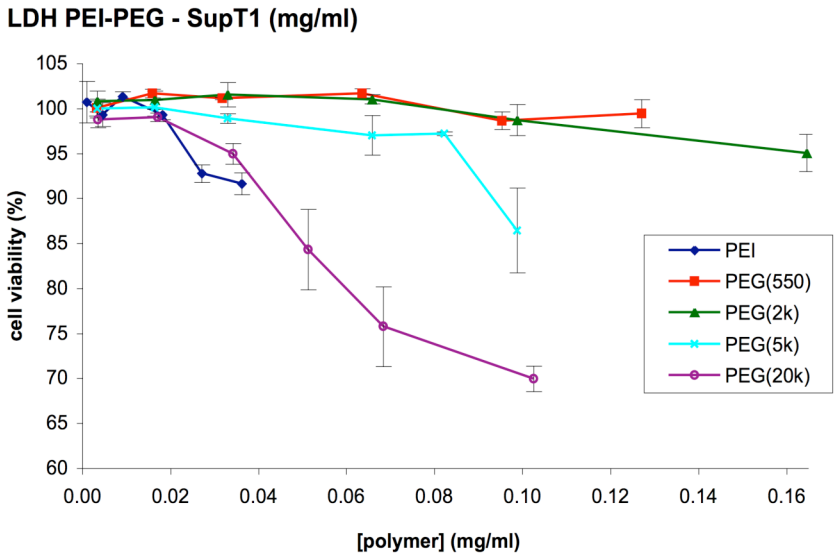

Figure 43. LDH release from SupT1 cells 3 h after being treated with PEI-PEG/siRNA polyplexes as a function of PEI-PEG polymer concentration (mg/ml). N/P ratios were constant for all concentrations: PEI, N/P=5; all PEI-PEG copolymers, N/P=10. (Cell viability was determined by LDH release relative to untreated cells, and 0% viability was established by cells treated with Triton X-100)

Different polymers with different PEG moieties can complex siRNA with more or less effectivity and likewise cause higher or lower levels of cytotoxicity. **Figure 44** shows how the cytotoxicity of the different polymers correlates to the quantity of siRNA in each treatment. Since all treatments for each polymer were mixed with siRNA at the same N/P ratio according to the optimal results in complexation and condensation studies, the concentration of polymer contained in each treatment was directly proportional to the concentration of siRNA. These results show that for treatments containing the maximum amount of siRNA that is likely necessary to achieve a biological effect (0.5 µM), the polyplex causes no cytotoxicity for any of the polymers. In fact, for all the polymers except for PEI(25k)-PEG(20k)$_1$ up to five times that concentration still did not cause cytotoxicity, and for PEI(25k)-PEG(20k)$_1$, two times the effective concentration could be safely administered.

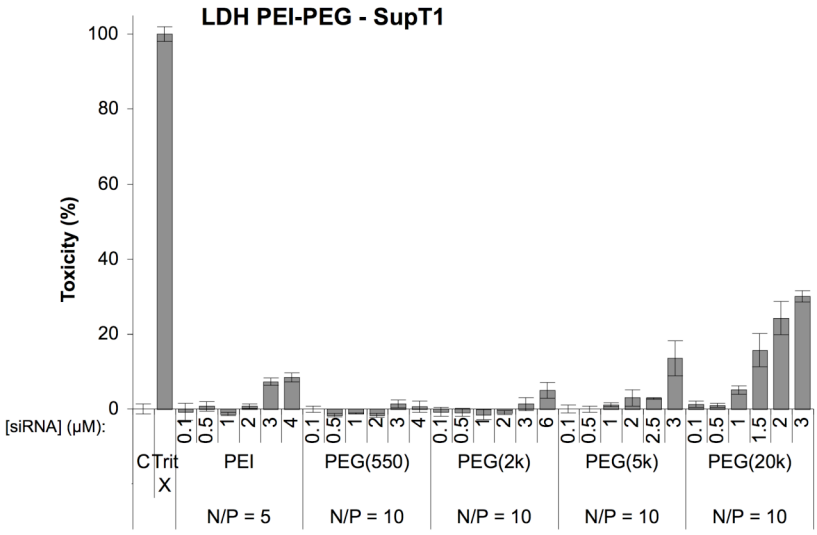

Figure 44. LDH release from SupT1 cells 3 h after being treated with polyplex as a function of siRNA concentration. N/P ratios were constant for all concentrations: PEI, N/P=5; all PEI-PEG copolymers, N/P=10. (Values are relative to cells treated with Triton X-100)

4.5.2.2.1.2 LDH release by PBMC

With the extent of membrane rupture caused by the PEI-PEG polymers on SupT1 cells established, next, LDH assays were carried out to measure the same effect on primary PBMCs. A similar trend was observed with these cells (Figure 45). Once again, PEI(25k) and PEI(25k)-PEG(20k)$_1$ were more toxic than the more highly grafted copolymers. PEI(25) was the most toxic, while PEI(25k)-PEG(550)$_{30}$ was the least.

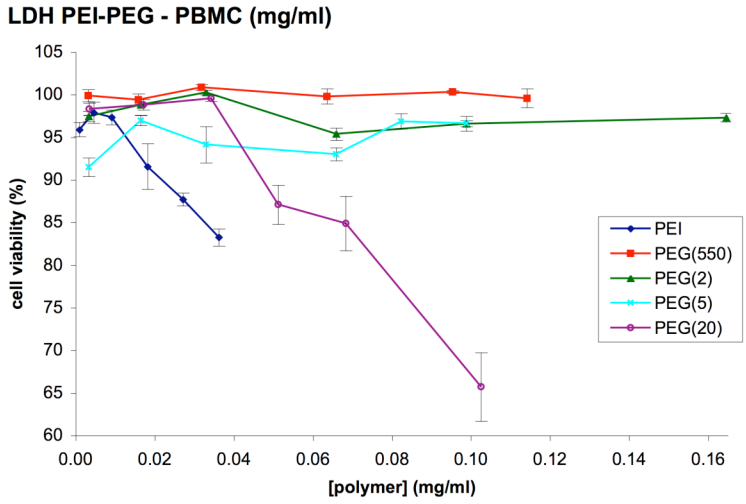

Figure 45. LDH release from PBMC primary cells 3h after being treated with PEI-PEG/siRNA polyplexes as a function of PEI-PEG polymer concentration (mg/ml). N/P ratios were constant for all concentrations: PEI, N/P=5; all PEI-PEG copolymers, N/P=10. (Cell viability was determined by

LDH release relative to untreated cells, and 0% viability was established by cells treated with Triton X-100)

Unsurprisingly, the results showed that PBMC were not more susceptible to toxic effects than the established cell line, SupT1, as treatments necessary to deliver working concentrations of siRNA all fell below the toxicity limit of 10% (**Figure 46**).

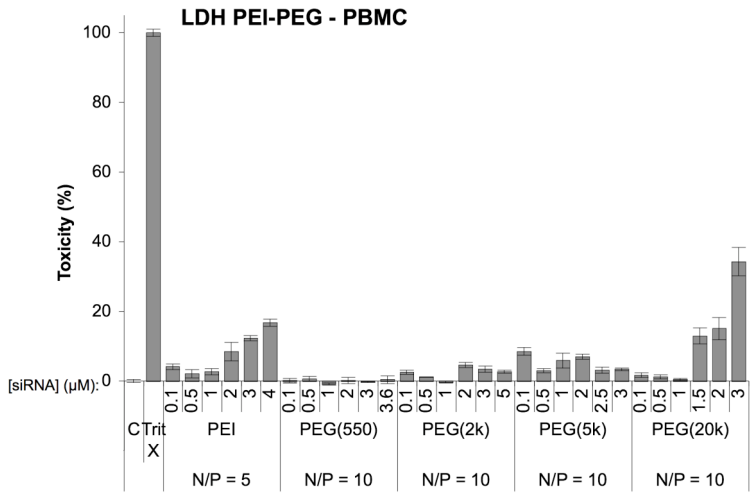

Figure 46. LDH release from PBMC primary cells 3 h after being treated with polyplex as a function of siRNA concentration. N/P ratios were constant for all concentrations: PEI, N/P=5; all PEI-PEG copolymers, N/P=10. (Values are relative to cells treated with Triton X-100)

4.5.2.2.2 Viability via Flow Cytometry

4.5.2.2.2.1 Viability of SupT1

Utilizing the same criteria for determining the cell viability as for flow cytometry experiments with dendriplex, percentages of viable cells was measured after treatments with varying polyplex concentrations. In these experiments, the siRNA concentration was held constant at 500 nM while the N/P ratio was varied resulting in a range of polymer concentrations in the polyplex treatments. With SupT1 cells, viability did not drop below 90% of control values after 24 h of incubation with the treatments for any of the polymers at all N/P ratios tested except for the highest N/P values each for PEI(25k) (N/P = 15) and PEI(25k)-PEG(20k)$_1$ (N/P = 20) which resulted in viability of 76% and 77%, respectively (**Figure 47**). PEI(25k) also seemed to have a more rapid effect on the cells as the polymer at an N/P value of 15 resulted in less than 70% viability after only 3 h.

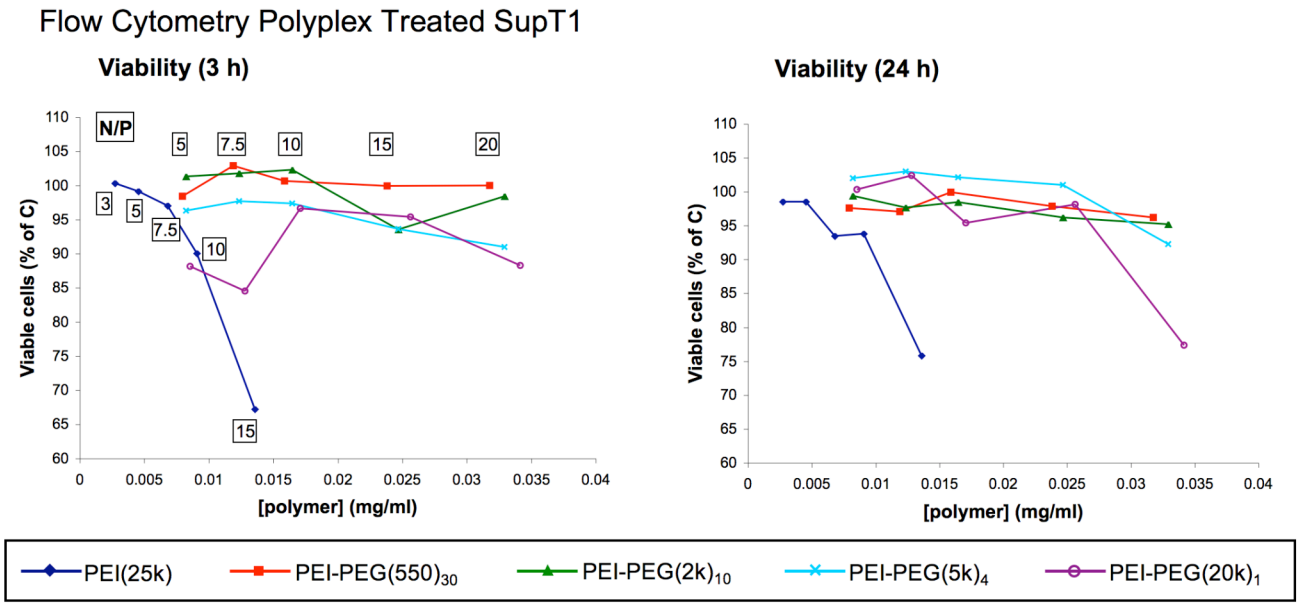

Figure 47. Graphs showing flow cytometry results for SupT1 cells 3 h (left) and 24 h (right) after treatment with polyplexes of varying concentration. Cell viability is based on viability gates in size/complexity dot plots (see **Figure 31**). Values are relative to untreated cells. [siP24-Cy3] = 500 nM; N/P ratios indicated in 3 h graph for all PEI-PEG copolymers in upper boxes and for PEI in lower boxes.

4.5.2.2.2.2 Viability of PBMC

As for PBMC, these cells were more susceptible to damage caused by the treatments with polyplexes. After only 3 h incubation, the cell viability was detected to drop below 90% for the same treatments that were seen to be toxic for SupT1 after 24 h, as well as the treatment of PEI(25k)-PEG(20k)$_1$ at an N/P ratio of 15. After 24 h incubation, the N/P ratio of 10 for PEI(25k)-PEG(20k)$_1$ also resulted in a cell viability slightly below 90% (86%), and the highest two N/P ratios (15 and 20) for both PEI(25k)-PEG(2k)$_{10}$ and PEI(25k)-PEG(5k)$_4$ also caused the cell viability to drop below 90% (**Figure 48**).

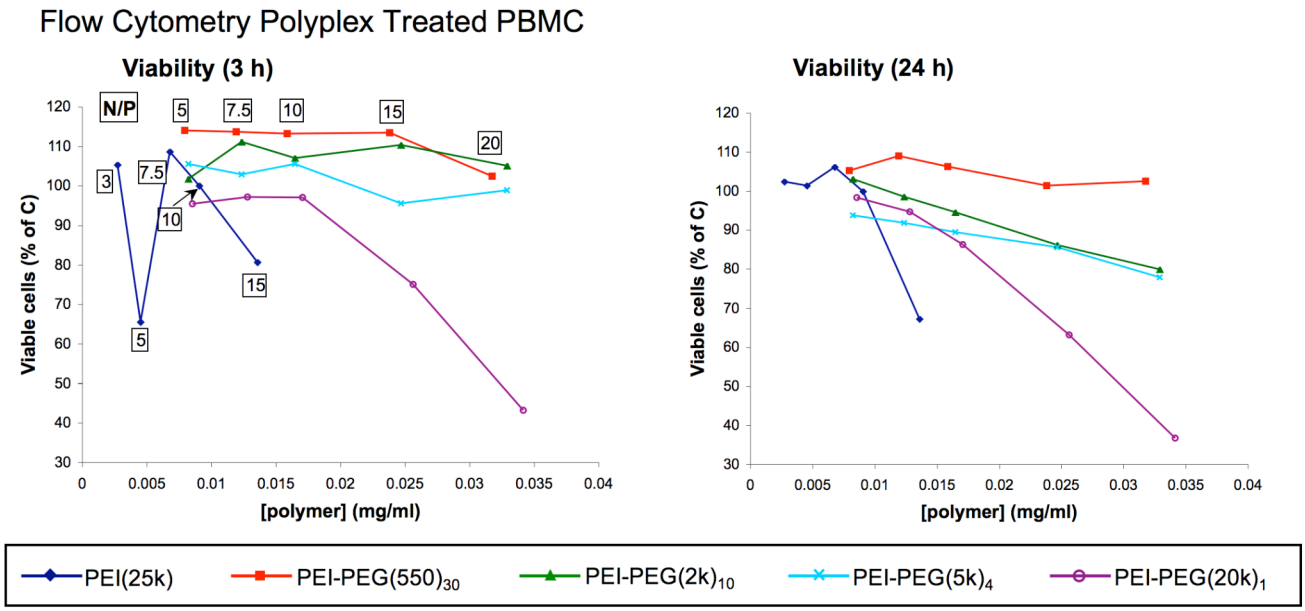

Figure 48. Graphs showing flow cytometry results for PBMC cells 3 h (left) and 24 h (right) after treatment with polyplexes of varying concentration. Cell viability is based on viability gates on size/complexity dot plots (see **Figure 31**). Values are relative to untreated cells. [siP24-Cy3] = 500 nM; N/P ratios indicated in 3 h graph for all PEI-PEG copolymers in upper boxes and for PEI in lower boxes.

4.5.2.3 Effect on erythrocytes

4.5.2.3.1 Hemolytic activity

As had been done with dendrimers, erythrocytes were utilized to determine cytotoxic effects on blood cells other than lymphocytes. The cytotoxicity was measured by release of hemoglobin as a result of cell membrane rupture. Similar to cytotoxicity results already obtained, PEI(25k) had the greatest cytotoxic effect, while the PEG grafted copolymers showed a negligible release of hemoglobin (**Figure 49**).

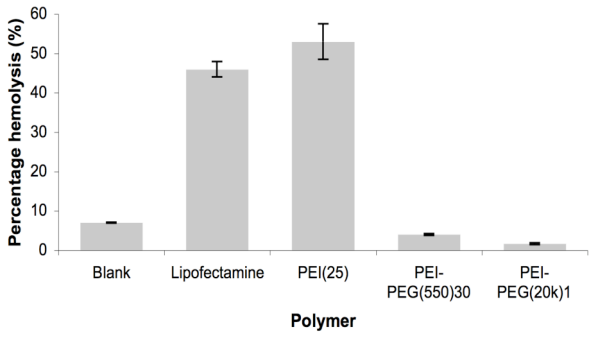

Figure 49. Percentage of erythrocyte hemolysis after treatments with polymers alone.

4.5.2.3.2 Erythrocyte aggregation

In addition to detecting erythrocyte rupture and the release of hemoglobin, these cells were assayed for more subtle effects, which can be seen when multiple cells aggregate or clump together. Erythrocyte aggregation occurs from slight morphological defects in the cells caused by the interaction with the molecules of a treatment and can result in problems in blood viscosity and microcirculation. Testing for erythrocyte aggregation is a good method for determining if a pharmaceutical will be toxic when used *in vivo* even if *in vitro* cytotoxicity results come up negative. Erythrocytes were treated with three of the five copolymers without siRNA and examined under a light microscope to detect aggregation and morphological changes in the cells **(Figure 50).** Treatment with PEI(25k) resulted in the most aggregation, while treatments with PEI(25k)-PEG$(550)_{30}$ or PEI(25k)-PEG$(20k)_1$ caused minimal aggregation and slight morphological deformity. When compared with cells treated with Lipofectamine, however, the copolymer treated cells appeared to be much less affected, as the Lipofectamine treated cells possessed a high percentage of poikilocytes with a large degree of deformation.

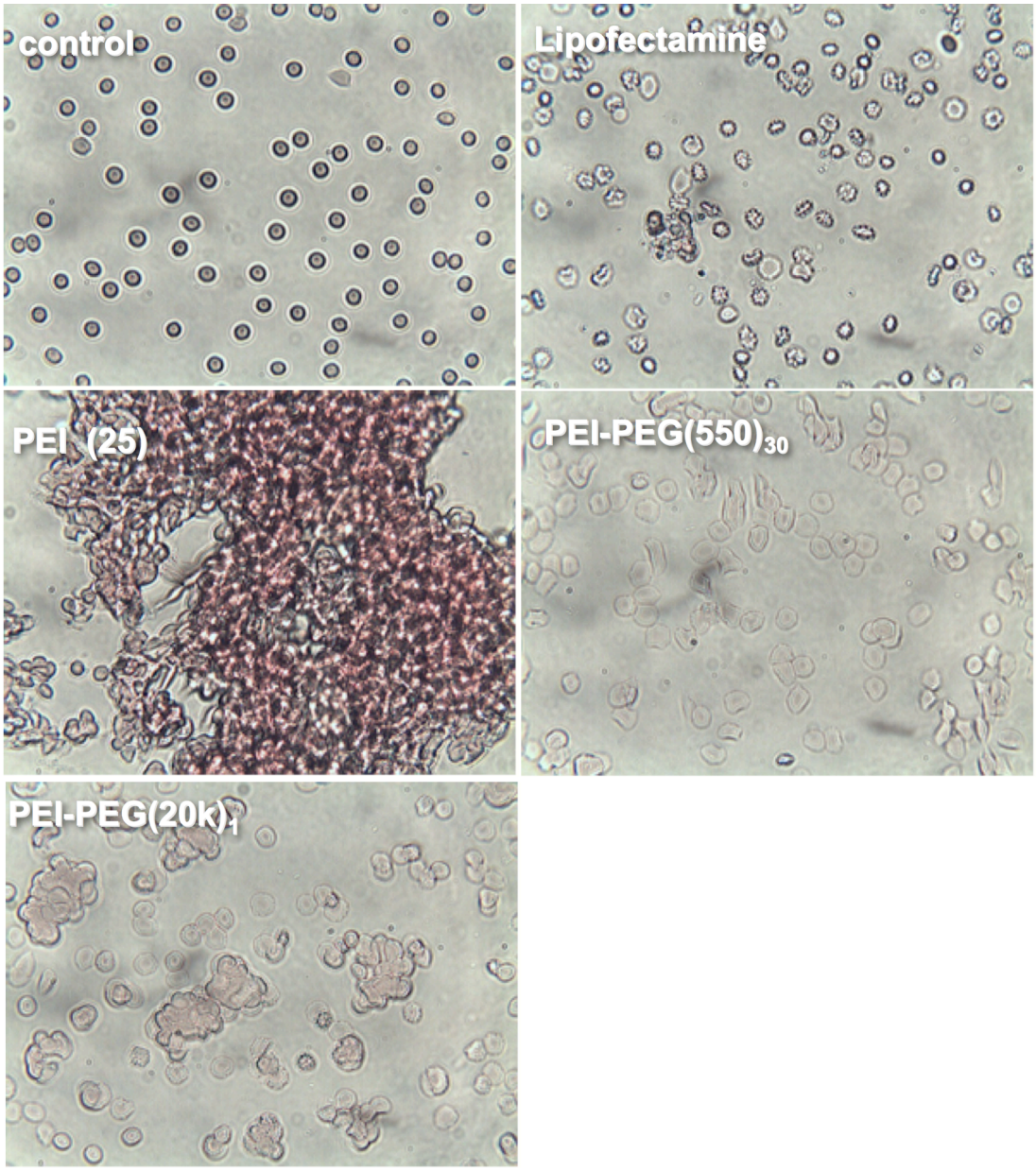

Figure 50. Erythrocyte aggregation when treated with polymers alone. Untreated cells and Lipofectamine treated cells were used as comparative controls.

4.6 Transfection efficiency

4.6.1 Dendriplex

4.6.1.1 Uptake by lymphocytes

4.6.1.1.1 Uptake by SupT1

Flow cytometry was used to detect the entrance of fluorochrome-labeled siRNA either alone or complexed with 2G-NN16 dendrimer into viable SupT1 cells.

At 3 h, the highest transfection efficiency was interestingly detected for siRNA alone and at +/- charge ratios of 2 and 1 (86, 84 and 81%, respectively) (**Figure 51A**). For higher +/- charge ratios, not only a lower transfection efficiency was measured, but also a diminished quantity of viable cells were seen inevitably due to toxic effects. By 24 h, the percentages of successfully transfected cells for all treatments with siRNA were all 100%, and the intensity of fluorescence emitted by the cells was substantially higher, as could be seen by the shift to the right of the histograms and according to x-median values (data not shown), indicating a large quantity of siRNA in the interior of each cell (**Figure 51B and C**). Note that B is an overlay plot of the data shown in A. Nearly identical results were obtained when PBMC were tested instead of SupT1 (data not shown).

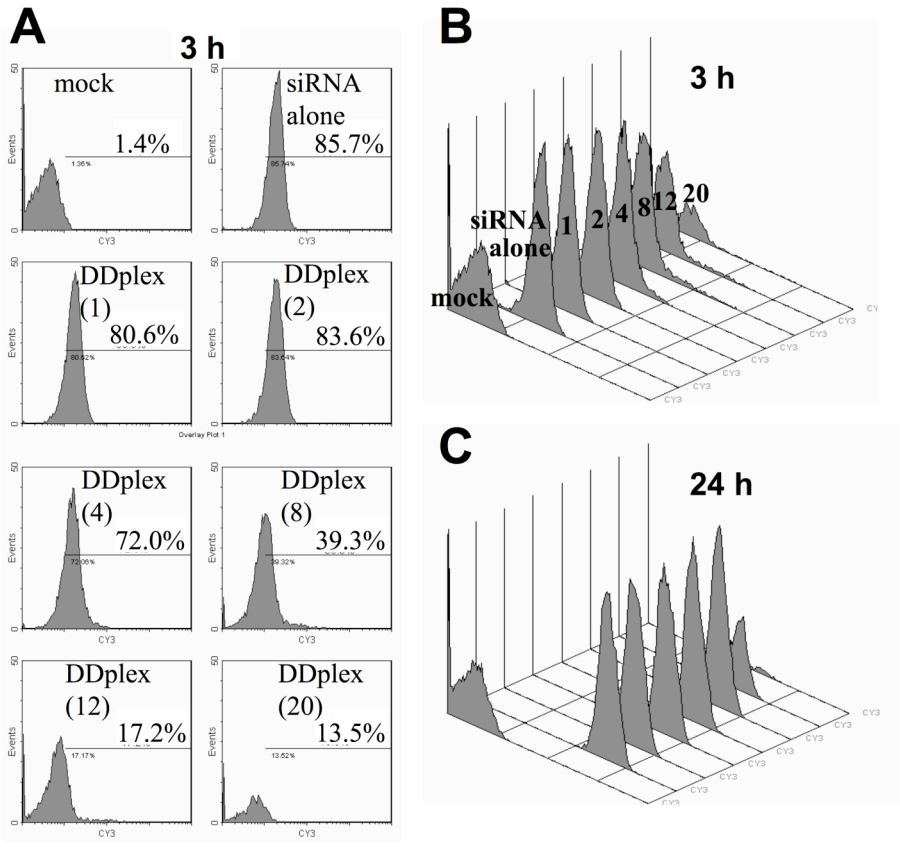

Figure 51. Histograms show successful transfection by dendriplex. Transfection efficiency is shown by flow cytometry of SupT1 cells 3 h after treatment with siRNA or dendriplexes (A) (+/- charge ratio indicated in parentheses) and overlay plots for all samples at both 3 (B) and 24 h (C). 500 nM siRNA for all points.

4.6.1.1.2 Uptake by HIV-infected PBMC

Next, toxicity and transfection efficiency were tested for siRNA and dendriplex treatments on HIV-infected PBMC. At 3 h, unlike with the SupT1 cells, naked siRNA was unable to enter the PBMC, but when complexed with 2G-NN16 successful transfection was obtained with a maximum at +/- ratio of 2 (41%) **(Figure 52A**). Despite this difference, toxicity profiles for these cells mimicked the results for SupT1. By 24 h, much higher transfection efficiency was seen for naked siRNA as well as +/- ratios of 1 and 2. Lipofectin® also exhibited higher transfection efficiency at 24 h compared to 3 h, however not to the extent of 2G-NN16 **(Figure 52B**). The percentage of viable cells was lower as a whole for these cells, as a result in part of the HIV infection, but no substantial difference was detected between control cells and those treated with dendriplex. Meanwhile, Lipofectin® exhibited a larger decrease in cell viability compared to the control cells.

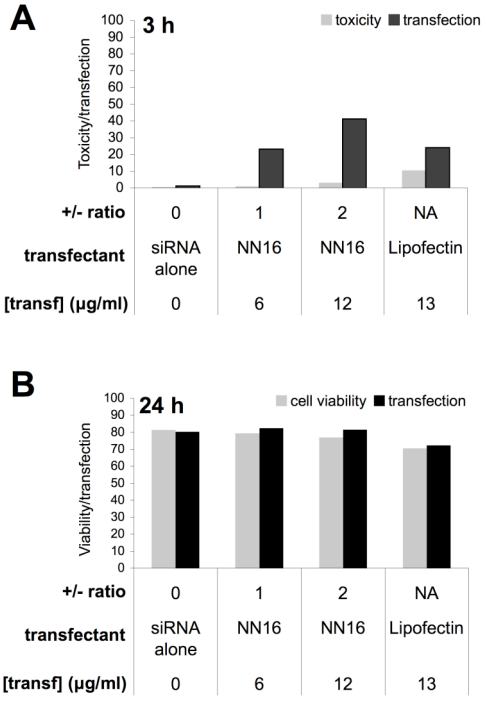

Figure 52. Transfection and toxicity profiles of dendriplexes on HIV-infected PBMC. Dendriplex at varying +/− charge ratios after 3 h incubation (A) and 24 h incubation (B). Toxicity was measured by LDH enzyme release (A), while transfection and cell viability was measured by flow cytometry (B). Lipofectin® was used as a comparative control for both toxicity and transfection.

4.6.1.2 Uptake by astrocytes

U87MG cells showed positive results for transfection with dendriplexes made of 2G-NN16 and Cy3-labeled siRNA. **Figure 53** indicates the percentage of viable cells with detectable fluorescence as measured via flow cytometry after 3 h for cells treated with 250 nM sP24-Cy3 alone or in dendriplex at +/- charge ratios of 2, 4, or 8. The highest transfection rate after this short time period corresponds with the highest +/- charge ratio for the dendriplex (i.e. the highest concentration of 2G-NN16). Unlike for lymphocytes, neither a lower +/- charge ratio such as 2 nor siRNA alone showed high positive transfection of the astrocytoma cells after only 3 h. With lymphocytes, the exact opposite trend had been observed.

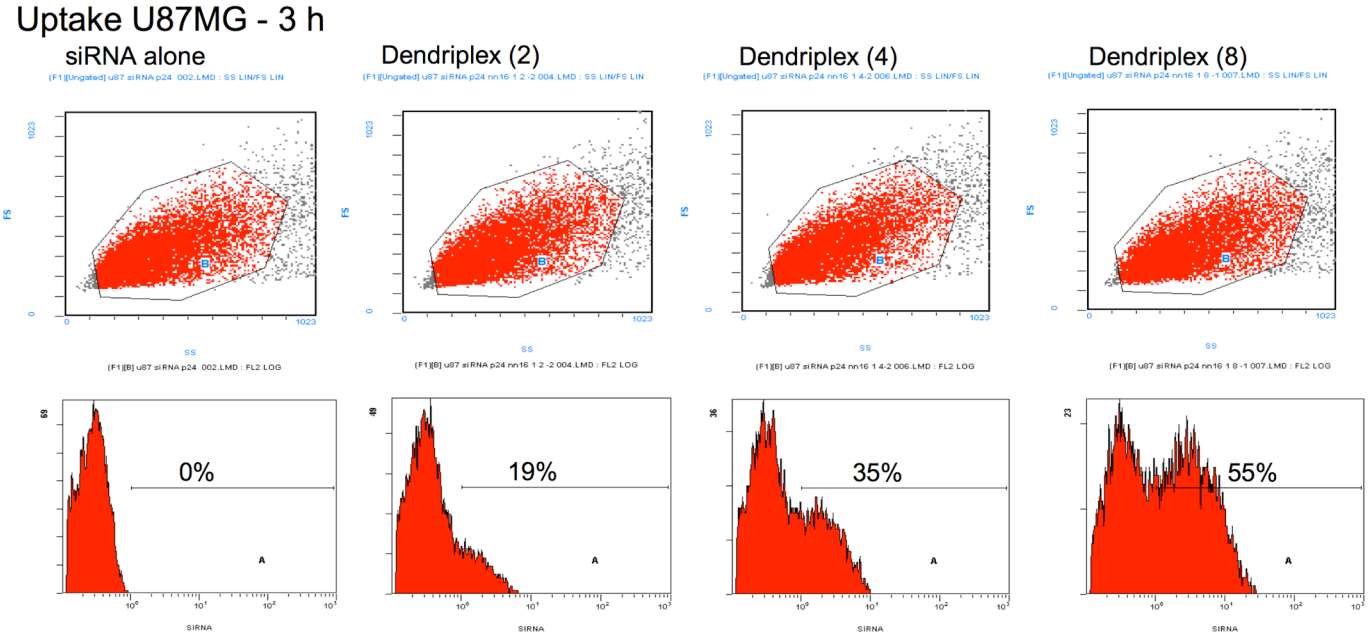

Figure 53. Dot plots and histograms indicate percentage uptake by viable U87MG cells 3 h after treatment with dendriplex of varying +/- charge ratios. ([siRNA] = 250 nM; +/- charge ratio indicated in parentheses)

Regardless of these differences, after 18 h, all treatment samples (siRNA alone or in dendriplex at +/- charge ratios of 2, 4 or 8) showed very high levels of transfection. **Figure 54** shows that 90% of all viable U87MG cells showed siP24-Cy3 uptake regardless of the amount of 2G-NN16.

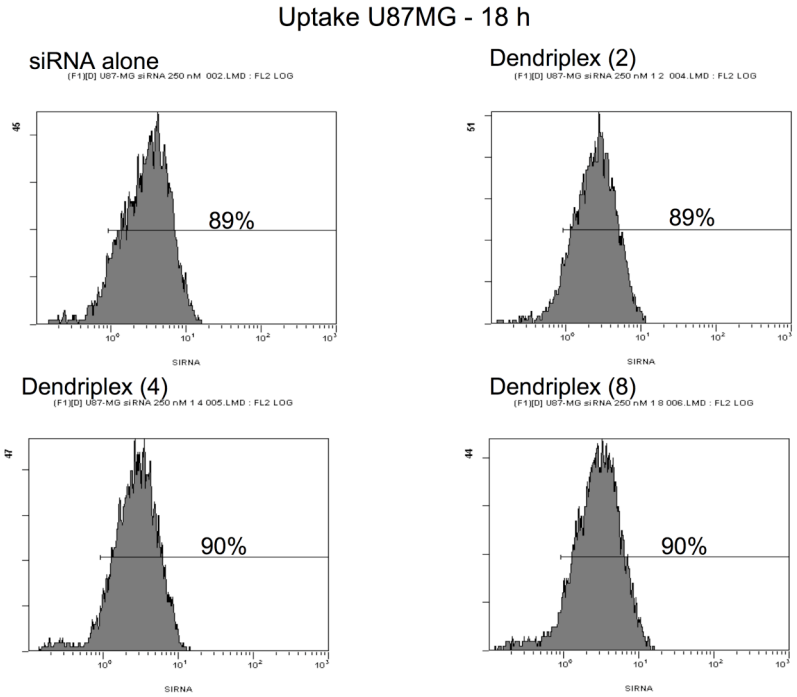

Figure 54. Histograms show successful transfection of U87MG cells 18 h after treatment with siRNA alone or dendriplexes at varying +/- charge ratios. ([siRNA] = 250 nM; +/- charge ratio indicated in parentheses)

In addition to achieving uptake in a high percentage of astrocytoma cells, the quantity of siRNA that was taken up by the cells was measured by quantifying the average intensity of the fluorescence for each cell showing sufficient fluorescence to be considered positive for siRNA uptake. This value, referred to as the x-median of fluorescence, appeared to increase as the +/- ratio of dendrimer to siRNA increased for dendriplex-treated cells when measured after 3 h (**Figure 55**). The highest +/- ratio tested was 8 and showed an equally high level of fluorescence intensity as cells treated with Lipofectin®. This indicates that dendriplexes were successful at transfecting siRNA into astrocytoma cells, and that a high amount of siRNA reached the interior of the cell when complexed with 2G-NN16. The importance of this is highlighted by the fact that the biological function of siRNA takes place in the cytoplasm, where the two strands of the siRNA are separated and incorporated into the RISC complex.

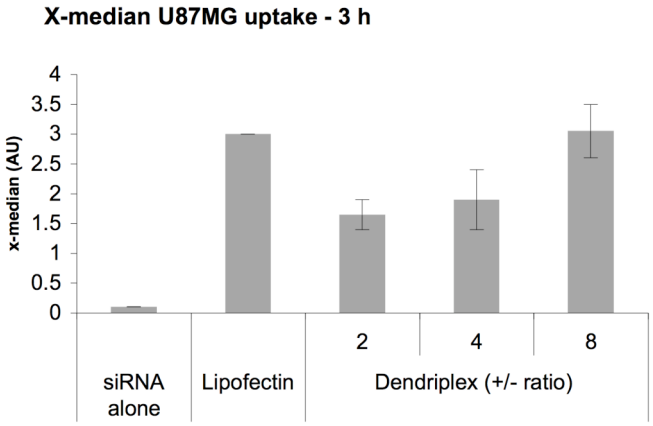

Figure 55. X-median of fluorescence intensity in U87 cells 3 h after treatment with dendriplexes. Lipofectin® was used as a comparative control. (Values represent the average intensity of fluorescence among all viable cells that show sufficient fluorescence intensity to be considered positive for siRNA uptake ($\geq 10^0$); [siRNA] = 250 nM)

4.6.2 Polyplex

4.6.2.1 Uptake by lymphocytes

4.6.2.1.1 Uptake by SupT1 and PBMC

To initially test transfection efficiency of the various PEGylated polymers, polyplexes made of polymers and Cy3-labeled siRNA were administered to either SupT1 cells or PBMC, and samples were collected and analyzed by flow cytometry after 3 or 24 hours to detect cells emitting fluorescence indicating a positive uptake of siRNA. All treatments were made with a constant concentration of siP24-Cy3 (500 nM), but the polymer concentrations varied as a scale of N/P ratios was tested. All the polymers were tested at N/P ratios of 5, 7.5, 10, 15 and 20 except PEI(25k) which was tested at N/P ratios of 3, 5, 7.5, 10 and 15 because of its better efficiency at complexing siRNA and since it had exhibited higher cytotoxicity in previous experiments. Cells were washed with glycine acid to remove any siRNA bound to the exterior of the cell membrane prior to being analyzed with the flow cytometer.

Figure 56A and **B** show the flow cytometry results for polyplex-treated SupT1 cells and PBMC, respectively. For all the polymers in both cell lines and following both short and long incubation times, the transfection efficiency increased with increasing N/P ratios (except for PEI-PEG(5k)$_4$ in SupT1 at 3 h which did not transfect the cells at any N/P ratio). This is possibly because a higher ratio of polymer to siRNA resulted in a more stable polyplex. Another possibility was that the

polyplexes of higher N/P ratios were more easily endocytosed by the cells because of the greater net positive charge. A third possibility is that the higher rate of uptake was a result of more cellular damage caused by the higher polymer concentrations. In general, there was a direct correlation between transfection efficiency and decreased cellular viability.

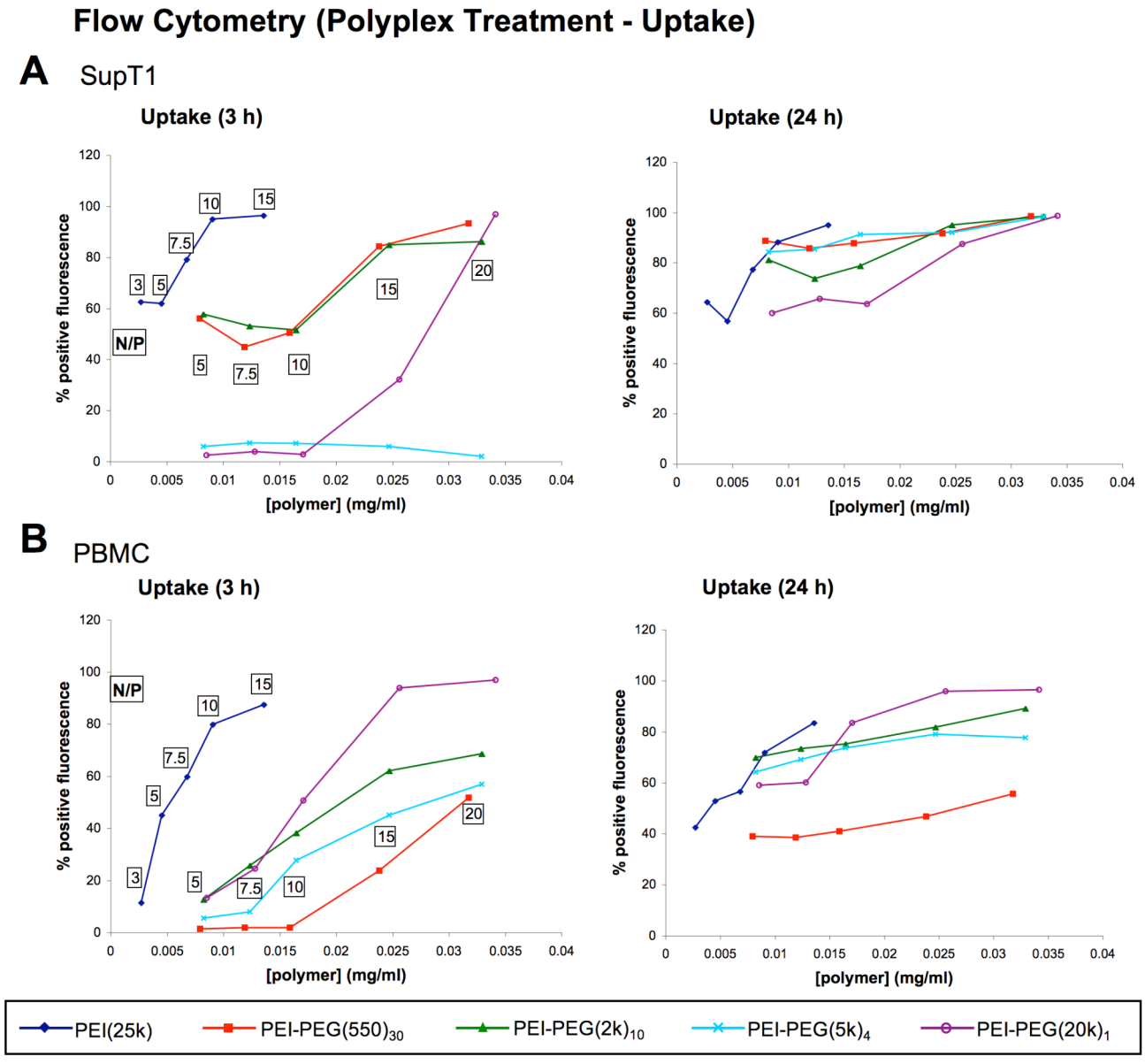

Figure 56. Graphs showing flow cytometry results for uptake of siP24-Cy3 by SupT1 cells (A) and PBMC (B) for 3 h (left) and 24 h (right) after treatment with polyplexes of varying concentration. Values are relative to untreated cells. [siP24-Cy3] = 500 nM; N/P ratios indicated in each 3 h graph for PEI in upper boxes and for all PEI-PEG copolymers in lower boxes.

PEI(25k) generally showed higher uptake than the rest of the polymers at 3 hours, but by 24 hours, it was no more effective than the others. Furthermore, its effect on cellular viability reached a detrimental level at concentrations lower than those for the other polymers (**Figure 47**). This is inevitably due to its higher charge density and lack of PEG molecules to damper its effect. The only other polymer that caused a significant effect on cellular viability was PEI-PEG(20k)$_1$, as the other three polymers did not exert much of a negative effect on the cells even at fairly high polymer concentrations (**Figure 47**).

4.7 Confocal and immunofluorescence microscopy

4.7.1 Lymphocytes

4.7.1.1 Dendriplex

To assure that flow cytometry results indicated a successful transfection into the cytoplasm of the cell as well as to further investigate the rare occurrence of successful uptake of naked siRNA, lymphocytes that had been treated with fluorochrome-labeled siRNA either alone or in dendriplex at +/- ratio of 1 or 2 were viewed with a scanning confocal microscope (**Figure 57**). The figure images are labeled with the percentages of cells with successful uptake of siRNA. For all treatments, the siRNA was clearly seen in the interior of a majority of the cells with the highest percentage of uptake for a +/- ratio of 1. The cells were clearly alive and viable as is seen in videos showing healthy, mobile cells with siRNA clearly located in the interior of the cells[*].

[*] Videos can be seen in the electronic version of this work.

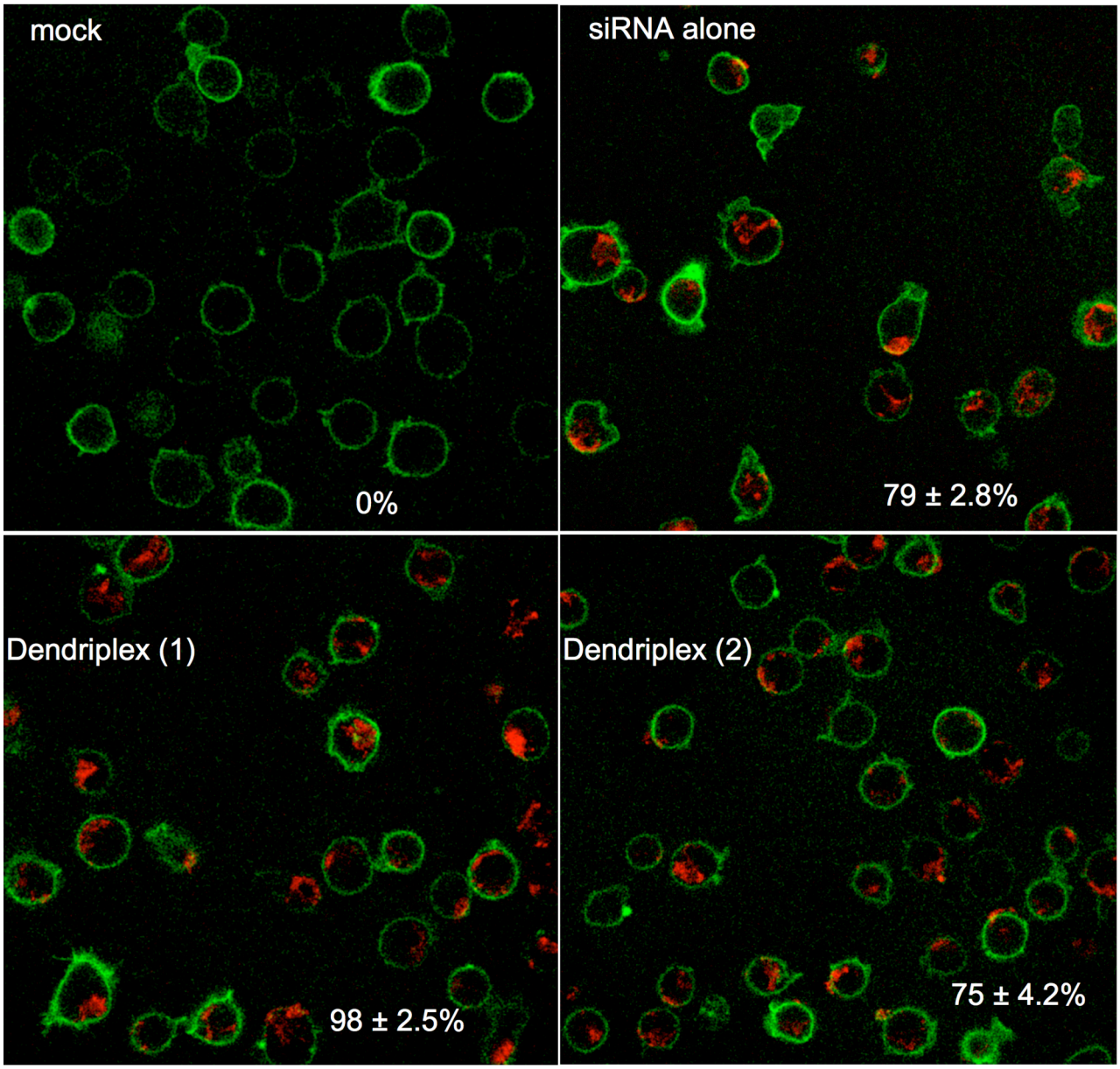

Figure 57. Confocal microscopy overlay images show complete internalization of siRNA into T cells. SupT1 cells after 20 h incubation with mock treatment (A) or with siP24-Cy3 (red) alone (B) or complexed with 2G-NN16 at a +/- charge ratio of 1 (C) or 2 (D). Cell membranes are labeled with αCD45-FITC antibodies (green). Percentages of cells positive for siRNA uptake are indicated ± SD.

4.7.1.2 Polyplex

The scanning confocal microscope was also used to image SupT1 cells treated with polyplexes composed of 1000 nM siP24-Cy3 and each of the five PEI-PEG copolymers after 24 h incubation. In order from the left, **Figure 58** showed light microscopy images, images of FITC-antibody-labeled cell membranes (green), overlay images of cell membranes with siP24-Cy3 (red), and overlay images of cell membranes, siP24-Cy3, and DAPI-labeled cell nuclei (blue). It was possible to examine both the extent of siRNA uptake and the cell morphology from the images. In particular, the status of the cell nuclei revealed the effects that the treatments had on the cells. In line with the flow cytometry results, there was a high level of siRNA uptake from all treatments.

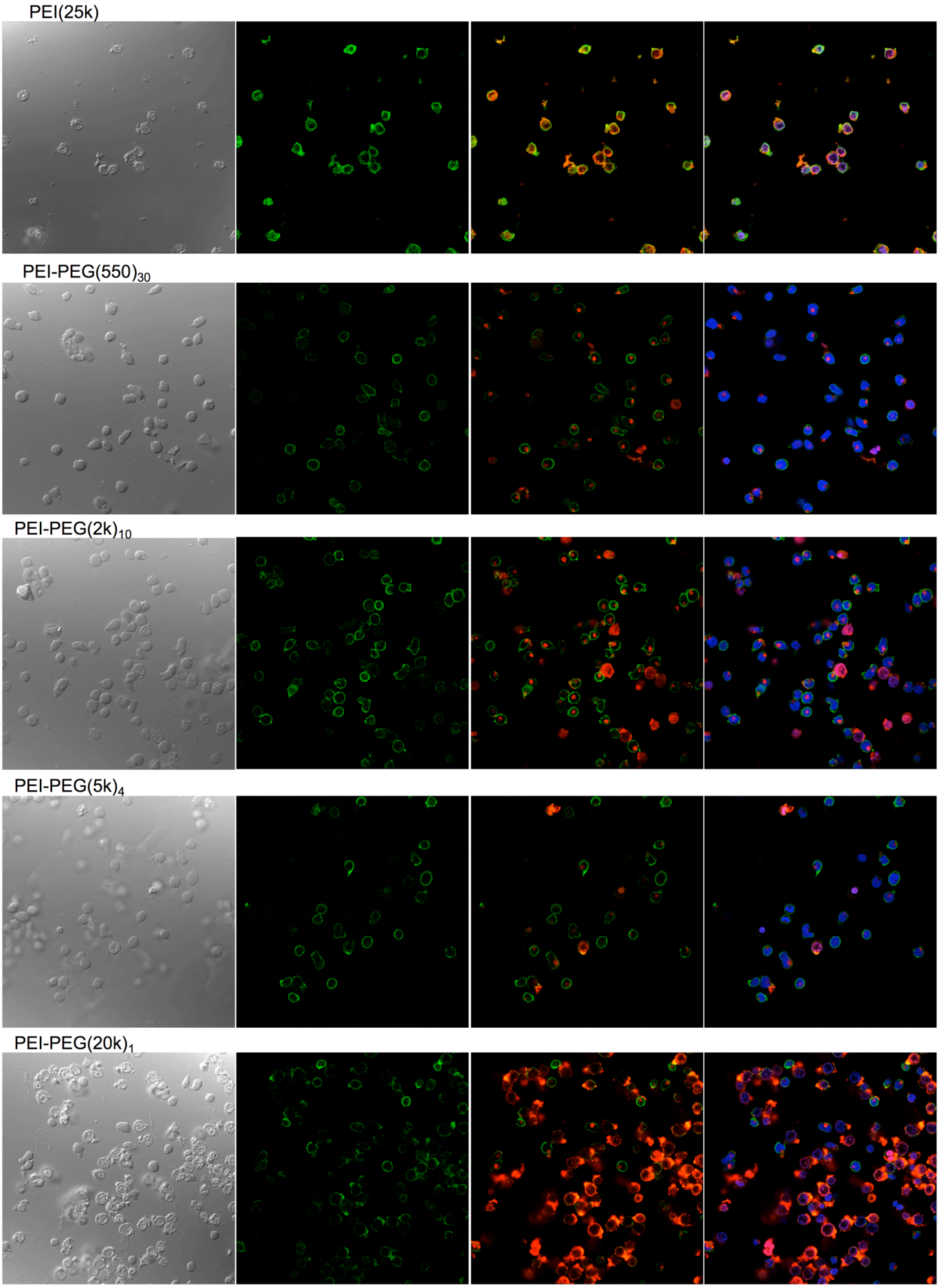

Figure 58. Confocal images of SupT1 cells 24 h after being treated with polyplexes containing siP24-Cy3 (1000 nM). N/P ratios were 5 for PEI(25K) and 10 for all others.

Figure 59 showed a quantitative analysis of the amount of siRNA uptake and the estimated cell viability for the four PEG-engrafted copolymers based on the viewing of the photographs by independent observers. From the images, negative effects on the cells by PEI(25k) and PEI(25k)-PEG(20k)$_1$ were easily observed. The percentages of cells that could be considered viable for these two treatments were quite low. In the case of PEI(25k)-PEG(20k)$_1$, this was inevitably the result of using twice the usual polymer concentration (0.033 mg/ml) in order to delivery 1000 nM siRNA (0.033 mg/ml PEI(25k)-PEG(20k)$_1$ had shown toxicity; see **Figure 47** and **Figure 48**). However, the other three copolymers showed positive results for cell viability and siRNA uptake. Specifically, the cells treated with these polyplexes showed siRNA uptake of greater than 70%. PEI(25k)-PEG(550)$_{30}$ and PEI(25k)-PEG(5k)$_4$ had the highest uptake (~85%) followed closely by PEI(25k)-PEG(2k)$_{10}$ and PEI(25k)-PEG(20k)$_1$. These results reflected precisely the same results that were obtained by flow cytometry (**Figure 56A, 24 h**).

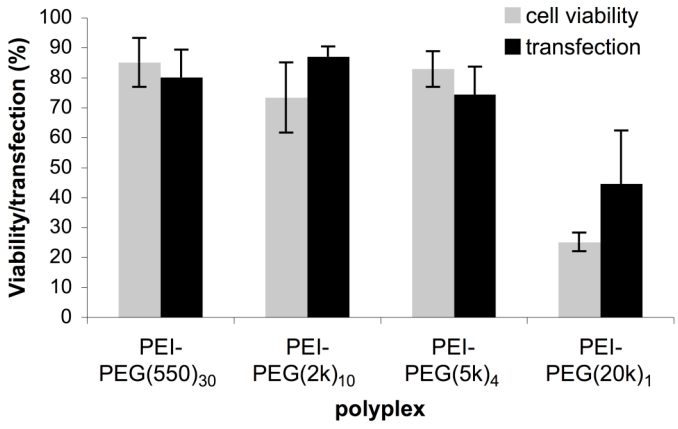

Figure 59. Visual analyses of confocal images in Figure 58 revealed viability and transfection data for the different polyplex treatments. [siRNA] = 1000 nM; [PEI-PEG] = 0.033 mg/ml.

4.7.2 Astrocytes

4.7.2.1 Dendriplex

Immunofluorescence microscopy was used to analyze uptake of Cy3-labeled siRNA by U87MG cells. Microscopy images corroborated flow cytometry results indicating no uptake for siRNA (250 nM) alone and increased uptake with higher +/- ratios when siRNA is complexed with 2G-NN16 dendrimer. Because of the adherent nature of this astrocytic cell line resulting in planar dendritic cells attached to the surface of the microscope slide, obtaining a quality confocal sectional cut showing the interior of the cells is difficult. Thus immunofluorescence microscopy was utilized instead. By labeling the nucleus with DAPI and attempting to bring the nucleus into focus, it could be estimated whether or not the fluorochrome-labeled siRNA had gained entrance into the interior of the cells. The images obtained appear to show the interior of the cells and show the aggregation of Cy3 fluorescence in small clusters as well as regions where the fluorescence is more dispersed (**Figure 60**). This is evidence that the dendriplexes were endocytosed and are located inside internal vesicles as well as having dispersed throughout the cytoplasm.

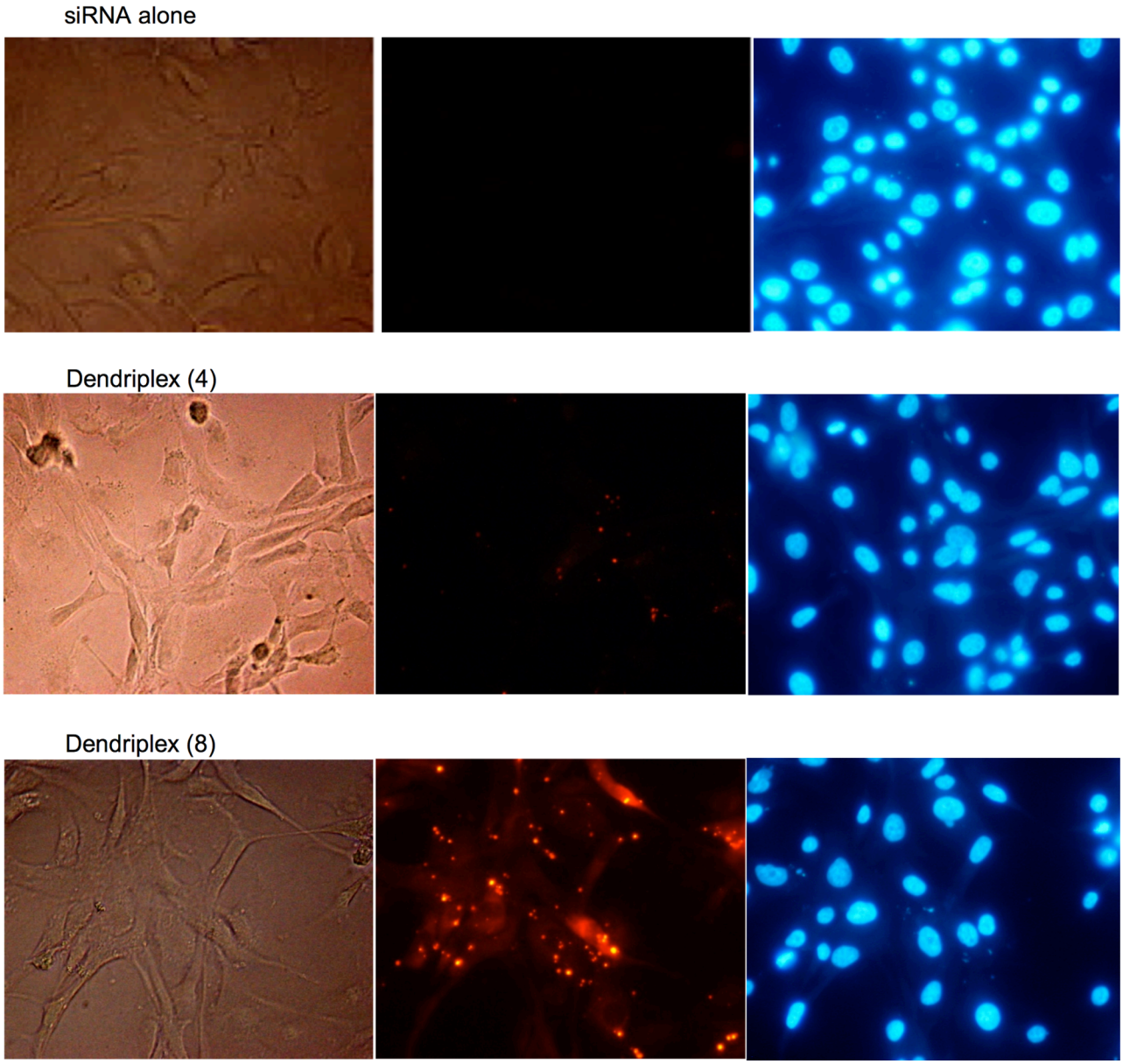

Figure 60. Immunofluorescence microscope images of U87MG cells 24 h after being treated with siP24-Cy3 alone (250 nM) or in dendriplex. siP24-Cy3 appears red and DAPI-labeled nuclei appear blue.

4.8 Dendriplexes pass through biological membranes

4.8.1 Monolayer of polarized epithelial cells

To evaluate the ability of dendriplexes to cross biological barriers, we used a human epithelial cell barrier (tight monolayer of polarized HEC-1A epithelial cells) in a transwell system. This method is inadequate at fully representing a model for the BBB, but most BBB models typically are not able to generate a tightly formed monolayer of cells without fenestrations. Therefore, in order to prevent passive diffusion of the

dendriplexes through discontinuities in the monolayer, polarized epithelial cells were used to form a tightly bound monolayer [117]. FITC-labeled-siRNA alone or complexed with NN16 dendrimers were added to the apical zone with previously activated PBMCs in the basolateral zone of the chamber of the transwell system. PBMCs were utilized to more easily determine uptake of the siRNA and, hence, the transcytosis of the dendriplex or siRNA alone through the biological barrier since the kinetics of PBMC transfection had been more thoroughly studied. Subsequently, the PBMCs were collected after 5 or 72 h and analyzed by flow cytometry for siRNA uptake. We did not find any fluorescence in cells after the short incubation times (5 h) (**Figure 61A**), whereas we did find an increase in the transfection capacity of cells treated with siRNA alone by 52% and in cells treated with dendriplexes by 83% after 72 hours (**Figure 61B**). The monolayer was viewed with a light microscope to assess its integrity and lack of apparent fenestrations prior to undergoing experiments (**Figure 61C**). However, even more convincing evidence that the monolayer was completely intact was the fact that there was no siRNA uptake after the shorter incubation times (5 h). Had there been holes in the monolayer allowing the dendriplex to freely diffuse across the barrier, the results would have more resembled the prior flow cytometry results of siRNA uptake for PBMCs in which transfection was detected after only 3 h (**Figure 52)**. In addition, treatments with dendriplexes were not toxic at the dose used.

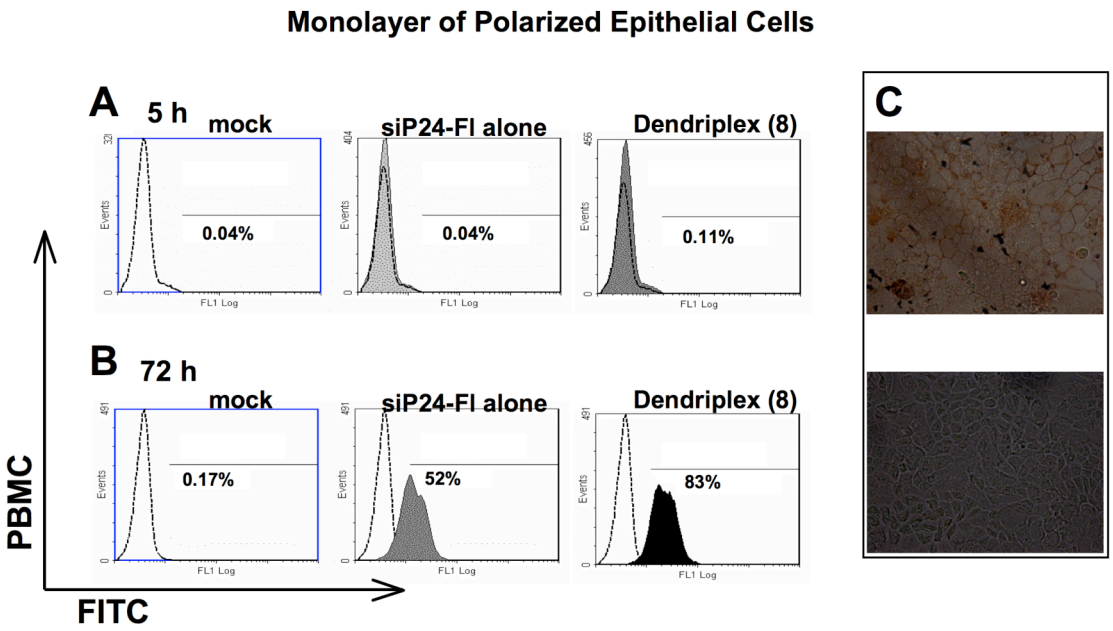

Figure 61. Transcytosis through an epithelial cell barrier. In a transwell chamber, FITC-labeled-siP24 alone or FITC-labeled-siP24/2G-NN16 was added to the apical face of a tight monolayer of polarized epithelial cells, HEC-1A. Five h (A) or 72 h (C) later, activated PBMCs were collected from the basolateral zone and the transfection was analyzed by flow cytometry. Prior to treatment the integrity of the epithelial monolayer was imaged by light microscopy (C) stained with AgNO3 (above) and without staining (below).

4.8.2 Monolayer of a bovine brain microvascular endothelial cells

An even better system for assessing the potential capability of crossing the BBB is accomplished through the use of bovine brain microvascular endothelial cells in a transwell chamber. The formation of a tight monolayer with 100% confluence was determined by measuring the transepithelial electric resistance and was monitored with a light microscope. An image of the monolayer can be seen in **Figure 62A**. As before, FITC-labeled siP24 either alone or complexed to 2G-NN16 was added to the apical zone. For these experiments, either PBMC or U87MG were seeded in the basolateral zone and tested for siRNA uptake by flow cytometry either 5 or 72 h after the treatment. As with the epithelial cell barrier system, uptake of siRNA by the cells in the basolateral zone indicated successful transcytosis of the cell monolayer barrier and subsequent transfection of the target cells. For PBMC, there was no siRNA uptake after only 5 h (**Figure 62B**), but positive transcytosis and transfection for both siRNA alone and dendriplex after 72 h (**Figure 62C**). With U87MG astrocytes in the basolateral zone, the experiment modelled the *in vivo* system in both the cells that form the blood brain barrier and the target cells. These experiments revealed no uptake after 5 h (**Figure 62D**), but a three-fold higher transfection than with the PBMC after 72 h (**Figure 62E**). Both siRNA alone and bound to dendrimers showed positive transcytosis and transfection by the target cells.

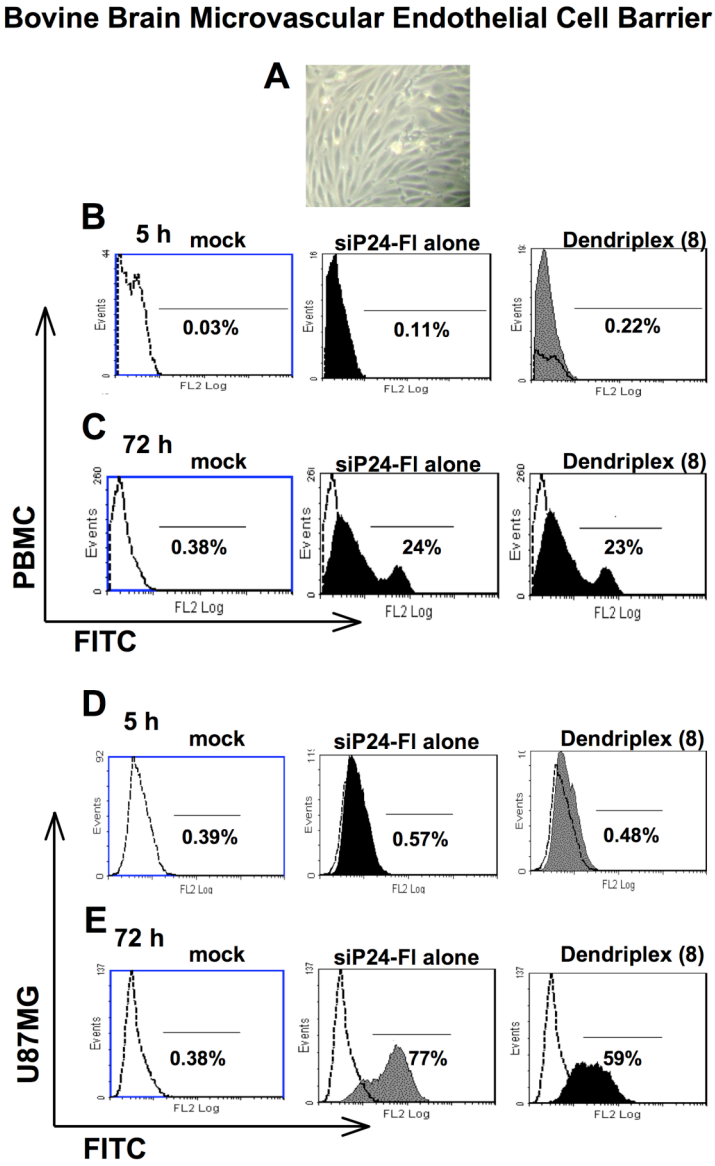

Figure 62. Transcytosis of a BBB model. Bovine brain microvascular endothelial cells were grown into a tight monolayer (A) in a transwell chamber. FITC-labeled siRNA (250 nM) alone or in dendriplex with 2G-NN16 (+/- ratio of 8) were added to the apical face of the transwell with either activated PBMC (B & C) or U87MG cells (D & E) in the basolateral zone. After 5 h (B & D) or 72 h (C & E), the cells from the basolateral zone were collected and analyzed by flow cytometry for siRNA uptake. Untreated cells were used as a mock control.

4.9 Biological activity of siRNA

4.9.1 Silencing effect by siRNA via electroporation

Prior to attempting HIV inhibition experiments using siRNA complexed with dendrimers or polymers, the efficacy of the siRNA at inhibiting HIV needed to be determined. To carry this out, HIV-infected PBMC were subjected to treatment with siRNA via electroporation. Flow cytometry data showed that electroporation resulted

in successful transfection of Cy3-labeled siRNA (**Figure 63**). Cells washed with trypsin to remove molecules on the membrane showed similar levels of Cy3 fluorescence indicating uptake into the cell interior.

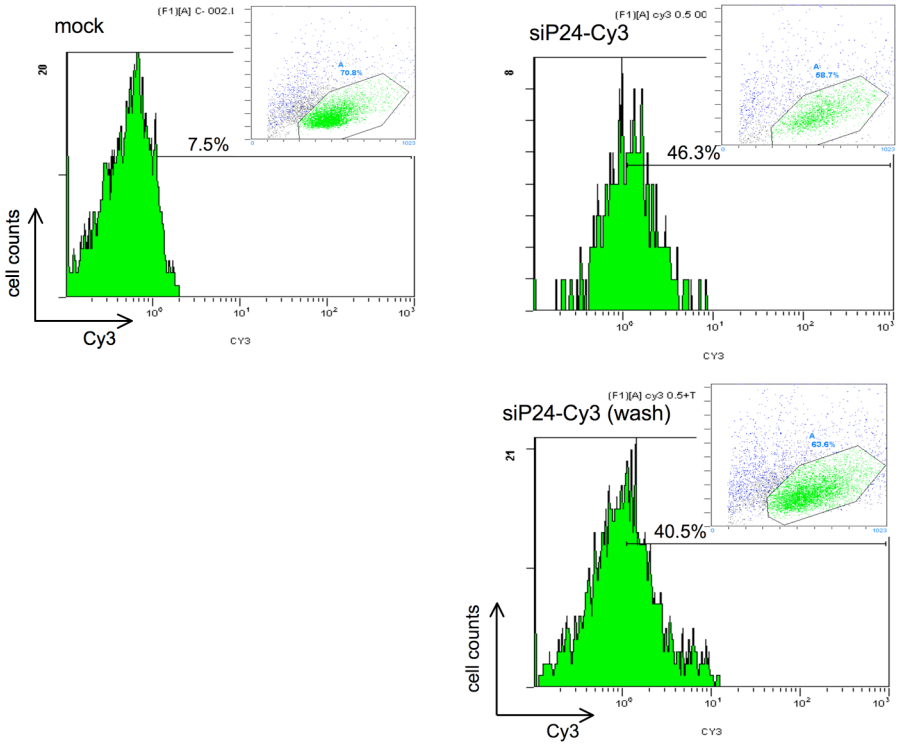

Figure 63. Flow cytometry indicates successful entrance of Cy3-labeled siRNA in HIV-infected PBMC 24h after electroporation

As a control for siRNA entrance and function, we performed parallel experiments with uninfected SupT1 cells that were electroporated with siRNA targeted to the housekeeping gene GAPDH. The siRNA was seen to be functional as cells electroporated with GAPDH siRNA (siGAPDH) exhibited up to 80% silencing. The GAPDH knockdown was seen to be sequence-specific and dependent on siRNA concentration. This was determined as points treated with less than 250 nM siGAPDH never achieved greater than 50% knockdown while 250 and 500 nM siGAPDH achieved 70% and 89% knockdown, respectively, while a negative control siRNA of random sequence (siRandom) had either no effect or a slight effect on GAPDH expression (**Figure 64A**). Additionally, the silencing affect was seen to last up to 6 days after only one treatment with siRNA (**Figure 64B**). Next, it was determined if this same effect could be achieved in HIV-infected PBMC via electroporation.

Results showed from 50% to 80% inhibition for 500 nM of a siRNA targeted to the HIV *p24* gene (siP24) and up to 85% inhibition when targeted to the HIV *gag* gene (siGAG1) compared to mock treated cells (**Figure 64C**). Furthermore, there was a difference of at least 40% between cells treated with siGAG1 and those treated with siRandom for all time points. This indicates a sequence-specific inhibition of HIV for siRNA at this concentration. At 3 times the siRNA concentration, there was no improvement in viral inhibition (data not shown). Because of these results, siRNA concentrations were limited to between 250 nM and 500 nM for all further gene-silencing experiments.

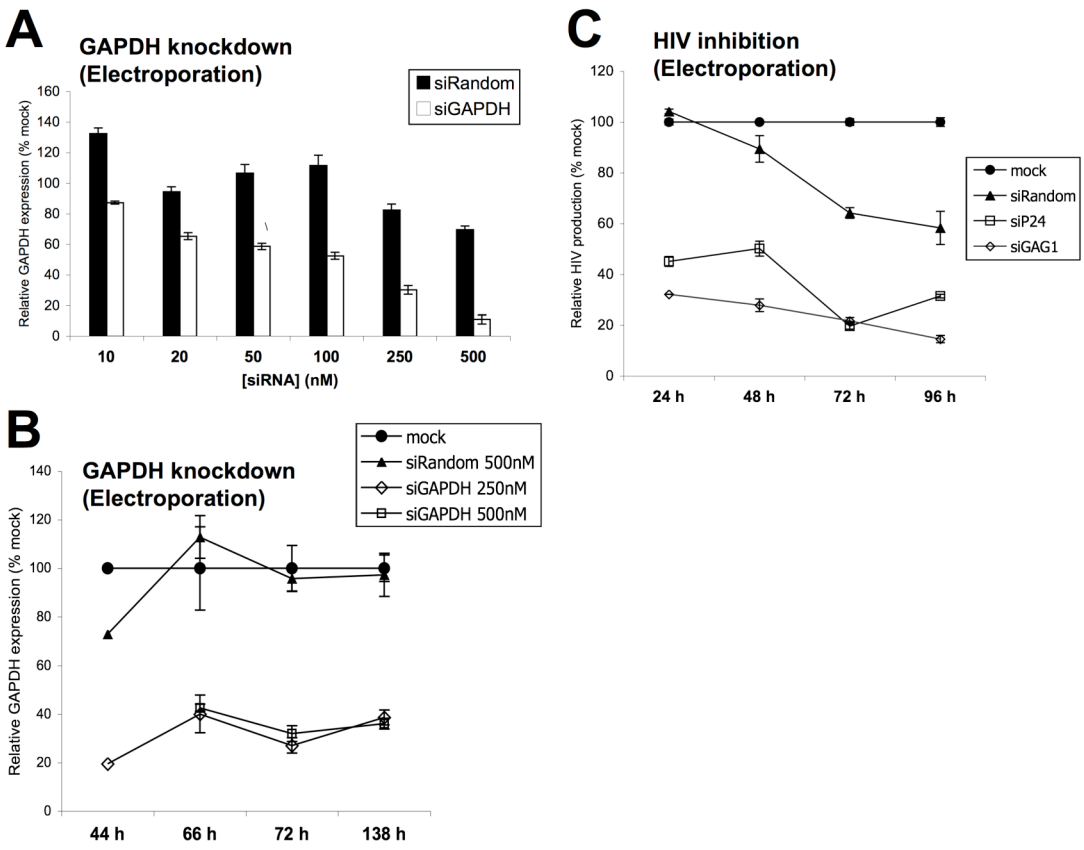

Figure 64. siRNA transfected by electroporation. SupT1 cells showed a downregulation of GAPDH that was sequence-specific, affected by siRNA concentration (A), and lasted at least 6 days (B). siRNA targeted to HIV also showed inhibition of HIV replication when delivered by electroporation (C).

4.9.2 Silencing by dendriplex-delivered siRNA

4.9.2.1 Lymphocytes

With the efficacy of siRNA at GAPDH knockdown and inhibition of HIV demonstrated via electroporation, GAPDH silencing and HIV inhibition experiments were next carried out with dendriplexes of 2G-NN16 and siRNA. Naked siRNA was also tested for biological effect, and Lipofectin® was used as a comparative control. Expression of GAPDH in normal SupT1 cells was shown to be reduced in a sequence specific way when the cells were treated with naked, Lipofectin®-delivered, and 2G-NN16-delivered siRNA (45, 46, and 47%, respectively) (**Figure 65A-C**).

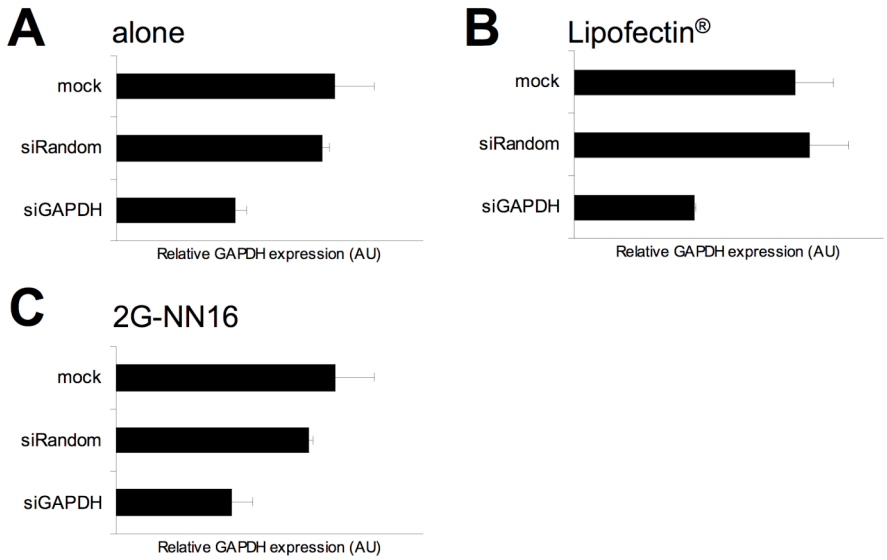

Figure 65. GAPDH expression in SupT1 cells 48 h after being treated with siRNA alone or complexed with Lipofectin or 2G-NN16. [siRNA] = 500 nM; +/- ratio for 2G-NN16 was 2.

siRNA was also able to inhibit HIV when bound to 2G-NN16. Inhibition was achieved by both siRNA targeted to the HIV *nef* gene (siNEF) and a cocktail mixture of the three siRNAs siP24, siGAG1 and siNEF (siCOCKTAIL) (15 and 22%, respectively) compared to control cells (**Figure 66**).

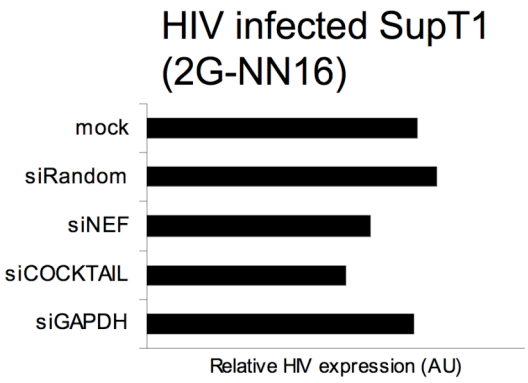

Figure 66. Ag p24 quantity for HIV-infected SupT1 cells 24 h after being treated with dendriplexes of 2G-NN16 and different siRNA. [siRNA] = 500 nM; +/- ratio = 2.

To further investigate the HIV inhibitory effect, dendriplexes at different +/- charge ratios along with naked siRNA were tested on HIV-infected PBMC. At 24 h, an inhibition of 25% is seen for siNEF and nearly 40% for siCOCKTAIL when bound to 2G-NN16 at a +/- charge ratio of 2 compared to control cells (**Figure 67**). The inhibition obtained with a +/- ratio of 2 is better than for a +/- ratio of 1 or naked siRNA. Moreover, LDH assays for these experiments show that the treatments cause minimal toxicity.

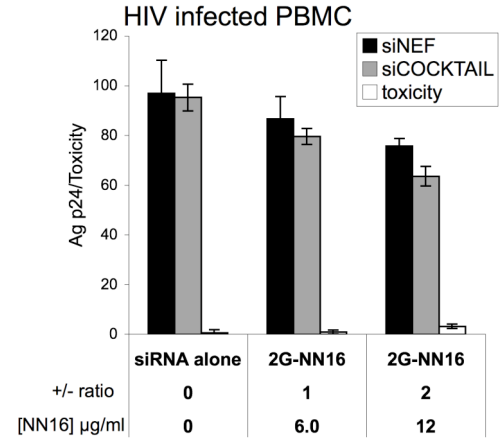

Figure 67. Graph showing Ag p24 quantities indicates HIV replication for HIV infected PBMC after 24 h incubation with siRNA alone or dendriplexes at +/- charge ratio of 1 or 2. White bars indicate toxicity as measured by LDH release 3 h after treatment (relative to cells treated with Triton X-100).

4.9.2.2 Astrocytes

Next, U87MG astrocytes were tested for an siRNA silencing effect. Initial GAPDH knockdown experiments with these cells showed slight gene silencing for siRNA treatment alone or in dendriplex to the amount of 12% and 37%, respectively, compared to mock-treated control cells (**Figure 68**). The silencing was sequence-specific, because treatments with either siRandom alone or complexed with 2G-NN16 did not result in a decrease in GAPDH expression. In addition, dendrimer alone did not negatively affect GAPDH expression, which indicated that cytotoxicity was not an issue.

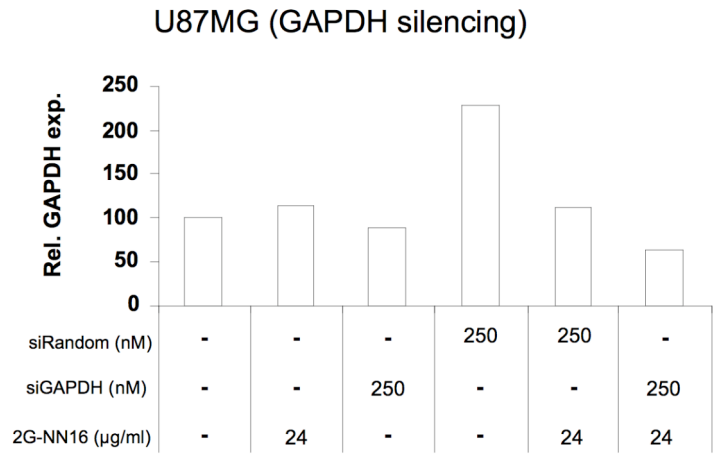

Figure 68. Initial GAPDH silencing experiment in U87MG cells for siRNA treatment alone or with 2G-NN16 (+/- ratio of 8).

When experiments on HIV inhibition were performed with these cells, dendriplexes containing anti-HIV siRNA had much better efficacy at reducing the viral replication (**Figure 69**). After infecting the cells with the T-tropic HIV strain NL4-3, treatments with siRNA targeted to the *p24* gene or the *nef* gene were administered either alone or in dendriplex. Seventy-two h later, supernatants from the cell plates were collected and viral RNA was quantified by qPCR. Results from the qPCR showed that the dendriplexes achieved the greatest level of viral inhibition. At an siRNA concentration of 100 nM, siNEF and siP24 reduced the viral replication by 50% and 55%, respectively, and when the concentration of siP24 was increased to 250 nM, the inhibitory effect improved to over 80% inhibition (**Figure 69A**). Similar results were obtained when the cells were infected with the M-tropic HIV strain Ba-L.

However, the maximum level of HIV inhibition with this viral strain was achieved with treatments of dendriplex containing 250 nM of siP24 in which the viral replication was reduced by 40% (**Figure 69B**).

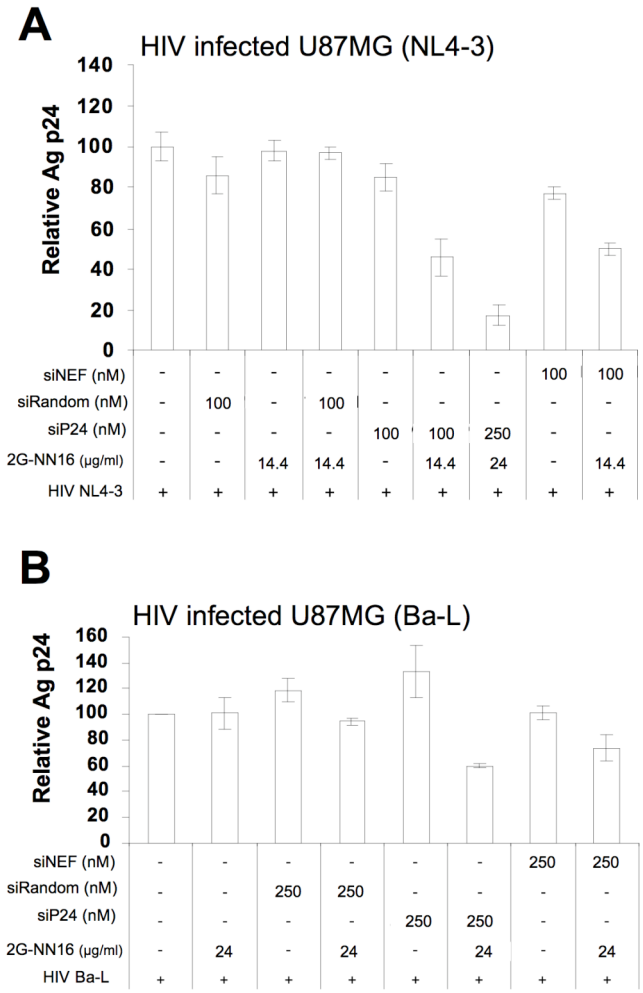

Figure 69. Graphs indicate a reduction in HIV replication in U87-MG cells 72 h after treatment with siNEF or siP24 alone or delivered by 2G-NN16. The cells were infected with the X4-HIV strain, NL4-3 (A), or the R5-HIV strain, Ba-L (B). Values represent Ag p24 concentration as determined by ELISA relative to untreated cells; siRandom was used as a control.

4.9.3 Silencing by polyplex-delivered siRNA

4.9.3.1 Lymphocytes

4.9.3.1.1 GAPDH knockdown from one-time treatment

Initial experiments on the biological effect of siRNA delivered by PEI-PEG polymers were attempts at GAPDH silencing following a one-time treatment and then, long-term GAPDH silencing through repetitive treatments. After the one time

treatment or polyplexes, GAPDH expression was reduced in a sequence-specific manner when the cells were collected 72 h after treatment for polyplexes made up of PEI(25k)-PEG(2k)$_{10}$, PEI(25k)-PEG(20k)$_1$, and PEI(25k)-PEG(550)$_{30}$ (**Figure 70B**). When the cells were collected one day earlier (48 h after treatment), only PEI(25k)-PEG(2k)$_{10}$ showed any amount of sequence-specific GAPDH silencing (**Figure 70A**).

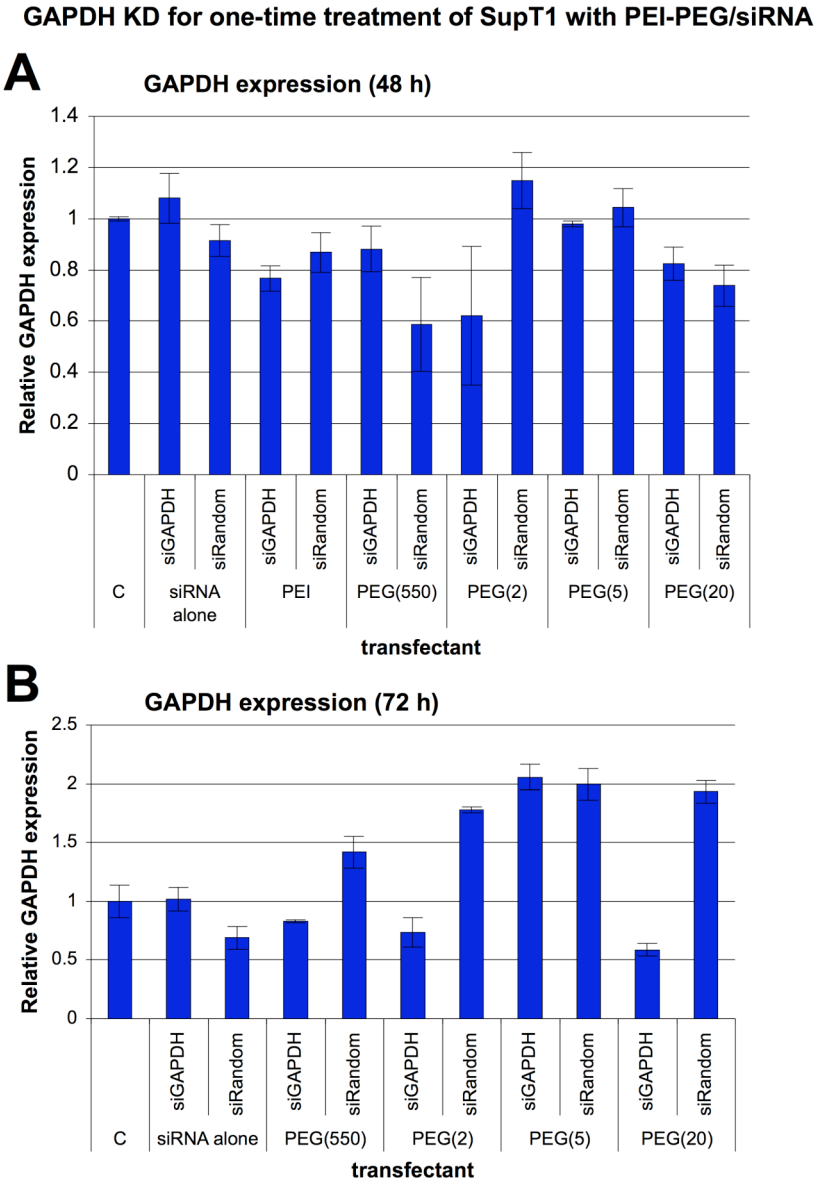

Figure 70. Graphs showing relative expression of GAPDH in SupT1 cells treated with siRNA alone or delivered by PEI-PEG polymers after incubations of 48 h (A) and 72 h (B). [siRNA] = 500 nM; N/P ratio 5 for PEI, 10 for all others.

4.9.3.1.2 GAPDH knockdown over an extended time period with repetitive doses

GAPDH silencing experiments were extended from 3 up to 22 days. In order for the cells to be maintained for this longer period, the cells were diluted by collecting samples and replacing the lost volume with fresh medium. This allowed measurements of GAPDH expression to be made and treatments of PEI-PEG/siRNA polyplex to be repeated every 2 or 3 days. A total of 9 treatment doses and 9 measurements were made over the course of 22 days. After taking into consideration all the results obtained thus far, including stability, cytotoxicity, transfection and biological effect, it was decided to continue experimentation with a focus on only two of the five polymers, PEI(25k)-PEG(2k)$_{10}$ and PEI(25k)-PEG(20k)$_1$. The results showed that siRNA targeted to the GAPDH gene had a greater effect on silencing GAPDH expression as the experiment went along when delivered by PEI(25k)-PEG(20k)$_1$ (**Figure 71**). Treatments with this polyplex reduced gene expression by 78% and 77% on days 13 and 20, respectively, while siRandom delivered by the same polymer consistently resulted in GAPDH expression either equal to or greater than the GAPDH expression for mock treated cells. PEI(25k)-PEG(2k)$_{10}$-delivered siGAPDH did not produce such positive results as it caused a reduction in GAPDH expression compared to siRandom -treated cells in only four out of nine time points.

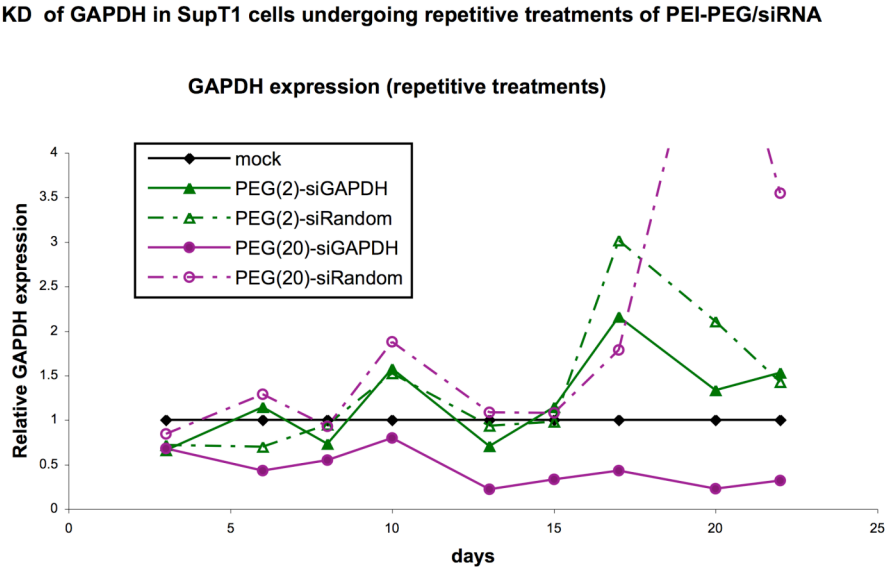

Figure 71. Graph showing relative GAPDH expression for SupT1 cells undergoing repeated treatments with PEI-PEG/siRNA polyplexes. [siRNA] = 500 nM; N/P ratio = 10.

4.9.3.1.3 HIV inhibition

4.9.3.1.3.1 Treatment with polyplexes prior to infection with HIV

The final experiments carried out with siRNA and PEI-PEG polymers were HIV inhibition experiments. First, attempts were made to inhibit HIV replication by submitting SupT1 cells to one-time treatments of polyplexes 24 h prior to infecting them with HIV. If the siRNA could transfect the cells and become functional at targeting the HIV RNA for degradation prior to the introduction of the viral genome, it could possibly prevent infection of the cell by stopping the viral cycle before retrotranscription took place by degrading the first template viral RNA introduced into the cell interior. Such a mechanism could offer the possibility of a prophylactic therapy for the prevention of HIV infection. The results, however, showed a very slight reduction in the production of p24 for cells treated with siNEF or siCOCKTAIL complexed to PEI(25k)-PEG(2k)$_{10}$ or PEI(25k)-PEG(20k)$_1$ compared to cells treated with siRandom (**Figure 72**).

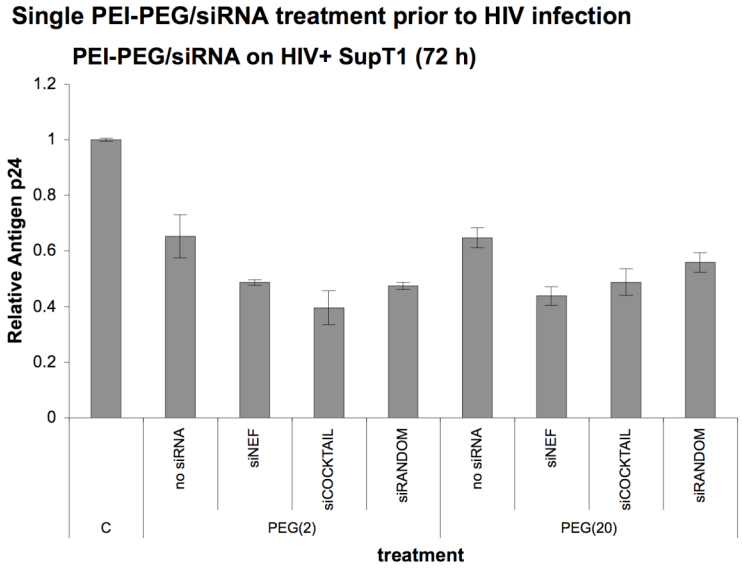

Figure 72. Relative Ag p24 for HIV infected SupT1 cells that had been treated with polyplexes one time 24 h prior to being infected with HIV. Ag p24 concentration was quantified by ELISA 72 h after infection with HIV.

4.9.3.1.3.2 Repetitive treatments with polyplexes over two weeks

Despite the less than positive results obtained from the pre-infection treatment experiments, further experiments on HIV inhibition were carried out. Utilizing

experimental protocols similar to those used for the experiments of long-term GAPDH silencing via repetitive treatments, HIV-infected SupT1 or PBMC were maintained in passage while undergoing repeated treatments to examine the more long-term effects that polyplexes had on the viral replication. Several days after SupT1 cells were infected with HIV and submitted to an initial treatment with polyplexes, samples were collected, the lost volume was replaced with fresh medium, and an additional treatment was added to each point. This procedure was repeated every two or three days up to 15 days. **Figure 73** shows the p24 quantification results for six time points from day 2 to day 15 for cells infected with 100 pg HIV per million cells. The greatest amount of HIV inhibition was achieved by siNEF delivered by PEI(25k)-PEG(20k)$_1$ which reduced the amount of HIV production by greater than 10^4 fold compared to mock-treated cells and around 100 fold compared to siRandom-treated cells. The HIV inhibition was not detected until day 7, and a difference between siNEF and siRandom was not seen until day 9. However, by day 15 of the experiment the siNEF polyplex-treated cells maintained a viral production below 100 pg of p24 protein. The level of HIV inhibition was equivalent to the inhibitory effect caused by treatments of 0.5 µM AZT.

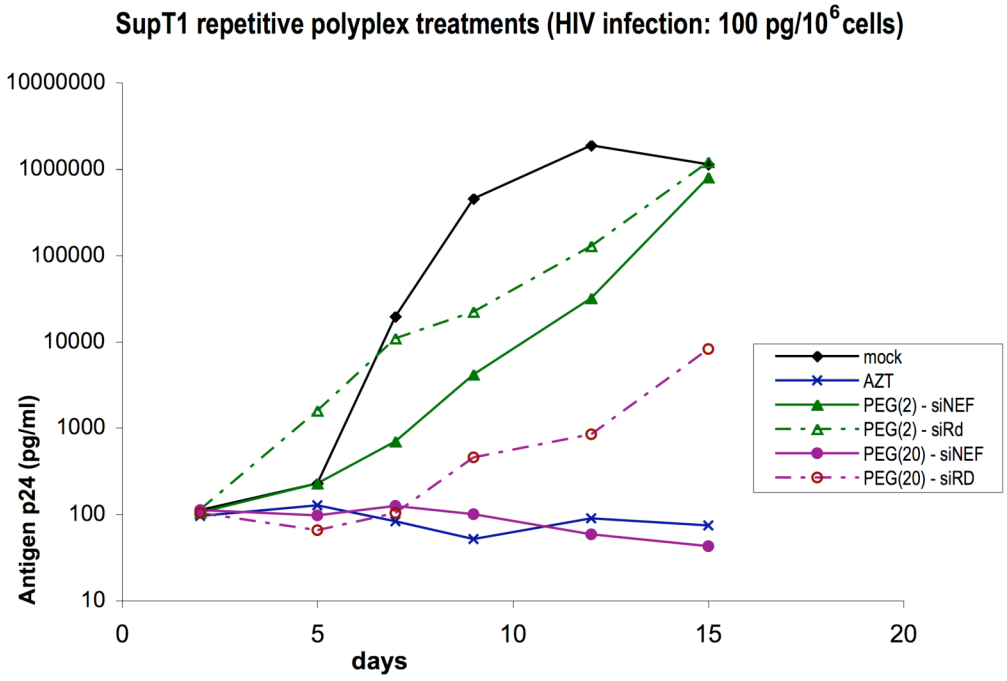

Figure 73. HIV replication is inhibited over an extended time period in HIV infected SupT1 cells undergoing repetitive treatments with polyplexes containing anti-HIV siRNA and PEI-PEG(2k)$_{10}$

or PEI-PEG(20k)$_1$. Cells were infected with HIV NL4-3 at a concentration of 100 pg/10^6 cells; y-axis is logarithmic Ag p24 concentration; [siRNA] = 500 nM; N/P ratio = 10; [AZT] = 500 nM.

When SupT1 cells were infected with ten times as much HIV (1000 pg HIV/10^6 cells), repetitive treatments still had an inhibitory effect on HIV replication. As before, siNEF delivered by PEI(25k)-PEG(20k)$_1$ resulted in the greatest amount of HIV inhibition and, once again, mirrored the effects of AZT treatments (**Figure 74**). With the higher multiplicity of infection, mock-treated cells experienced an explosion in HIV replication by day 7 when p24 levels peaked and dropped off because of a high amount of cell death due to the high viral titer. This peak did not occur for the mock-treated cells infected with the lower MOI until day 12. This higher MOI was also responsible for the fact that the siNEF-polyplex did not maintain the viral replication from increasing like it had when infected with the lower MOI. Regardless, the difference between siNEF-polyplex treated cells and the rest of the points in the experiment was consistently around 100 fold.

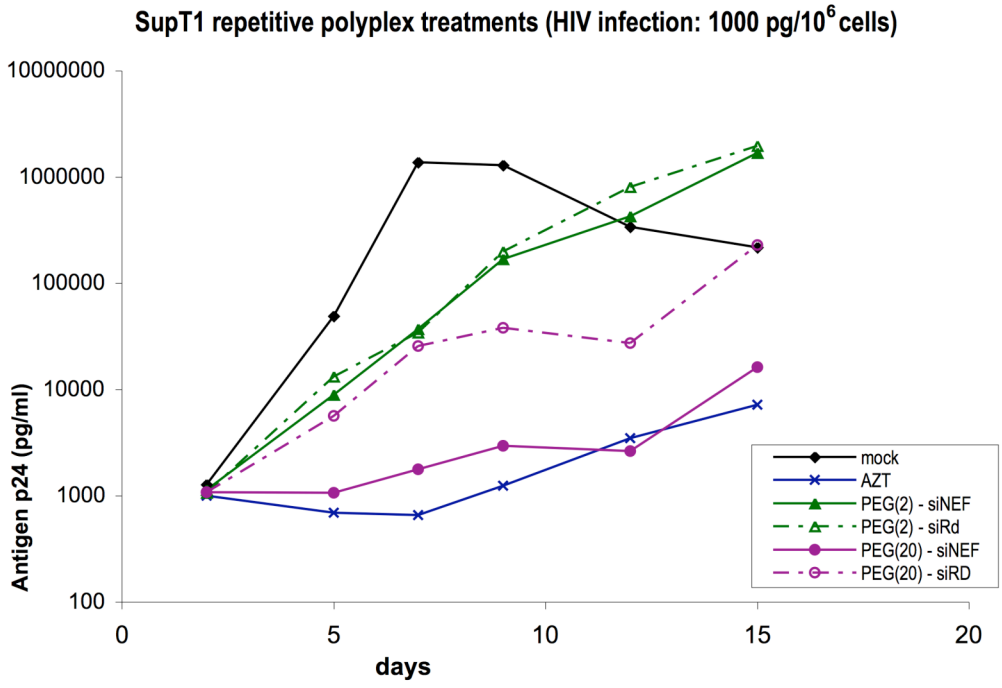

Figure 74. Equivalent results for HIV inhibition by repetitive doses of polyplexes over an extended time period in SupT1 cells infected with HIV NL4-3 at a concentration of 1000 pg/10^6 cells. y-axis is logarithmic Ag p24 concentration; [siRNA] = 500 nM; N/P ratio = 10; [AZT] = 500 nM.

5. DISCUSSION

The goal of bringing gene therapy techniques such as RNAi to the fight against HIV infection holds a great deal of promise. The main hurdle to overcome in utilizing these powerful tools appears to be delivery and transfection of the infected cells. The development of a system that could address these issues could immensely expand the therapeutic possibilities of RNAi.

This work presents research on two types of drug delivery vehicles and their capability to transport and deliver siRNA to two different cell types. In the first instance, amine-terminated carbosilane dendrimers are a monodisperse, low molecular weight dendrimer. Second, a group of PEG-engrafted PEI copolymers possess a high charge density coupled with exterior protective PEG moieties to improve their biocompatibility. The experimental research that was carried out can be divided into three sections. First, analysis on the stability and characterization of the interaction between each delivery vehicle and siRNA was performed. Second, the effects these molecules (either alone or complexed with siRNA) had on cells when treated *in vitro* were carefully examined. The effects of the treatment on the cells that were measured included unwanted effects such as cytotoxicity, and desirable effects like successful transfection. Also, the ability of these macromolecules to transverse biological barriers in order to reach the target cells was considered among the effects resulting from the interaction between the complexes and cells. Finally, the primary objective of this research, achieving a biological effect from the delivery of siRNA to the cells and, in particular, achieving gene silencing, was thoroughly assayed at the end of this work.

The structural differences between the two vehicles provide evidence for the advantages and disadvantages that each vehicle offers. CBS dendrimers are a smaller molecule with a more defined structure possessing internal Si–O bonds that allow for time-controlled liberation of the exterior branches. On the other hand, PEI-PEG polymers have a higher density of positively charged amines (PEI = 43 g/charge; 2G-NN16 = 287 g/charge), which allows for both a higher N/P ratio and a lower polymer concentration to achieve delivery of the same amount of siRNA. Also, the attachment of PEG moieties on the periphery functions to shield the high charge density of the PEI core and greatly improves the biocompatibility of the molecules. This is an improvement over the dendrimer structure, which has its positive charges exposed on the surface of the molecule. Finally, the larger molecular weight of the polymers

allows for complexation with a larger amount of siRNA. The molar ratio of siRNA to PEI is 13.8 mol siRNA for every mol PEI, compared to 0.38 mol siRNA to every mol 2G-NN16. With the experimental +/- charge ratios utilized, the polymer is added at a ratio of ten times the amount of siRNA compared to the ratio of only two for dendrimer. Even so, the resulting molar ratios are 1.38 mol siRNA per mol PEI and 0.19 mol siRNA per mol 2G-NN16. Clearly, the polymer can achieve the same delivery at a substantially lower concentration than the dendrimer.

The first results reported here dealt with the stability and characterization of the complex formed between the vehicles and siRNA. The first conclusion to be made was that gel electrophoresis is adequate in visualizing the formation of a stable complex. The siRNA complexation and condensation gels showed that PEI-PEG copolymers require higher N/P ratios to fully complex siRNA compared to PEI and 2G-NN16 (**Figures 20 and 23**). As described before, the presence of the PEG moieties shield the charged amines of the PEI core thus minimizing the exposure of the positive charges to components of the cell where it would have toxic effects, but also partially impedes the ability for the positive charges to fully and efficiently bind siRNA. Therefore, a higher concentration of PEG-engrafted polymer is needed to fully complex the siRNA. 2G-NN16 has no such protective shield, so its positive charges are fully exposed and able to bind siRNA more efficiently. The fact that 2G-NN16 possesses two charged amines on each branch with one inside of the other is likely the reason that the +/- charge ratio to adequately complex siRNA is two, as only one of the amine pairs per branch on average can capably bind the siRNA.

The strength of union assay simply showed that the electrostatic union between the vehicle and siRNA was not an entirely static interaction (**Figure 21**). 2G-NN16 binds siRNA less strongly than 2G-NN8 by a slight amount. This could indicate a greater tendency to release the siRNA after cell transfection has occurred. It could also, however, indicate less protection en route to the target cells. The only accurate way to answer this question would be further investigation, including *in vivo* trials. The PEI-PEG copolymers 2k, 5k, and 20k* showed similar results to the dendrimers in heparin competition assays in that partial release was seen at 0.21

* Throughout the discussion, the PEI-PEG polymers may be referred to simply by the mass of their PEG attachments or without including the PEI in the name. Thus, "2k" and PEG(2k)$_{10}$ refer to PEI(25k)-PEG(2k)$_{10}$ unless otherwise specified.

IU/µg with full release at 0.31 IU/µg [89]. It was also shown that the presence of PEG moieties prevented the polymer from binding the siRNA much more strongly, which is further evidence of their effect at shielding the high charge density of the PEI core.

Dynamic light scattering assays on dendriplexes showed that both size and zeta potential depended on +/- charge ratio (**Figure 22**) and [121]. Utilizing the zeta potential assay, it was determined that the naturally occurring +/- charge ratio of dendriplexes between 2G-NN16 and siRNA was about 3:1. At smaller +/- ratios, there was not sufficient protection by the dendrimer and the zeta potential reflected the high density of negative charges of the siRNA in the complex. The assays also showed that beginning at 3, as the +/- charge ratio increased, there was a greater likelihood of aggregation. Particle size at +/- ratio of 3 was greater than 300 nm, whereas at +/- ratio of 2 it was smaller at just over 200 nm. Meanwhile, polyplexes tested at an N/P ratio of ten had a smaller particle size and a positive zeta potential (**Figure 24**). The difference between this and the zeta potential of dendriplexes is clearly because of the difference in charge ratios utilized. Among the different copolymers, it appears that the larger PEG chains condensed the siRNA better and resulted in particle sizes of around 150 nm. It is likely that the PEG moieties also helped significantly in preventing aggregation, supported by the fact that PEI(25k) showed a gradual increase in particle size during the 20 min duration of the experiment (data not shown), probably because of aggregation [89]. The PEG(550)-engrafted polymer seemed to not be sufficient to condense the siRNA fully as particle size was over 300 nm.

The most intriguing attribute of the CBS dendrimer was its ability to enact a time-controlled release. The difficulty in synthesizing gradually degrading dendrimers was finding a balance between achieving water solubility and avoiding rapid hydrolysis of the Si–O bonds. In fact, only at the point when dendrimers of second generation were created having $CH_2CH_2NMe_2$ branches outside of the Si–O were the dendrimers able to be dissolved in water without the immediate hydrolysis of the Si–O bonds [109]. Thus, the quaternized version, possessing $CH_2CH_2N^+Me_3$ branches, offered all three characteristics of water solubility, a positively charged periphery and gradually hydrolysable internal Si–O bonds. Time-controlled hydrolysis was demonstrated clearly via NMR spectroscopy, and established the timeframe for a dendrimer possessing only a single ethylamine on each branch (2G-N8) to degrade

between 1 and 12 hours with a large percentage of it occurring after 5 h (**Figure 25**). More in-depth NMR analysis on concentration of intact dendrimer versus time showed a first-order decomposition that also was dependent on initial dendrimer concentration [109]. Due to the dependency on dendrimer concentration for the rate of Si–O hydrolysis, the dendrimer concentrations utilized *in vivo* would decompose at a slower rate than the higher concentrations of laboratory experiments. This timeframe for degradation would provide adequate time for transit in the blood stream to the target cells, cell transfection and escape from the endosome all to occur prior to liberation of the cargo. Furthermore, gel electrophoresis showed the liberation of siRNA to begin between 8 and 12 h and continue until the last of the siRNA had been freed between 18 and 24 h (**Figure 26)**. A gradual but constant liberation would enhance therapy by providing a constantly replenishing supply of active siRNA molecules.

The best way to observe protection of the delivery vehicle over its cargo was by monitoring siRNA using GE. The presence of liberated siRNA versus the absence of siRNA indicated degradation by RNases. The first protection assay gel (**Figure 27**) showed intact siRNA in the presence of RNase when complexed to 2G-NN16. The fact that the siRNA band was retained in the well made quantitative analysis difficult, but visual inspection offered sound evidence of a high degree of protection. The gel showing heparin-freed siRNA (**Figure 28**) allowed for quantitative analysis using gel band intensity quantification software. Results showed at least 40% of the siRNA was protected and subsequently liberated by heparin. PEI-PEG polymers had also been tested for protection from RNase by Mao, et al. [89]. Their research showed that polymers engrafted with larger PEG chains were the best at protecting siRNA. 20k maintained protection over at least 80% of the siRNA even when exposed to high concentrations of RNase; 5k protected at least 50% and 2k protected over 30% up until the two highest RNase concentrations were added to the polyplex. Meanwhile PEI(25k) and PEG(550) offered very little or no protection from RNase degradation. The capability of protecting siRNA from RNase is of fundamental importance for the siRNA to be able to exert an effect once in the interior of the cell [89]. Previously, we found that CBS similarly protected oligonucleotides from sequestration and degradation by serum proteins [122] and [123]. Protection from RNase degradation and sequestration by other proteins is a major benefit of these delivery vehicles as

naked siRNA cannot be administered intravenously without being rapidly lost to the body's natural defenses contained in the blood system.

The next section of results revealed the cytotoxicity levels caused by the delivery vehicles and the complexes they formed with siRNA on the two types of cells under investigation. First off, dendriplexes at concentrations up to 25 μg/ml did not cause sufficient membrane rupture to cause cytotoxicity in any of the cells tested. They did not damage cell metabolism as measured by MTT assays. They did not cause loss of cell viability according to flow cytometry scatter plots. The results from these experiments came about while assaying for siRNA uptake by cells treated with varying concentrations of dendriplex. It was seen that the percentages of total events that fell within the "viable" gates varied according to the treatment. This resulted in a simple assay for testing viability without staining. Some forms of staining could have further distinguished apoptotic or necrotic cells from live cells [124], but possibly would have interfered with quantification of uptake. Next, it was found that dendriplex at these concentrations did not cause cell proliferation as measured by absolute cell counts or DNA synthesis. However, the BrdU incorporation into newly synthesized DNA assay is less accurate than others at estimating cell viability because it only indicates the extent of DNA replication, not cell proliferation. Dendrimers did not result in over- or under-expression of any gene in astrocytes compared to control cells as seen in the genome-wide microarray. Most importantly, no apoptosis inducing or cell cycle arrest promoting genes were affected by 24 μg/ml 2G-NN16 treatments. True, dendrimers alone were more toxic than dendriplexes. However, neither dendrimers alone nor dendriplexes were as toxic as Lipofectin at working concentrations. Additionally, dendriplexes did not have a toxic effect on HIV-infected PBMC, even though productive HIV infection can substantially weaken the cells' fitness making them more susceptible to cytotoxic damage.

It is relevant that 2G-NN16 did not produce cytotoxicity in the human astrocytoma cells. The results of MTT and LDH screening showed that the upper limit of the 2G-NN16 concentration for biological assays is no less than 24 μg/ml. Toxicity profiles of dendriplexes formed from 2G-NN16 CBS and siRNA showed very similar values to those obtained for dendrimers alone, as has been reported elsewhere [107, 113, 125, 126]. Both assays indicate a lack of toxicity of 2G-NN16 at the concentrations used in HIV inhibition experiments. Until now, gene expression

studies about toxicity of delivery reagents are not routinely performed. Here, we have performed a microarray analysis of the U87MG astrocytoma cell line treated with 24 µg/ml of 2G-NN16 compared to control cells. These studies did not show any statistically significant gene expression change [127, 128], so we can consider 2G-NN16 to be a transfection agent with minimal secondary effects in gene regulation in astrocytoma cells. To test for possible off-target effects by the siRNA, further microarray analyses must be performed on cells treated with dendriplexes containing siRNA or siRNA alone. These results contrast with changes in gene expression profiles [129, 130] and higher cytotoxic effects [104, 131, 132] described for other dendrimers.

For cytotoxicity testing of PEI-PEG polymers, initially, they were tested on mouse cells. The order of toxicity from most to least was PEI25k, $PEG(5k)_2$, $PEG(30k)_1$ and $PEG(550)_{30}$. Testing on SupT1 and PBMCs revealed practically the same results showing the order of toxicity to be PEI25k, $PEG(20k)_1$, $PEG(5k)_4$, $PEG(2k)_{10}$, and $PEG(550)_{30}$. Differences between the toxic effects of $PEG(5k)_2$ and $PEG(5k)_4$ in these two assays revealed that only two PEG blocks of 5k in size were not sufficient to protect cells from the PEI core while four 5k blocks appeared to be. The use of flow cytometry to estimate cell viability was also utilized with PEI-PEG treated cells. Both SupT1 and PBMC treated with polyplexes (**Figures 47 and 48**) produced results in accordance with LDH assays (**Figures 43 and 45**). The similarities in the viability graphs produced by these two methods give support to the validity of flow cytometry to detect cytotoxicity. Finally, PEI(25k) at high concentrations was seen to cause both erythrocyte rupture and aggregation, but neither $PEG(20k)_1$ nor $PEG(550)_{30}$ appeared to cause negative effects on these cells, except for a possible slight tendency to aggregate for treatment with $PEG(20k)_1$. These results must be interpreted with the fact that the polymer concentrations were 15 times the usual amount administered (0.25 mg/ml for the PEI-PEG copolymers).

When assessing the transfection efficiency of the various delivery agents, both flow cytometry and confocal/immunofluorescence microscopy were used. Accurate quantification of uptake was measured by flow cytometry, while qualitative assessment of the nature of the uptake was done via confocal and immunofluorescence microscope images. Positive results showed that dendriplex was

successful at transfecting SupT1, HIV-infected PBMC and U87MG cells. Also, siRNA alone was taken up by all the cells. For incubation times of 24 h, dendrimer-delivered siRNA improved the transfection efficiency over siRNA alone. The gradual degradation of the dendrimer could feasibly explain this difference, as siRNA is more easily detected after being liberated from the dendrimer. For astrocytes, the higher the +/- ratio, the better the transfection, while for lymphocytes, the highest transfection efficiency was at a +/- ratio of 2. This is possibly explained by astrocytes' reduced tendency to endocytose foreign particles [133], and the increased zeta potential of the dendriplexes at higher +/- charge ratios greatly facilitates this process. Meanwhile, the higher zeta potential dendriplexes causes more harm than good to lymphocytes. It is worth noting, however, that dendriplexes showed equal or better transfection than the commercially available Lipofectin. This is a noteworthy result considering that Lipofectin is among the top of the line transfection reagents used for laboratory settings.

The fact that we observed complete entrance of naked siRNA in the primary lymphocytes and the U87MG within 24 hours and almost immediately in the established cell line merits attention. This is not the first time that we have noticed this occurrence as we also observed the uptake of free oligonucleotides in PBMC [134]. It can be assumed that the small size of the siRNA and antisense oligonucleotides is the determining factor in their uptake since we have not witnessed the entrance of larger plasmids alone (data not shown). Regardless of their uptake by these cells, naked siRNA and oligonucleotides would face more significant obstacles in the *in vivo* setting, precisely for which the dendrimers and polymers were designed to overcome. The design of these delivery vehicles not only intends to improve transfection efficiency, stability and protection *in vivo*, but also to possess a time-dependent release capability in the case of dendrimers, and an exterior layer of PEG moieties to improve biocompatibility in the case of polymers.

For polyplex treatments administered with a constant siRNA concentration, successful transfection was achieved in lymphocytes by almost all polymers even after short incubation times. $PEG(20k)_1$, interestingly, was better at transfecting PBMC than SupT1, while $PEG(550)_{30}$ showed the exact opposite characteristic. PEI(25k) achieved quicker transfection in both cell types, but by 24 h, its high transfection efficiency was equaled by the other copolymers. It is also uncertain if the

high uptake at short time periods was because of cellular damage caused by the PEI25k polymer, which is a possibility considering the toxicity results for this polymer after 3 h. showed consistent transfection capability for all times, N/P ratios and cell types. This result, in particular, was of more significance when considering the results obtained for biological effect achieved with $PEG(2k)_{10}$-delivered siRNA.

Confocal and immunofluorescence images proved that flow cytometry results indicated uptake into the interior of the cell and not just association of the siRNA with the cell membrane. Additionally, the videos of live cells positive for siRNA uptake proved that the transfection was not the result of fixating the cells (which was not performed, in this case) or any other process of the cell preparation that would have created pores in the cell membrane, but rather by natural uptake. For confocal images of polyplex treated cells, double the siRNA concentration was administered to increase the probability of obtaining a clearer detection of the siRNA. The drawback was that this resulted in double the concentration of polymer, which resulted in a cytotoxic effect for $PEG(20k)_1$ and especially PEI(25k).

A substantial problem in investigating gene therapy or RNAi in the fight against HIV lies in the fact that practically all HIV-susceptible cells are very difficult to transfect [135, 136]. To overcome the inherent difficulties in transfecting suspension T cell lines or primary cell cultures such as PBMC or NHA [137], investigators have made use of innovative techniques such as nucleofection [138] or antibody fused proteins [139]. The confocal microscopy images indicate uptake of siRNA by CD4+ T lymphocytes via our transfection methods. Moreover, the similarity of the compartmentalized fluorescent siRNA with perinuclear endosomes in terms of morphology and spatial localization indicate the possibility of entrance via endocytosis. In several polarized T cells seen in the videos, fluorescence appears clearly accumulated in the uropod. This peculiar localization only occurs in polarized lymphocytes [140], offering further evidence of endocytosis. Even though the exact internalization pathway has not yet been determined, it is most likely that the pathway is mediated by internal vesicle formation.

In order to better assess the potential for dendrimers to treat cells of the CNS, quality assays on biological barrier transcytosis of the molecules were needed. The first assays involved a monolayer of polarized epithelial cells, which is used in the laboratory to model the genital mucosal membrane [141]. After obtaining positive

results for the ability to cross the epithelial cell layer, bovine brain microvascular endothelial cells were obtained. These cells form a monolayer that more closely mimics the cells contained in the BBB [142, 143]. In order for the models to function, it was essential that the cells formed tight junctions without fenestrations [117]. We analyzed the monolayers during their growth using several methods capable of detecting gaps and fenestrations. First, visual analysis of the monolayer was accomplished with the aid of a light microscope, a Nomarski prism for depth perception and AgNO3 staining, which highlights tight junctions [144]. Monolayer-forming cells were seeded and grown concurrently both in the transwell dishes and in separate plaques which could be viewed under a microscope. This allowed for the determination of the progress of the development of the monolayer. Second, an epithelial voltohmmeter was used to measure the TEER, and only a reading of greater than 300 Ωcm^2 was considered sufficient to indicate the absence of junction gaps. However, the strongest evidence for the integrity of the tight monolayer was the fact that after 5 h, there was no uptake of either siRNA alone or dendriplex in either PBMC or U87MG for either of the barrier models. Had there existed gaps, there most certainly would have been transfection in these cells after 5 h, because transfection studies had already shown that 3 h is enough for the transfection of these cells with dendriplex or siRNA in most cases. Therefore, the high transfection rate after 72 h can only be considered a result of the dendriplexes crossing the barrier.

The CNS is not the primary target for HIV infection. However, the existence of neuropathological disorders caused by HIV infection such as HIV associated dementia (HAD) combined with the inaccessibility of the CNS for large molecule pharmaceuticals creates the need for research into anti-HIV therapy for the CNS including drugs with the capability of crossing the blood brain barrier. Although the introduction of HAART has greatly reduced the severity of HAD, still a great number of HIV-infected individuals manifest a plethora of CNS diseases unrelated to opportunistic infections, including HAD [22-24]. The majority of antiretroviral drugs may not cross the BBB sufficiently to reduce the viral load and inflammation in the CNS. Thus, HAART is currently insufficient in many cases. However, the emergence of nanotechnology provides some hope that treatment of CNS disorders in HIV-infected patients will be improved.

The final section of results presented in this work dealt with achieving a desired outcome from treatment with the complexes, namely, specific gene silencing. For many of the gene silencing experiments, the housekeeping gene GAPDH was targeted as an easily measured control for the detection of effective gene silencing. When siRNA targeted to either GAPDH or the HIV genes was transfected into lymphocytes via electroporation, the result was a sequence-specific, lasting downregulation of the target genes. These results supported the effectivity of the siRNA if transfection and release could be accomplished with the delivery agents. They also revealed that the silencing activity was dependent on the siRNA concentration and established the most effective concentration to be at least 250 nM. Experiments in delivery of siRNA to lymphocytes by 2G-NN16 showed nearly 50% silencing of GAPDH and 22% inhibition of HIV. In astrocytes the maximum silencing efficiency was 37% and over 80%, respectively. Furthermore, in astrocytes, the treatment was able to have an effect at reducing the viral replication for both an X4-HIV isolate (NL4-3) and an R5-HIV isolate (Ba-L). Being able to silence both viral isolates is promising, as the exact mechanism of how HIV infects CNS cells is not fully understood.

As for polymer-delivered siRNA to lymphocytes, the short-term silencing effect was less promising. However, when repetitive treatments were administered throughout the duration of longer experiments, both GAPDH and HIV were silenced with much higher effectivity. Two copolymers stood out over the remaining three polymers in their ability to affect gene expression. These were $PEG(2k)_{10}$ and $PEG(20k)_1$. Delivery by $PEG(2k)_{10}$ had somewhat less of a sequence-specific effect in the longer duration experiments. However, it seemed to have a bit more effectivity after shorter incubation times, and was indeed able to inhibit HIV replication during the long-term experiments by delivering siNEF by an average of 74% compared to siRandom starting from day 5 in cells that had been infected with HIV at a MOI of 100 pg/10^6 cells (**Figure 73**). The logarithmic scale of the antigen p24 production in this graph causes the results to be misleading in the extent of the differences between the treatments. That, and the fact that $PEG(20k)_1$-delivered siNEF achieved an almost total degree of inhibition compared either to untreated cells or siRandom treated cells. The most astonishing results of this work were the capability of $PEG(20k)_1$-delivered siNEF at inhibiting HIV when administered regularly every few days for multiple

weeks. In cells infected with a MOI of 100 pg/10^6 cells, PEG(20k)$_1$-delivered siNEF resulted in an average inhibition of 90 % compared to siRandom and 99.8% compared to untreated cells after day 7. Naturally, it is difficult to extrapolate what kind of inhibitory effect this treatment would have in patients, as the level of virus production in laboratory experiments is purposely maintained at very high levels in order to detect sometimes-subtle differences in replication rates. Of course, *in vivo* tests would provide much needed information about the effect of these treatments when applied to whole organisms.

Currently there exist many limits in the overall efficacy of current HIV therapy because of the ability of HIV to develop drug resistant strains. Likewise, viral latency is a significant problem when addressing treatment for HIV infection [145] and [146]. RNAi could potentially improve this weakness in HIV therapy by attacking very specific targets of the viral life cycle [147], reducing the opportunities for the emergence of resistant strains, and making use of a cocktail of siRNA to attack the virus on multiple fronts. As we have shown, a mixture of several siRNA targeted specifically to the virus resulted in an inhibitory effect of nearly 40%. This inhibition was achieved by only targeting a mixture of HIV genes, however the possibility of combining [64] siRNA targeted to HIV with other siRNA designed to downregulate endogenous cellular genes [37, 148] essential for HIV replication could feasibly improve results. Furthermore, dendriplexes or polyplexes could be utilized to selectively target HIV infected cells or harbors of latently infected cell pools.

This work has combined three separate but equally interesting aspects of molecular biology research. First, nanotechnology is a field continually expanding and offering new nanoparticles and nanosystems for a huge variety of applications. Research into the utilization of nanoparticles such as dendrimers and polymers as biocompatible drug delivery cell-transfecting vehicles requires inorganic structural chemistry combined with cellular biology. Second, RNAi is an exciting laboratory tool currently at the perusal of molecular biologists for a myriad of research applications. It is also being developed and tested for potential uses outside the laboratory and in the realm of the hospital for clinical uses including, as one example, the fight against infectious diseases [147]. Finally, HIV is a raging pandemic of huge proportions that requires the development and availability of as many weapons and defenses against it as possible. By examining the possibility of bringing

nanotechnology and RNAi together as a therapy against HIV infection, this work, hopefully, will in some way contribute to the ongoing research towards a solution to this disease and in the process add to the ever expanding base of knowledge being constantly generated in the scientific laboratory.

6. CONCLUSIONS

1. 2G-NN16 dendrimer forms a stable dendriplex with siRNA at an optimal +/- ratio between 2 and 4, which possesses a particle size from 250 to 350 nm, protects the siRNA from RNases, and exhibits a time-controlled liberation of its siRNA cargo from 12 to 24 h.

2. The non-grafted PEI polymer forms a stable polyplex at an N/P ratio of 5, while the PEG-grafted PEI polymers form polyplexes starting from an N/P ratio of 8. The larger PEG moieties allow for the formation of particles around 150 nm in size, which possesses a zeta potential of +15 mV.

3. When treated at working concentrations, 2G-NN16 dendrimer and dendriplex do not cause cytotoxicity or cell proliferation on immortalized or primary lymphocytes or astrocytes. Neither do they cause erythrocyte hemolysis. Furthermore, 2G-NN16 alone does not cause gene expression variations in astrocytes.

4. PEG engraftments improve the biocompatibility profile of PEI polymers on lymphocytes, especially PEG chains of the sizes 0.55, 2 and 5 kDa. Regardless, none of the polymers were cytotoxic when administered at twice the necessary working concentrations.

5. By 24 h, 2G-NN16 dendriplex can achieve very high transfection efficiencies in lymphocytes and astrocytes. The optimal +/- charge ratio for transfection is 2 for lymphocytes and 8 for astrocytes.

6. Ungrafted PEI polymer achieves cell transfection more quickly than grafter copolymer, but by 24 h, all the polymers show relatively equal transfection efficiencies.

7. Transfection facilitated by polyplex or dendriplex resulted in access to the cell interior by siRNA.

8. 2G-NN16 dendriplex was capable of crossing biological barrier models made of polarized epithelial or bovine brain microvascular endothelial cells and achieving transfection of lymphocytes or astrocytes on the opposite side of the barrier.

9. siRNA delivered by 2G-NN16 successfully reduced GAPDH expression or HIV replication in lymphocytes or astrocytes in a sequence-specific manner.

10. Treatment of lymphocytes with polyplexes composed of siRNA and PEI(25k)-PEG(20k)$_1$ resulted in nearly 80% gene silencing of GAPDH when administered regularly every few days for multiple weeks. The ability to inhibit viral replication in HIV-infected lymphocytes with siRNA targeted to viral genes by this same treatment regimen was achieved to the extent of at least a 10-fold reduction in virus production.

7. BIBLIOGRAPHY

1. Center for Disease Control. Pneumocystis pneumonia--Los Angeles. *MMWR* 1981; **30**: 250-2.
2. UNAIDS. 2008 Report on the global AIDS epidemic. 2008.
3. Kallings LO. The first postmodern pandemic: 25 years of HIV/ AIDS. *J Intern Med* 2008; **263**: 218-43.
4. World Population Prospects: The 2008 Revision. In: United Nations Population Division; 2008.
5. Fauci AS, Pantaleo G, Stanley S, Weissman D. Immunopathogenic mechanisms of HIV infection. *Ann Intern Med* 1996; **124**: 654-63.
6. Kahn JO, Walker BD. Acute human immunodeficiency virus type 1 infection. *N Engl J Med* 1998; **339**: 33-9.
7. Mellors JW, Rinaldo CR, Jr., Gupta P, et al. Prognosis in HIV-1 infection predicted by the quantity of virus in plasma. *Science* 1996; **272**: 1167-70.
8. Libman H. Pathogenesis, natural history, and classification of HIV infection. *Prim Care* 1992; **19**: 1-17.
9. Coffin JM, Hughes SH, Varmus H. **Retroviruses**. Plainview, N.Y.: Cold Spring Harbor Laboratory Press; 1997.
10. Trono D. HIV accessory proteins: leading roles for the supporting cast. *Cell* 1995; **82**: 189-92.
11. Briggs JA, Grunewald K, Glass B, et al. The mechanism of HIV-1 core assembly: insights from three-dimensional reconstructions of authentic virions. *Structure* 2006; **14**: 15-20.
12. Greene WC, Peterlin BM. Charting HIV's remarkable voyage through the cell: Basic science as a passport to future therapy. *Nat Med* 2002; **8**: 673-80.
13. Miller MD, Farnet CM, Bushman FD. Human immunodeficiency virus type 1 preintegration complexes: studies of organization and composition. *J Virol* 1997; **71**: 5382-90.
14. Cullen BR. Retroviruses as model systems for the study of nuclear RNA export pathways. *Virology* 1998; **249**: 203-10.
15. Alcamo IE. AIDS in the modern world. In: *AIDS in the modern world*; 2001:25-6.
16. Gupta P, Balachandran R, Ho M, Enrico A, Rinaldo C. Cell-to-cell transmission of human immunodeficiency virus type 1 in the presence of azidothymidine and neutralizing antibody. *J Virol* 1989; **63**: 2361-5.
17. Phillips DM. The role of cell-to-cell transmission in HIV infection. *AIDS* 1994; **8**: 719-31.
18. Kramer-Hammerle S, Rothenaigner I, Wolff H, Bell JE, Brack-Werner R. Cells of the central nervous system as targets and reservoirs of the human immunodeficiency virus. *Virus Res* 2005; **111**: 194-213.
19. Schwartz L, Major EO. Neural progenitors and HIV-1-associated central nervous system disease in adults and children. *Curr HIV Res* 2006; **4**: 319-27.
20. Gonzalez-Scarano F, Martin-Garcia J. The neuropathogenesis of AIDS. *Nat Rev Immunol* 2005; **5**: 69-81.
21. Coleman CM, Wu L. HIV interactions with monocytes and dendritic cells: viral latency and reservoirs. *Retrovirology* 2009; **6**: 51.
22. McArthur JC, Haughey N, Gartner S, et al. Human immunodeficiency virus-associated dementia: an evolving disease. *J Neurovirol* 2003; **9**: 205-21.

23. Neuenburg JK, Brodt HR, Herndier BG, et al. HIV-related neuropathology, 1985 to 1999: rising prevalence of HIV encephalopathy in the era of highly active antiretroviral therapy. *J Acquir Immune Defic Syndr* 2002; **31**: 171-7.
24. Dore GJ, McDonald A, Li Y, Kaldor JM, Brew BJ. Marked improvement in survival following AIDS dementia complex in the era of highly active antiretroviral therapy. *Aids* 2003; **17**: 1539-45.
25. Melton ST, Kirkwood CK, Ghaemi SN. Pharmacotherapy of HIV dementia. *Ann Pharmacother* 1997; **31**: 457-73.
26. Clifford DB. Central Neurologic Complications of HIV Infection. *Curr Infect Dis Rep* 1999; **1**: 187-91.
27. Gonzalo T, Garcia Goni M, Munoz-Fernandez MA. Socio-economic impact of antiretroviral treatment in HIV patients. An economic review of cost savings after introduction of HAART. *AIDS Rev* 2009; **11**: 79-90.
28. Gottfredsson M, Bohjanen PR. Human immunodeficiency virus type I as a target for gene therapy. *Front Biosci* 1997; **2**: d619-34.
29. Hirsch MS, Conway B, D'Aquila RT, et al. Antiretroviral drug resistance testing in adults with HIV infection: implications for clinical management. International AIDS Society--USA Panel. *JAMA* 1998; **279**: 1984-91.
30. Bermejo M, Sanchez-Palomino S, Usan L, Alcami J. Dynamics of HIV replication in lymphocytes and the efficacy of protease inhibitors. *J Med Virol* 2004; **73**: 502-7.
31. US Food and Drug Administration. . In: Drugs used in the treatment of HIV infection. http://www.fda.gov/oashi/aids/virals.html.
32. Fire A, Xu S, Montgomery MK, et al. Potent and specific genetic interference by double-stranded RNA in Caenorhabditis elegans. *Nature* 1998; **391**: 806-11.
33. Sharp PA. RNA interference--2001. *Genes Dev.* 2001; **15**: 485-90.
34. Whitehead KA, Langer R, Anderson DG. Knocking down barriers: advances in siRNA delivery. *Nat Rev Drug Discov* 2009; **8**: 129-38.
35. Ma JB, Ye K, Patel DJ. Structural basis for overhang-specific small interfering RNA recognition by the PAZ domain. *Nature* 2004; **429**: 318-22.
36. Filipowicz W, Bhattacharyya SN, Sonenberg N. Mechanisms of post-transcriptional regulation by microRNAs: are the answers in sight? *Nat Rev Genet* 2008; **9**: 102-14.
37. Shimizu S, Kamata M, Kittipongdaja P, et al. Characterization of a potent non-cytotoxic shRNA directed to the HIV-1 co-receptor CCR5. *Genet Vaccines Ther* 2009; **7**: 8.
38. Echeverri CJ, Perrimon N. High-throughput RNAi screening in cultured cells: a user's guide. *Nat Rev Genet* 2006; **7**: 373-84.
39. Sepp KJ, Hong P, Lizarraga SB, et al. Identification of neural outgrowth genes using genome-wide RNAi. *PLoS Genet* 2008; **4**: e1000111.
40. Kohn DB, Candotti F. Gene therapy fulfilling its promise. *N Engl J Med* 2009; **360**: 518-21.
41. Hacein-Bey-Abina S, Von Kalle C, Schmidt M, et al. LMO2-associated clonal T cell proliferation in two patients after gene therapy for SCID-X1. *Science* 2003; **302**: 415-9.
42. Howe SJ, Mansour MR, Schwarzwaelder K, et al. Insertional mutagenesis combined with acquired somatic mutations causes leukemogenesis following gene therapy of SCID-X1 patients. *J Clin Invest* 2008; **118**: 3143-50.

43. Kurreck J. RNA interference: from basic research to therapeutic applications. *Angew Chem Int Ed Engl* 2009; **48**: 1378-98.
44. Peer D, Shimaoka M. Systemic siRNA delivery to leukocyte-implicated diseases. *Cell Cycle* 2009; **8**: 853-9.
45. Han W, Wind-Rotolo M, Kirkman RL, Morrow CD. Inhibition of human immunodeficiency virus type 1 replication by siRNA targeted to the highly conserved primer binding site. *Virology* 2004; **330**: 221-32.
46. Lee MT, Coburn GA, McClure MO, Cullen BR. Inhibition of human immunodeficiency virus type 1 replication in primary macrophages by using Tat- or CCR5-specific small interfering RNAs expressed from a lentivirus vector. *J. Virol.* 2003; **77**: 11964-72.
47. Novina CD, Murray MF, Dykxhoorn DM, et al. siRNA-directed inhibition of HIV-1 infection. *Nat. Med.* 2002; **8**: 681-6.
48. Pomerantz RJ. RNA interference meets HIV-1: will silence be golden? *Nat. Med.* 2002; **8**: 659-60.
49. Malim MH, Hauber J, Le SY, Maizel JV, Cullen BR. The HIV-1 rev trans-activator acts through a structured target sequence to activate nuclear export of unspliced viral mRNA. *Nature* 1989; **338**: 254-7.
50. Scherer L, Rossi JJ, Weinberg MS. Progress and prospects: RNA-based therapies for treatment of HIV infection. *Gene Ther* 2007; **14**: 1057-64.
51. Westerhout EM, Ooms M, Vink M, Das AT, Berkhout B. HIV-1 can escape from RNA interference by evolving an alternative structure in its RNA genome. *Nucleic Acids Res.* 2005; **33**: 796-804.
52. Qin XF, An DS, Chen IS, Baltimore D. Inhibiting HIV-1 infection in human T cells by lentiviral-mediated delivery of small interfering RNA against CCR5. *Proc Natl Acad Sci U S A* 2003; **100**: 183-8.
53. Song E, Lee SK, Dykxhoorn DM, et al. Sustained small interfering RNA-mediated human immunodeficiency virus type 1 inhibition in primary macrophages. *J. Virol.* 2003; **77**: 7174-81.
54. Kumar P, Ban HS, Kim SS, et al. T cell-specific siRNA delivery suppresses HIV-1 infection in humanized mice. *Cell* 2008; **134**: 577-86.
55. Nishitsuji H, Kohara M, Kannagi M, Masuda T. Effective suppression of human immunodeficiency virus type 1 through a combination of short- or long-hairpin RNAs targeting essential sequences for retroviral integration. *J. Virol.* 2006; **80**: 7658-66.
56. Turner JJ, Fabani M, Arzumanov AA, Ivanova G, Gait MJ. Targeting the HIV-1 RNA leader sequence with synthetic oligonucleotides and siRNA: chemistry and cell delivery. *Biochim. Biophys. Acta.* 2006; **1758**: 290-300.
57. Capodici J, Kariko K, Weissman D. Inhibition of HIV-1 infection by small interfering RNA-mediated RNA interference. *J. Immunol.* 2002; **169**: 5196-201.
58. Morris KV, Chung CH, Witke W, Looney DJ. Inhibition of HIV-1 replication by siRNA targeting conserved regions of gag/pol. *RNA Biol* 2005; **2**: 17-20.
59. ter Brake O, Konstantinova P, Ceylan M, Berkhout B. Silencing of HIV-1 with RNA interference: a multiple shRNA approach. *Mol Ther* 2006; **14**: 883-92.
60. Lee SK, Dykxhoorn DM, Kumar P, et al. Lentiviral delivery of short hairpin RNAs protects CD4 T cells from multiple clades and primary isolates of HIV. *Blood* 2005; **106**: 818-26.

61. Son J, Uchil PD, Kim YB, et al. Effective suppression of HIV-1 by artificial bispecific miRNA targeting conserved sequences with tolerance for wobble base-pairing. *Biochem Biophys Res Commun* 2008; **374**: 214-8.
62. Jacque JM, Triques K, Stevenson M. Modulation of HIV-1 replication by RNA interference. *Nature* 2002; **418**: 435-8.
63. Coburn GA, Cullen BR. Potent and specific inhibition of human immunodeficiency virus type 1 replication by RNA interference. *J. Virol.* 2002; **76**: 9225-31.
64. Li MJ, Kim J, Li S, et al. Long-term inhibition of HIV-1 infection in primary hematopoietic cells by lentiviral vector delivery of a triple combination of anti-HIV shRNA, anti-CCR5 ribozyme, and a nucleolar-localizing TAR decoy. *Mol Ther* 2005; **12**: 900-9.
65. Senserrich J, Pauls E, Armand-Ugon M, et al. HIV-1 resistance to the anti-HIV activity of a shRNA targeting a dual-coding region. *Virology* 2008; **372**: 421-9.
66. Park WS, Hayafune M, Miyano-Kurosaki N, Takaku H. Specific HIV-1 env gene silencing by small interfering RNAs in human peripheral blood mononuclear cells. *Gene Ther* 2003; **10**: 2046-50.
67. Das AT, Brummelkamp TR, Westerhout EM, et al. Human immunodeficiency virus type 1 escapes from RNA interference-mediated inhibition. *J. Virol.* 2004; **78**: 2601-5.
68. Wolff JA, Malone RW, Williams P, et al. Direct gene transfer into mouse muscle in vivo. *Science* 1990; **247**: 1465-8.
69. Inoue T, Sugimoto M, Sakurai T, et al. Modulation of scratching behavior by silencing an endogenous cyclooxygenase-1 gene in the skin through the administration of siRNA. *J Gene Med* 2007; **9**: 994-1001.
70. Fattal E, Bochot A. Ocular delivery of nucleic acids: antisense oligonucleotides, aptamers and siRNA. *Adv Drug Deliv Rev* 2006; **58**: 1203-23.
71. Palliser D, Chowdhury D, Wang QY, et al. An siRNA-based microbicide protects mice from lethal herpes simplex virus 2 infection. *Nature* 2006; **439**: 89-94.
72. Grzelinski M, Urban-Klein B, Martens T, et al. RNA interference-mediated gene silencing of pleiotrophin through polyethylenimine-complexed small interfering RNAs in vivo exerts antitumoral effects in glioblastoma xenografts. *Hum Gene Ther* 2006; **17**: 751-66.
73. Dykxhoorn DM, Novina CD, Sharp PA. Killing the messenger: short RNAs that silence gene expression. *Nat. Rev. Mol. Cell Biol.* 2003; **4**: 457-67.
74. Song E, Zhu P, Lee SK, et al. Antibody mediated in vivo delivery of small interfering RNAs via cell-surface receptors. *Nat. Biotechnol.* 2005; **23**: 709-17.
75. Verma IM, Somia N. Gene therapy -- promises, problems and prospects. *Nature* 1997; **389**: 239-42.
76. Alvarez Losada S, Canto-Nogues C, Munoz-Fernandez MA. A new possible mechanism of human immunodeficiency virus type 1 infection of neural cells. *Neurobiol Dis* 2002; **11**: 469-78.
77. Douglas KL. Toward development of artificial viruses for gene therapy: a comparative evaluation of viral and non-viral transfection. *Biotechnol Prog* 2008; **24**: 871-83.

78. Midoux P, Pichon C, Yaouanc JJ, Jaffres PA. Chemical vectors for gene delivery: a current review on polymers, peptides and lipids containing histidine or imidazole as nucleic acids carriers. *Br J Pharmacol* 2009; **157**: 166-78.
79. Bareford LM, Swaan PW. Endocytic mechanisms for targeted drug delivery. *Adv Drug Deliv Rev* 2007; **59**: 748-58.
80. Weber N, Ortega P, Clemente MI, et al. Characterization of carbosilane dendrimers as effective carriers of siRNA to HIV-infected lymphocytes. *J Control Release* 2008; **132**: 55-64.
81. Walther W, Stein U. Viral vectors for gene transfer: a review of their use in the treatment of human diseases. *Drugs* 2000; **60**: 249-71.
82. Mintzer MA, Simanek EE. Nonviral vectors for gene delivery. *Chem Rev* 2009; **109**: 259-302.
83. Meade BR, Dowdy SF. Enhancing the cellular uptake of siRNA duplexes following noncovalent packaging with protein transduction domain peptides. *Adv Drug Deliv Rev* 2008; **60**: 530-6.
84. Garnett MC. Gene-delivery systems using cationic polymers. *Crit Rev Ther Drug Carrier Syst* 1999; **16**: 147-207.
85. Wagner E, Cotten M, Foisner R, Birnstiel ML. Transferrin-polycation-DNA complexes: the effect of polycations on the structure of the complex and DNA delivery to cells. *Proc Natl Acad Sci U S A* 1991; **88**: 4255-9.
86. Boussif O, Lezoualc'h F, Zanta MA, et al. A versatile vector for gene and oligonucleotide transfer into cells in culture and in vivo: polyethylenimine. *Proc Natl Acad Sci U S A* 1995; **92**: 7297-301.
87. Pouton CW, Wagstaff KM, Roth DM, Moseley GW, Jans DA. Targeted delivery to the nucleus. *Adv Drug Deliv Rev* 2007; **59**: 698-717.
88. Veronese FM, Pasut G. PEGylation, successful approach to drug delivery. *Drug Discov Today* 2005; **10**: 1451-8.
89. Mao S, Neu M, Germershaus O, et al. Influence of polyethylene glycol chain length on the physicochemical and biological properties of poly(ethylene imine)-graft-poly(ethylene glycol) block copolymer/SiRNA polyplexes. *Bioconjug. Chem.* 2006; **17**: 1209-18.
90. Standard Terminology Relating to Nanotechnology. In. West Conshohocken, PA: ASTM International; 2006.
91. Pantarotto D, Singh R, McCarthy D, et al. Functionalized carbon nanotubes for plasmid DNA gene delivery. *Angew Chem Int Ed Engl* 2004; **43**: 5242-6.
92. Cai D, Mataraza JM, Qin ZH, et al. Highly efficient molecular delivery into mammalian cells using carbon nanotube spearing. *Nat Methods* 2005; **2**: 449-54.
93. Yang R, Yang X, Zhang Z, et al. Single-walled carbon nanotubes-mediated in vivo and in vitro delivery of siRNA into antigen-presenting cells. *Gene Ther* 2006; **13**: 1714-23.
94. Zhang Z, Yang X, Zhang Y, et al. Delivery of telomerase reverse transcriptase small interfering RNA in complex with positively charged single-walled carbon nanotubes suppresses tumor growth. *Clin Cancer Res* 2006; **12**: 4933-9.
95. Boas U, Heegaard PM. Dendrimers in drug research. *Chem. Soc. Rev.* 2004; **33**: 43-63.

96. D'Emanuele A, Attwood D, Abu-Rmaileh R. Dendrimers. *Encyclopedia of Pharmaceutical Technology: Third Edition* 2006: 872 - 90.
97. Bai S, Thomas C, Rawat A, Ahsan F. Recent progress in dendrimer-based nanocarriers. *Crit Rev Ther Drug Carrier Syst* 2006; **23**: 437-95.
98. Tomalia DA, Baker H, Dewald J, et al. A New Class of Polymers: Starburst-Dendritic Macromolecules. *Polym. J.* 1985; **17**: 117-32.
99. Klajnert B, Bryszewska M. Dendrimers: properties and applications. *Acta Biochim Pol* 2001; **48**: 199-208.
100. Castriciano MA, Romeo A, Baratto MC, Pogni R, Scolaro LM. Supramolecular mimetic peroxidase based on hemin and PAMAM dendrimers. *Chem Commun (Camb)* 2008: 688-90.
101. Bielinska A, Kukowska-Latallo JF, Johnson J, Tomalia DA, Baker JR, Jr. Regulation of in vitro gene expression using antisense oligonucleotides or antisense expression plasmids transfected using starburst PAMAM dendrimers. *Nucleic Acids Res* 1996; **24**: 2176-82.
102. Esfand R, Tomalia DA. Poly(amidoamine) (PAMAM) dendrimers: from biomimicry to drug delivery and biomedical applications. *Drug Discov Today* 2001; **6**: 427-36.
103. Dufes C, Uchegbu IF, Schatzlein AG. Dendrimers in gene delivery. *Adv. Drug. Deliv. Rev.* 2005; **57**: 2177-202.
104. Duncan R, Izzo L. Dendrimer biocompatibility and toxicity. *Adv. Drug Deliv. Rev.* 2005; **57**: 2215-37.
105. Zinselmeyer BH, Mackay SP, Schatzlein AG, Uchegbu IF. The lower-generation polypropylenimine dendrimers are effective gene-transfer agents. *Pharm Res* 2002; **19**: 960-7.
106. Boas U, Christensen JB, Heegaard PM. **Dendrimers: design, synthesis and chemical properties**. In: *Dendrimers in Medicine and Biotechnology: New Molecular Tools*. Edited by Boas U, Christensen JB, Heegaard PM: RSC Publishing; 2006:3785-98.
107. Bermejo JF, Ortega P, Chonco L, et al. Water-soluble carbosilane dendrimers: synthesis biocompatibility and complexation with oligonucleotides; evaluation for medical applications. *Chemistry* 2007; **13**: 483-95.
108. Svenson S, Tomalia DA. Dendrimers in biomedical applications--reflections on the field. *Adv. Drug. Deliv. Rev.* 2005; **57**: 2106-29.
109. Ortega P, Bermejo JF, Chonco L, et al. Novel Water-Soluble Carbosilane Dendrimers: Synthesis and Biocompatibility. *Eur. J. Inorg. Chem.* 2006; **2006**: 1388 - 96.
110. Petersen H, Fechner PM, Fischer D, Kissel T. Synthesis, Characterization, and Biocompatibility of Polyethylenimine-graft-poly(ethylene glycol) Block Copolymers. *Macromolecules* 2002; **35**: 6867-74.
111. Adachi A, Gendelman HE, Koenig S, et al. Production of acquired immunodeficiency syndrome-associated retrovirus in human and nonhuman cells transfected with an infectious molecular clone. *J Virol* 1986; **59**: 284-91.
112. Gartner S, Markovits P, Markovitz DM, et al. The role of mononuclear phagocytes in HTLV-III/LAV infection. *Science* 1986; **233**: 215-9.
113. Fischer D, Li Y, Ahlemeyer B, Krieglstein J, Kissel T. In vitro cytotoxicity testing of polycations: influence of polymer structure on cell viability and hemolysis. *Biomaterials* 2003; **24**: 1121-31.

114. Petersen H, Fechner PM, Martin AL, et al. Polyethylenimine-graft-poly(ethylene glycol) copolymers: influence of copolymer block structure on DNA complexation and biological activities as gene delivery system. *Bioconjug Chem* 2002; **13**: 845-54.
115. Kloeckner J, Wagner E, Ogris M. Degradable gene carriers based on oligomerized polyamines. *Eur J Pharm Sci* 2006; **29**: 414-25.
116. Clemente MI, Gonzalo T, Jiménez JL, et al. A promising vector for gene therapy in HIV/AIDS produce highly efficient transfection of primary and cell line cultures. *Pharm Res* Sep 2009; **Submitted**.
117. Bomsel M. Transcytosis of infectious human immunodeficiency virus across a tight human epithelial cell line barrier. *Nat Med* 1997; **3**: 42-7.
118. Saidi H, Magri G, Nasreddine N, Requena M, Belec L. R5- and X4-HIV-1 use differentially the endometrial epithelial cells HEC-1A to ensure their own spread: implication for mechanisms of sexual transmission. *Virology* 2007; **358**: 55-68.
119. Jiménez JL, Clemente MI, Weber N, et al. Inhibition of HIV replication by siRNA in human astrocytoma cells using Carbosilane Dendrimers. Sep 2009; **Submitted**.
120. Evans LH, Alamgir AS, Owens N, Weber N, et al. Mobilization of endogenous retroviruses in mice after infection with an exogenous retrovirus. *J Virol* 2009; **83**: 2429-35.
121. Shcharbin D, Pedziwiatr E, Bryszewska M. How to study dendriplexes I: Characterization. *J Control Release* 2009; **135**: 186-97.
122. Chonco L, Bermejo-Martin JF, Ortega P, et al. Water-soluble carbosilane dendrimers protect phosphorothioate oligonucleotides from binding to serum proteins. *Org. Biomol. Chem.* 2007; **5**: 1886-93.
123. Shcharbin D, Pedziwiatr E, Chonco L, et al. Analysis of interaction between dendriplexes and bovine serum albumin. *Biomacromolecules* 2007; **8**: 2059-62.
124. Liegler TJ, Hyun W, Yen TS, Stites DP. Detection and quantification of live, apoptotic, and necrotic human peripheral lymphocytes by single-laser flow cytometry. *Clin Diagn Lab Immunol* 1995; **2**: 369-76.
125. Ortega P, Bermejo JF, Chonco L, et al. Novel Water-soluble carbosilane dendrimers: synthesis and biocompatibility. *Eur J Inorg Chem* 2006: 1388-96.
126. Jevprasesphant R, Penny J, Jalal R, et al. The influence of surface modification on the cytotoxicity of PAMAM dendrimers. *Int J Pharm* 2003; **252**: 263-6.
127. Gentleman RC, Carey VJ, Bates DM, et al. Bioconductor: open software development for computational biology and bioinformatics. *Genome Biol* 2004; **5**: R80.
128. Smyth GK. Linear Models and Empirical Bayes Methods for Assessing Differential Expression in Microarray Experiments. *Statistical Applications in Genetics and Molecular Biology* 2004; **3**: Article 3.
129. Omidi Y, Hollins AJ, Drayton RM, Akhtar S. Polypropylenimine dendrimer-induced gene expression changes: the effect of complexation with DNA, dendrimer generation and cell type. *J Drug Target* 2005; **13**: 431-43.
130. Hollins AJ, Omidi Y, Benter IF, Akhtar S. Toxicogenomics of drug delivery systems: Exploiting delivery system-induced changes in target gene expression to enhance siRNA activity. *J Drug Target* 2007; **15**: 83-8.

131. Dutta T, Agashe HB, Garg M, et al. Poly (propyleneimine) dendrimer based nanocontainers for targeting of efavirenz to human monocytes/macrophages in vitro. *J. Drug Target.* 2007; **15**: 89-98.
132. Tziveleka LA, Psarra AM, Tsiourvas D, Paleos CM. Synthesis and characterization of guanidinylated poly(propylene imine) dendrimers as gene transfection agents. *J. Control. Release* 2007; **117**: 137-46.
133. Magnus T, Chan A, Linker RA, Toyka KV, Gold R. Astrocytes are less efficient in the removal of apoptotic lymphocytes than microglia cells: implications for the role of glial cells in the inflamed central nervous system. *J Neuropathol Exp Neurol* 2002; **61**: 760-6.
134. Bermejo JF, Chonco L, Samaniego R, et al. Comparative Uptake of Phosphorothioate Oligonucleotides by Human Peripheral Blood Mononuclear Cells from Newborns and Adults. *Eur. J. Sci. Res.* 2006; **15**: 113-21.
135. Keller H, Yunxu C, Marit G, et al. Transgene expression, but not gene delivery, is improved by adhesion-assisted lipofection of hematopoietic cells. *Gene Ther* 1999; **6**: 931-8.
136. Brahmamdam P, Watanabe E, Unsinger J, et al. Targeted delivery of siRNA to cell death proteins in sepsis. *Shock* 2009; **32**: 131-9.
137. Lingor P, Michel U, Scholl U, Bahr M, Kugler S. Transfection of "naked" siRNA results in endosomal uptake and metabolic impairment in cultured neurons. *Biochem Biophys Res Commun* 2004; **315**: 1126-33.
138. Yin J, Ma Z, Selliah N, et al. Effective gene suppression using small interfering RNA in hard-to-transfect human T cells. *J. Immunol. Methods* 2006; **312**: 1-11.
139. Peer D, Zhu P, Carman CV, Lieberman J, Shimaoka M. Selective gene silencing in activated leukocytes by targeting siRNAs to the integrin lymphocyte function-associated antigen-1. *Proc. Natl. Acad. Sci. U. S. A.* 2007; **104**: 4095-100.
140. Samaniego R, Sanchez-Martin L, Estecha A, Sanchez-Mateos P. Rho/ROCK and myosin II control the polarized distribution of endocytic clathrin structures at the uropod of moving T lymphocytes. *J Cell Sci* 2007; **120**: 3534-43.
141. Anderson DJ. **HIV Prevention: A Comprehensive Approach**: Academic Press; 2009.
142. Chan MP, Morisawa S, Nakayama A, Kawamoto Y, Yoneda M. Development of an in vitro blood-brain barrier model to study the effects of endosulfan on the permeability of tight junctions and a comparative study of the cytotoxic effects of endosulfan on rat and human glial and neuronal cell cultures. *Environ Toxicol* 2006; **21**: 223-35.
143. Ma SH, Lepak LA, Hussain RJ, Shain W, Shuler ML. An endothelial and astrocyte co-culture model of the blood-brain barrier utilizing an ultra-thin, nanofabricated silicon nitride membrane. *Lab Chip* 2005; **5**: 74-85.
144. Hirata A, Baluk P, Fujiwara T, McDonald DM. Location of focal silver staining at endothelial gaps in inflamed venules examined by scanning electron microscopy. *Am J Physiol* 1995; **269**: L403-18.
145. Persaud D, Zhou Y, Siliciano JM, Siliciano RF. Latency in human immunodeficiency virus type 1 infection: no easy answers. *J. Virol.* 2003; **77**: 1659-65.

146. Finzi D, Blankson J, Siliciano JD, et al. Latent infection of CD4+ T cells provides a mechanism for lifelong persistence of HIV-1, even in patients on effective combination therapy. *Nat. Med.* 1999; **5**: 512-7.
147. Lopez-Fraga M, Wright N, Jimenez A. RNA interference-based therapeutics: new strategies to fight infectious disease. *Infect Disord Drug Targets* 2008; **8**: 262-73.
148. Coley W, Kehn-Hall K, Duyne RV, Kashanchi F. Novel HIV-1 therapeutics through targeting altered host cell pathways. *Expert Opin Biol Ther* 2009.